A Unified Framework for Simulating Impact-Induced Detonation of a Combustible Material in an Elasto-Plastic Confiner

Haran Jackson

The Centre for Scientific Computing

University of Cambridge

This dissertation is submitted for the degree of

Doctor of Philosophy in Scientific Computing

Fitzwilliam College

Supervisor: Dr N. Nikiforakis

Declaration

This dissertation is the result of my own work and includes nothing which is the outcome of work done in collaboration except where specifically indicated in the text.

Word Count (including tables, figure legends, and appendices):

Haran Jackson
January 4th 2018

Acknowledgements

I would like to thank my supervisor, Dr Nikos Nikiforakis, for all the help and guidance he has given me. Additionally, I would like to thank Dr Louisa Michael, Geraint Harcombe, Tomé Gouveia, Knut Sverdrup, and Bruno Dog for the many useful discussions we had.

Research Output

The following materials were produced over the course of my PhD.

Publications

- H Jackson, N Nikiforakis, *Fast numerical schemes for plastic simulation with the Godunov-Peshkov-Romenski model* (in preparation)
- H Jackson, G Harcombe, N Nikiforakis, *A solver based on eigendecomposition of the Cauchy tensor for Godunov-Romenski-type continuum models* (in preparation)
- H Jackson, N Nikiforakis, *A Riemann ghost fluid method for modeling multimaterial interfaces with the GPR model* (in preparation)
- H Jackson, *The Montecinos-Balsara ADER-FV polynomial basis: convergence properties & extension to non-conservative multidimensional systems* (Computers & Fluids, 2018)
- H Jackson, *A fast numerical scheme for the Godunov-Peshkov-Romenski model of continuum mechanics* (Journal of Computational Physics, 2017)
- H Jackson, *On the eigenvalues of the ADER-WENO Galerkin predictor* (Journal of Computational Physics, 2017)

Conference Presentations

- International Conference on Computational Science 2017 (Zürich, CH), *Paper: A Fast Numerical Scheme for the Godunov-Peshkov-Romenski Model of Continuum Mechanics*
- SIAM International Conference on Numerical Combustion 2017 (Orlando, FL), *Minisymposium: A New Approach for Cook-off Modeling*

- Scientific Computation in the University of Cambridge Seminar Day 2017 (Cambridge, UK), *Poster: A Numerical Method based on Operator Splitting for the GPR Model of Continuum Mechanics*

- Cavendish Graduate Student Conference 2016 (Cambridge, UK), *Poster: A New Framework for Simulating Multimaterial Systems and Gaseous Cookoff*

Open-Source Software

- ADER (github.com/haranjackson/ADER): The ADER method for solving any (potentially very stiff) hyperbolic system of PDEs (6 watchers, 6 stars, 4 forks)

- Julia-WENO (github.com/haranjackson/Julia-WENO): An optimized Julia implementation of the WENO reconstruction algorithm, of any order of accuracy

- Euler1D (github.com/haranjackson/Euler1D): A few first- and second-order methods for solving the 1D Euler equations, implemented in C++

- ProjectionMethod (github.com/haranjackson/ProjectionMethod): A C++ implementation of Chorin's Project Method

- NewtonKrylov (github.com/haranjackson/NewtonKrylov): A C++ implementation of the Newton-Krylov algorithm, with Python bindings

- LGMRES (github.com/haranjackson/LGMRES): A C++ implementation of the LGMRES algorithm, with Python bindings (1star, 1 fork)

- LegendreGauss (github.com/haranjackson/LegendreGauss): C++ code to compute the Legendre-Gauss nodes and weights on [-1,1], based on NumPy's leggauss function

Abstract

Contents

List of Figures

List of Tables

Nomenclature

Roman Symbols

$\boldsymbol{J}$ Thermal impulse vector

$\boldsymbol{q}$ Heat flux vector

$\boldsymbol{v}$ Velocity

A Distortion tensor

c_0 Adiabatic speed of sound

c_h Characteristic velocity of heat waves

c_p Specific heat capacity at constant pressure

c_s Characteristic velocity of transverse perturbations

c_v Specific heat capacity at constant volume

E Total specific energy

p Pressure

p_∞ Pressure constant in stiffened gas equation of state

s Entropy

T Temperature

t Time variable

x Space variable

Greek Symbols

α Constant related to characteristic velocity of heat waves

δ Kronecker delta

γ Ratio of specific heat capacities, equal to $\frac{c_p}{c_v}$

ρ Density

ρ_0 Reference density

σ Viscous shear stress tensor

τ_1 Strain dissipation time

τ_2 Thermal impulse dissipation time

Other Symbols

$\|\cdot\|$ Euclidean vector norm

$\|\cdot\|_F$ Frobenius matrix norm

Acronyms / Abbreviations

DG Discontinuous Galerkin

EOS Equation of State

FV Finite Volume

WENO Weighted Essentially Non-Oscillatory

Notes

Unless otherwise stated, repeated indices in vector, matrix and tensor quantities are to be summed over. If M is a matrix, then $\boldsymbol{M_i}$ is taken to be the ith column of M (note, not the ith row). MATLAB-style index notation is used, such that $M_{i:j}$ refers to the matrix consisting of the columns $i \dots j$ of M (including columns i and j). $M_{i:j,m:n}$ refers to the submatrix of M with corners at M_{im} and M_{jn}.

Chapter 0

Introduction

0.1 Background

0.2 Objectives of this Study

0.3 Mathematical Model

The GPR model, first introduced in Peshkov and Romenski [41] and expanded upon in Dumbser et al. [14], takes the following form:

$$\frac{\partial \rho}{\partial t} + \frac{\partial \left(\rho v_k\right)}{\partial x_k} = 0 \tag{1a}$$

$$\frac{\partial \left(\rho v_i\right)}{\partial t} + \frac{\partial (\rho v_i v_k + p\delta_{ik} - \sigma_{ik})}{\partial x_k} = 0 \tag{1b}$$

$$\frac{\partial A_{ij}}{\partial t} + \frac{\partial \left(A_{ik} v_k\right)}{\partial x_j} + v_k \left(\frac{\partial A_{ij}}{\partial x_k} - \frac{\partial A_{ik}}{\partial x_j}\right) = -\frac{\psi_{ij}}{\theta_1} \tag{1c}$$

$$\frac{\partial \left(\rho J_i\right)}{\partial t} + \frac{\partial \left(\rho J_i v_k + T\delta_{ik}\right)}{\partial x_k} = -\frac{\rho H_i}{\theta_2} \tag{1d}$$

$$\frac{\partial \left(\rho s\right)}{\partial t} + \frac{\partial \left(\rho s v_k + H_k\right)}{\partial x_k} = \frac{\rho}{T}\left(\frac{\psi_{kl}\psi_{kl}}{\theta_1} + \frac{H_k H_k}{\theta_2}\right) \tag{1e}$$

where θ_1 and θ_2 are positive scalar functions, and $\psi = \frac{\partial E}{\partial A}$ and $\boldsymbol{H} = \frac{\partial E}{\partial \boldsymbol{J}}$. Entropy does not decrease during the dissipative time evolution:

$$\frac{\partial \left(\rho s\right)}{\partial t} + \frac{\partial \left(\rho s v_k + H_k\right)}{\partial x_k} \geq 0 \tag{2}$$

(1e) can be replaced with the following equation, which will be used instead when solving the model in this study:

$$\frac{\partial \left(\rho E\right)}{\partial t} + \frac{\partial \left(\rho E v_k + \left(p\delta_{ik} - \sigma_{ik}\right) v_i + q_k\right)}{\partial x_k} = 0 \tag{3}$$

Note that (1a), (1b), (1c), (1d), (3) can be written in the following form:

$$\frac{\partial \boldsymbol{Q}}{\partial t} + \boldsymbol{\nabla} \cdot \boldsymbol{F} + \boldsymbol{B} \cdot \nabla \boldsymbol{Q} = \boldsymbol{S} \tag{4}$$

The following definitions are given:

$$p = \rho^2 \left. \frac{\partial E}{\partial \rho} \right|_{s,A} \tag{5a}$$

$$\sigma = -\rho A^T \left. \frac{\partial E}{\partial A} \right|_{\rho,s} \tag{5b}$$

$$T = \left. \frac{\partial E}{\partial s} \right|_{\rho,A} \tag{5c}$$

$$\boldsymbol{q} = T \frac{\partial E}{\partial \boldsymbol{J}} \tag{5d}$$

To close the system, the EOS must be specified, from which the above quantities and the sources can be derived. E is the sum of the contributions of the energies at the molecular scale (microscale), the material element[1] scale (mesoscale), and the flow scale (macroscale):

$$E = E_1(\rho, s) + E_2(\rho, s, A, \boldsymbol{J}) + E_3(\boldsymbol{v}) \tag{6}$$

In previous studies, E_1 has to been taken to be either the ideal gas EOS, the stiffened gas EOS, or the shock Mie-Gruneisen EOS. A more general set of choices for E_1 is given in Section 1.1.

E_2 has the following quadratic form:

$$E_2 = \frac{c_s(\rho, s)^2}{4} \|\mathrm{dev}(G)\|_F^2 + \frac{\alpha(\rho, s)^2}{2} \|\boldsymbol{J}\|^2 \tag{7}$$

c_s is the characteristic velocity of transverse perturbations. In previous studies, c_s has always been constant. In this study, it will be extended to have a ρ dependence, as outlined in Section 1.1. α is related to the characteristic velocity of propagation of heat waves:

$$c_h = \frac{\alpha}{\rho} \sqrt{\frac{T}{c_v}} \tag{8}$$

[1]The concept of a *material element* corresponds to that of a fluid parcel from fluid dynamics, applied to both fluids and solids.

In previous studies, α has been taken to be constant, as it will in this study.

$G = A^T A$ is the Gramian matrix of the distortion tensor, and $\mathrm{dev}\left(G\right)$ is the deviator (trace-free part) of G:

$$\mathrm{dev}\left(G\right) = G - \frac{1}{3}\mathrm{tr}\left(G\right) I \tag{9}$$

E_3 is the usual specific kinetic energy per unit mass:

$$E_3 = \frac{1}{2}\left\|\boldsymbol{v}\right\|^2 \tag{10}$$

The following forms are taken:

$$\theta_1 = \frac{\tau_1 c_s^2}{3\left|A\right|^{\frac{5}{3}}} \tag{11a}$$

$$\theta_2 = \tau_2 \alpha^2 \frac{\rho T_0}{\rho_0 T} \tag{11b}$$

$$\tau_1 = \begin{cases} \frac{6\mu}{\rho_0 c_s^2} & viscous\,fluids \\ \tau_0 \left(\frac{\sigma_0}{\left\|\mathrm{dev}(\sigma)\right\|_F}\right)^n & elastoplastic\,solids \end{cases} \tag{12a}$$

$$\tau_2 = \frac{\rho_0 \kappa}{T_0 \alpha^2} \tag{12b}$$

The justification of these choices is that classical Navier–Stokes–Fourier theory is recovered in the stiff limit $\tau_1, \tau_2 \to 0$ (see [14]). The power law for elastoplastic solids is based on the work [5].

Finally, we have the following relations:

$$\sigma = -\rho c_s^2 G\,\mathrm{dev}\left(G\right) \tag{13a}$$

$$\boldsymbol{q} = \alpha^2 T \boldsymbol{J} \tag{13b}$$

$$-\frac{\psi}{\theta_1(\tau_1)} = -\frac{3}{\tau_1}\left|A\right|^{\frac{5}{3}} A\,\mathrm{dev}\left(G\right) \tag{13c}$$

$$-\frac{\rho \boldsymbol{H}}{\theta_2\left(\tau_2\right)} = -\frac{T\rho_0}{T_0 \tau_2}\boldsymbol{J} \tag{13d}$$

The following constraint also holds (see [41]):

$$\det(A) = \frac{\rho}{\rho_0} \tag{14}$$

The GPR model and Godunov and Romenski's 1970s model of elastoplastic deformation in fact relies upon the same equations. The realization of Peshkov and Romenski was that these are the equations of motion for an arbitrary continuum - not just a solid - and so the model can be applied to fluids too. Unlike in previous continuum models, material elements have not only finite size, but also internal structure, encoded in the distortion tensor.

The strain dissipation time τ_1 of the HPR model is a continuous analogue of Frenkel's "particle settled life time" [20]; the characteristic time taken for a particle to move by a distance of the same order of magnitude as the particle's size. Thus, τ_1 characterizes the time taken for a material element to rearrange with its neighbors. $\tau_1 = \infty$ for solids and $\tau_1 = 0$ for inviscid fluids. It is in this way that the HPR model seeks to describe all three major phases of matter, as long as a continuum description is appropriate for the material at hand.

The evolution equation for $\boldsymbol{J}$ and its contribution to the energy of the system are derived from Romenski's model of hyperbolic heat transfer, originally proposed in [33, 44], and implemented in [42, 43]. In this model, $\boldsymbol{J}$ is effectively defined as the variable conjugate to the entropy flux, in the sense that the latter is the derivative of the specific internal energy with respect to $\boldsymbol{J}$. Romenski remarks that it is more convenient to evolve $\boldsymbol{J}$ and E than the heat flux or the entropy flux, and thus the equations take the form given here. τ_2 characterizes the speed of relaxation of the thermal impulse due to heat exchange between material elements.

0.4 Numerical Methods

The GPR model, being non-conservative, with stiff source terms, represents a particularly challenging set of PDEs. In this study they are solved by an ADER-WENO method. First, the cell-wise constant state variable data from the current time step is reconstructed using high-order spatial polynomials according to the WENO method. This reconstruction is then extended to a reconstruction in both space and time for each individual cell in the domain, using the Discontinuous Galerkin method. A finite volume solver is then used to couple neighboring cells and produce the cell-wise constant data at the next time step.

0.4.1 The WENO Reconstruction

First introduced by Liu et al. [32] and developed by Jiang and Shu [27], WENO methods are used to produce high order polynomial approximations to piece-wise constant data. Many variations exist. In this study, the method of [18] is used.

Consider the domain $[0, L]$. Take $K, N \in \mathbb{N}$. The order of accuracy of the resulting method will be $N + 1$. Take the set of grid points $x_i = \frac{i \cdot L}{K}$ for $i = 0, \ldots, K$ and let $\Delta x = \frac{L}{K}$. Denote cell $[x_i, x_{i+1}]$ by C_i. Given cell-wise constant data u on $[0, L]$, an order N polynomial reconstruction of u in C_i will be performed. Define the scaled space variable:

$$\chi^i = \frac{1}{\Delta x} \left(x - x_i \right) \tag{15}$$

Denoting the Gauss-Legendre abscissae on $[0, 1]$ by $\{\chi_0, \ldots, \chi_N\}$, define the nodal basis of order N: the Lagrange interpolating polynomials $\{\psi_0, \ldots, \psi_N\}$ with the following property:

$$\psi_i \left(\chi_j \right) = \delta_{ij} \tag{16}$$

If N is even, take the stencils:

$$\begin{cases} S_1 & = \left\{ C_{i-\frac{N}{2}}, \ldots, C_{i+\frac{N}{2}} \right\} \\ S_2 & = \left\{ C_{i-N}, \ldots, C_i \right\} \\ S_3 & = \left\{ C_i, \ldots, C_{i+N} \right\} \end{cases} \tag{17}$$

If N is odd, take the stencils:

$$\begin{cases} S_1 & = \left\{ C_{i-\left\lfloor \frac{N}{2} \right\rfloor}, \ldots, C_{i+\left\lceil \frac{N}{2} \right\rceil} \right\} \\ S_2 & = \left\{ C_{i-\left\lceil \frac{N}{2} \right\rceil}, \ldots, C_{i+\left\lfloor \frac{N}{2} \right\rfloor} \right\} \\ S_3 & = \left\{ C_{i-N}, \ldots, C_i \right\} \\ S_4 & = \left\{ C_i, \ldots, C_{i+N} \right\} \end{cases} \tag{18}$$

The data is reconstructed on S_j as:

$$\sum_p \psi_p \left(\chi^i \left(x \right) \right) \hat{w}_p^{ij} \tag{19}$$

where the $\hat{w}_p^{ij}$ are solutions to the following linear system:

$$\frac{1}{\Delta x}\int_{x_k}^{x_{k+1}}\sum_p \psi_p\left(\chi^k\left(x\right)\right)\hat{w}_p^{ij}dx = u_k \qquad \forall C_k \in S_j \tag{20}$$

where u_k is the value of u in C_k. This can be written as $M_j\boldsymbol{\hat{w}^{ij}} = \boldsymbol{u_{[j_0:j_N]}}$ where $\{j_0,\ldots,j_N\}$ indexes the cells in S_j. In this study reconstructions with $N=2$ are used. The matrices of these linear systems and their inverses are precomputed to accelerate the solution of these systems.

Define the oscillation indicator matrix:

$$\Sigma_{mn} = \sum_{\alpha=1}^{N}\int_0^1 \psi_m^{(\alpha)}\psi_n^{(\alpha)}d\chi \tag{21}$$

and the oscillation indicator for each stencil:

$$o_j = \Sigma_{mn}\hat{w}_m^{ij}\hat{w}_n^{ij} \tag{22}$$

The full reconstruction in C_i is:

$$w_i\left(x\right) = \sum_p \psi_p\left(\chi^i\left(x\right)\right)\bar{w}_p^i \tag{23}$$

where $\bar{w}_p^i = \omega_j\hat{w}_p^{ij}$ is the weighted coefficient of the pth basis function, with weights:

$$\omega_j = \frac{\tilde{\omega}_j}{\sum_k\tilde{\omega}_k} \qquad \tilde{\omega}_j = \frac{\zeta_j}{\left(o_j+\varepsilon\right)^r} \tag{24}$$

In this study, $r=8$, $\varepsilon=10^{-14}$, $\zeta_j=10^5$ if S_j is a central stencil, and $\zeta_j=1$ if S_j is a side stencil, as in [13].

The reconstruction can be extended to two dimensions by taking:

$$\upsilon^i = \frac{1}{\Delta y}\left(y-y_i\right) \tag{25}$$

and defining stencils in the y-axis in an analogous manner. The data in C_i is then reconstructed using stencil S_j as:

$$\sum_{p,q} \psi_p\left(\chi^i(x)\right) \psi_q\left(\upsilon^i(x)\right) \tilde{w}_{pq}^{ij} \tag{26}$$

where the coefficients of the weighted 1D reconstruction are used as cell averages:

$$M_j \tilde{\boldsymbol{w}}_{\boldsymbol{p}}^{\boldsymbol{ij}} = \bar{\boldsymbol{w}}_{\boldsymbol{p}}^{[\boldsymbol{j_0}:\boldsymbol{j_N}]} \qquad \forall p \in \{0, \ldots, N\} \tag{27}$$

The oscillation indicator is calculated for each p in the same manner as the 1D case. The reconstruction method is easily further extensible to three dimensions, now using the coefficients $\bar{w}_{pq}$ of the weighted 2D reconstruction as cell averages.

0.4.2 The Galerkin Predictor

Take a non-conservative, hyperbolic system of the form:

$$\frac{\partial \boldsymbol{Q}}{\partial t} + \frac{\partial \boldsymbol{F}(\boldsymbol{Q})}{\partial x} + B(\boldsymbol{Q}) \cdot \frac{\partial \boldsymbol{Q}}{\partial x} = \boldsymbol{S}(\boldsymbol{Q}) \tag{28}$$

where $\boldsymbol{Q}$ is the vector of conserved variables, $\boldsymbol{F}$ is the conservative nonlinear flux, B is the block matrix corresponding to the purely non-conservative component of the system, and $\boldsymbol{S}(\boldsymbol{Q})$ is the algebraic source vector.

Take the grid for the previous section, and time steps $t_0 < t_1 < \ldots$ while defining $\Delta t_n = t_{n+1} - t_n$. Combining the techniques presented in [11, 13], the Discontinuous Galerkin method produces at each time step t_n a local polynomial approximation to $\boldsymbol{Q}$ on each space-time cell $C_i \times [t_n, t_{n+1}]$.

Now define the scaled time variable:

$$\tau^n = \frac{1}{\Delta t_n}(t - t_n) \tag{29}$$

Thus, (28) becomes:

$$\frac{\partial \boldsymbol{Q}}{\partial \tau^n} + \frac{\partial \boldsymbol{F}^*(\boldsymbol{Q})}{\partial \chi^i} + B^*(\boldsymbol{Q}) \cdot \frac{\partial \boldsymbol{Q}}{\partial \chi^i} = \boldsymbol{S}^*(\boldsymbol{Q}) \tag{30}$$

where

$$\boldsymbol{F}^* = \frac{\Delta t_n}{\Delta x}\boldsymbol{F} \qquad B^* = \frac{\Delta t_n}{\Delta x}B \qquad \boldsymbol{S}^* = \Delta t_n \boldsymbol{S} \tag{31}$$

The non-dimensionalization notation and spacetime cell indexing notation will be dropped for simplicity in what follows. Now define the set of spatio-temporal basis functions:

$$\{\theta_k(\chi,\tau)\} = \{\psi_p(\chi)\,\psi_s(\tau) : 0 \le p, s \le N\} \tag{32}$$

Denoting the Galerkin predictor by $\boldsymbol{q}$, take the following set of approximations:

$$\boldsymbol{Q} \approx \boldsymbol{q} = \theta_\beta \boldsymbol{q}_\beta \tag{33a}$$
$$\boldsymbol{F}(\boldsymbol{Q}) \approx \theta_\beta \boldsymbol{F}_\beta \tag{33b}$$
$$B(\boldsymbol{Q}) \cdot \frac{\partial \boldsymbol{Q}}{\partial \chi} \approx \theta_\beta \boldsymbol{B}_\beta \tag{33c}$$
$$\boldsymbol{S}(\boldsymbol{Q}) \approx \theta_\beta \boldsymbol{S}_\beta \tag{33d}$$

for some coefficients $\boldsymbol{q}_\beta, \boldsymbol{F}_\beta, \boldsymbol{B}_\beta, \boldsymbol{S}_\beta$.

If $\{\psi_0, ..., \psi_N\}$ is a nodal basis, the *nodal basis representation* may be used:

$$\boldsymbol{F}_\beta = \boldsymbol{F}(\boldsymbol{q}_\beta) \tag{34a}$$
$$\boldsymbol{B}_\beta = B(\boldsymbol{q}_\beta) \cdot \left(\frac{\partial \theta_\gamma(\chi_\beta, \tau_\beta)}{\partial \chi}\boldsymbol{q}_\gamma\right) \tag{34b}$$
$$\boldsymbol{S}_\beta = \boldsymbol{S}(\boldsymbol{q}_\beta) \tag{34c}$$

where (χ_β, τ_β) are the coordinates of the node corresponding to basis function θ_β.

If a modal basis is used, $\boldsymbol{F}_\beta, \boldsymbol{B}_\beta, \boldsymbol{S}_\beta$ may be found from the previous values of $\boldsymbol{q}_\beta$ in the iterative processes described below.

For functions $f(\chi,\tau) = f_\chi(\chi)\,f_\tau(\tau)$ and $g(\chi,\tau) = g_\chi(\chi)\,g_\tau(\tau)$, define the following integral operators:

$$[f,g]^t = f_\tau(t)\,g_\tau(t)\,\langle f_\chi, g_\chi\rangle \tag{35a}$$
$$\{f,g\} = \langle f_\tau, g_\tau\rangle\,\langle f_\chi, g_\chi\rangle \tag{35b}$$

Multiplying (30) by test function θ_α, using the polynomial approximations for $\boldsymbol{Q}, \boldsymbol{F}, \boldsymbol{B}, \boldsymbol{S}$, and integrating over space and time gives:

$$\left\{\theta_\alpha, \frac{\partial \theta_\beta}{\partial \tau}\right\} \boldsymbol{q}_\beta = -\left\{\theta_\alpha, \frac{\partial \theta_\beta}{\partial \chi}\right\} \boldsymbol{F}_\beta + \left\{\theta_\alpha, \theta_\beta\right\} \left(\boldsymbol{S}_\beta - \boldsymbol{B}_\beta\right) \tag{36}$$

0.4.2.1 The Discontinuous Galerkin Method

This method of computing the Galerkin predictor allows solutions to be discontinuous at temporal cell boundaries, and is also suitable for stiff source terms.

Integrating (36) by parts in time gives:

$$\begin{aligned}\left(\left[\theta_\alpha, \theta_\beta\right]^1 - \left\{\frac{\partial \theta_\alpha}{\partial \tau}, \theta_\beta\right\}\right) \boldsymbol{q}_\beta = \left[\theta_\alpha, \boldsymbol{w}\right]^0 - \left\{\theta_\alpha, \frac{\partial \theta_\beta}{\partial \chi}\right\} \boldsymbol{F}_\beta \\ + \left\{\theta_\alpha, \theta_\beta\right\} \left(\boldsymbol{S}_\beta - \boldsymbol{B}_\beta\right)\end{aligned} \tag{37}$$

where $\boldsymbol{w}$ is the reconstruction obtained at the start of the time step with the WENO method. Define the following:

$$U_{\alpha\beta} = \left[\theta_\alpha, \theta_\beta\right]^1 - \left\{\frac{\partial \theta_\alpha}{\partial \tau}, \theta_\beta\right\} \tag{38a}$$

$$V_{\alpha\beta} = \left\{\theta_\alpha, \frac{\partial \theta_\beta}{\partial \chi}\right\} \tag{38b}$$

$$\boldsymbol{W_\alpha} = \left[\theta_\alpha, \psi_\gamma\right]^0 \boldsymbol{w}_\gamma \tag{38c}$$

$$Z_{\alpha\beta} = \left\{\theta_\alpha, \theta_\beta\right\} \tag{38d}$$

Thus:

$$U_{\alpha\beta} \boldsymbol{q}_\beta = \boldsymbol{W_\alpha} - V_{\alpha\beta} \boldsymbol{F}_\beta + Z_{\alpha\beta} \left(\boldsymbol{S}_\beta - \boldsymbol{B}_\beta\right) \tag{39}$$

This nonlinear system in $\boldsymbol{q}_\beta$ is solved by a Newton method. The source terms must be solved implicitly if they are stiff. Note that $\boldsymbol{W}$ has no dependence on $\boldsymbol{q}$.

0.4.2.2 The Continuous Galerkin Method

This method of computing the Galerkin predictor is not suitable for stiff source terms, but it provides substantial savings on computational cost and ensures continuity across temporal cell boundaries.

$\{\psi_0, ..., \psi_N\}$ must be chosen in such a way that the first $N+1$ elements of $\{\theta_\beta\}$ have only a spatial dependence. The first $N+1$ elements of $\boldsymbol{q}$ are then fixed by demanding continuity at $\tau = 0$:

$$\boldsymbol{q}\left(\chi, 0\right) = \boldsymbol{w}\left(\chi\right) \tag{40}$$

where $\boldsymbol{w}$ is spatial the reconstruction obtained at the start of the time step with the WENO method.

For a given vector $\boldsymbol{v} \in \mathbb{R}^{(N+1)^2}$ and matrix $X \in M_{(N+1)^2,(N+1)^2}\left(\mathbb{R}\right)$, let $\boldsymbol{v} = \left(\boldsymbol{v^0}, \boldsymbol{v^1}\right)$ and $X = \begin{pmatrix} X^{00} & X^{01} \\ X^{10} & X^{11} \end{pmatrix}$ where $\boldsymbol{v^0}, X^{00}$ are the components relating solely to the first $N+1$ components of $\boldsymbol{v}$. We only need to find the latter components of $\boldsymbol{q}$, and thus, from (36), we have:

$$\begin{aligned} \left\{\theta_\alpha, \frac{\partial \theta_\beta}{\partial \tau}\right\}^{11} \boldsymbol{q_\beta^1} = \left\{\theta_\alpha, \theta_\beta\right\}^{11} \left(\boldsymbol{S_\beta^1} - \boldsymbol{B_\beta^1}\right) - \left\{\theta_\alpha, \frac{\partial \theta_\beta}{\partial \chi}\right\}^{11} \boldsymbol{F_\beta^1} \\ + \left\{\theta_\alpha, \theta_\beta\right\}^{10} \left(\boldsymbol{S_\beta^0} - \boldsymbol{B_\beta^0}\right) - \left\{\theta_\alpha, \frac{\partial \theta_\beta}{\partial \chi}\right\}^{10} \boldsymbol{F_\beta^0} \end{aligned} \tag{41}$$

Define the following:

$$U_{\alpha\beta} = \left\{\theta_\alpha, \frac{\partial \theta_\beta}{\partial \tau}\right\}^{11} \tag{42a}$$

$$V_{\alpha\beta} = \left\{\theta_\alpha, \frac{\partial \theta_\beta}{\partial \chi}\right\}^{11} \tag{42b}$$

$$\boldsymbol{W_\alpha} = \left\{\theta_\alpha, \theta_\beta\right\}^{10} \left(\boldsymbol{S_\beta} - \boldsymbol{B_\beta}\right)^0 - \left\{\theta_\alpha, \frac{\partial \theta_\beta}{\partial \chi}\right\}^{10} \boldsymbol{F_\beta^0} \tag{42c}$$

$$Z_{\alpha\beta} = \left\{\theta_\alpha, \theta_\beta\right\}^{11} \tag{42d}$$

Thus:

$$U_{\alpha\beta}\boldsymbol{q}_{\boldsymbol{\beta}}^{\mathbf{1}} = \boldsymbol{W}_{\boldsymbol{\alpha}} - V_{\alpha\beta}\boldsymbol{F}_{\boldsymbol{\beta}}^{\mathbf{1}} + Z_{\alpha\beta}\left(\boldsymbol{S}_{\boldsymbol{\beta}}^{\mathbf{1}} - \boldsymbol{B}_{\boldsymbol{\beta}}^{\mathbf{1}}\right) \tag{43}$$

Note that, as with the discontinuous Galerkin method, $\boldsymbol{W}$ has no dependence on the degrees of freedom in $\boldsymbol{q}$.

0.4.3 The Finite Volume Scheme

Following the formulation of [13], integrating (28) over $[t_n, t_{n+1}] \times C_i$ gives:

$$\boldsymbol{Q}_{\boldsymbol{i}}^{\boldsymbol{n+1}} = \boldsymbol{Q}_{\boldsymbol{i}}^{\boldsymbol{n}} + \Delta t_n\left(\boldsymbol{S}_{\boldsymbol{i}}^{\boldsymbol{n}} - \boldsymbol{P}_{\boldsymbol{i}}^{\boldsymbol{n}}\right) - \frac{\Delta t_n}{\Delta x}\left(\boldsymbol{D}_{\boldsymbol{i+1}}^{\boldsymbol{n}} - \boldsymbol{D}_{\boldsymbol{i}}^{\boldsymbol{n}}\right) \tag{44}$$

where

$$\boldsymbol{Q}_{\boldsymbol{i}}^{\boldsymbol{n}} = \frac{1}{\Delta x}\int_{x_i}^{x_{i+1}} \boldsymbol{Q}\left(x, t_n\right) dx \tag{45a}$$

$$\boldsymbol{S}_{\boldsymbol{i}}^{\boldsymbol{n}} = \frac{1}{\Delta t_n \Delta x}\int_{t_n}^{t_{n+1}}\int_{x_i}^{x_{i+1}} \boldsymbol{S}\left(\boldsymbol{Q}\right) dx dt \tag{45b}$$

$$\boldsymbol{P}_{\boldsymbol{i}}^{\boldsymbol{n}} = \frac{1}{\Delta t_n \Delta x}\int_{t_n}^{t_{n+1}}\int_{x_i}^{x_{i+1}} B\left(\boldsymbol{Q}\right) \cdot \frac{\partial \boldsymbol{Q}}{\partial x} dx dt \tag{45c}$$

$$\boldsymbol{D}_{\boldsymbol{i}}^{\boldsymbol{n}} = \frac{1}{\Delta t_n}\int_{t_n}^{t_{n+1}} \boldsymbol{\mathcal{D}}\left(\boldsymbol{Q}^-\left(x_i, t\right), \boldsymbol{Q}^+\left(x_i, t\right)\right) dt \tag{45d}$$

$\boldsymbol{Q^-, Q^+}$ are the left and right extrapolated states at the x_i boundary. $\boldsymbol{S}_{\boldsymbol{i}}^{\boldsymbol{n}}, \boldsymbol{P}_{\boldsymbol{i}}^{\boldsymbol{n}}, \boldsymbol{D}_{\boldsymbol{i}}^{\boldsymbol{n}}$ are calculated using an $N+1$-point Gauss-Legendre quadrature, replacing $\boldsymbol{Q}$ with $\boldsymbol{q_h}$.

M, as defined in Section 0.4.2, is a diagonalizable matrix with decomposition $M = R\Lambda R^{-1}$ where the columns of R are the right eigenvectors and Λ is the diagonal matrix of eigenvalues. Define the following matrix:

$$|M| = R\left|\Lambda\right| R^{-1} \tag{46}$$

Using these definitions, the interface terms arising in the FV formula have the following form:

$$\boldsymbol{\mathcal{D}}\left(\boldsymbol{q}^-, \boldsymbol{q}^+\right) = \frac{1}{2}\left(\boldsymbol{F}\left(\boldsymbol{q}^-\right) + \boldsymbol{F}\left(\boldsymbol{q}^+\right) + \hat{B} \cdot \left(\boldsymbol{q}^+ - \boldsymbol{q}^-\right) - \hat{M} \cdot \left(\boldsymbol{q}^+ - \boldsymbol{q}^-\right)\right) \tag{47}$$

$\hat{M}$ is chosen to either correspond to a Rusanov/Lax-Friedrichs flux [47]:

$$\hat{M} = \max\left(\max\left|\Lambda\left(\boldsymbol{q}^-\right)\right|, \max\left|\Lambda\left(\boldsymbol{q}^+\right)\right|\right) \tag{48}$$

or a Roe flux [16]:

$$\hat{M} = \left|\int_0^1 M\left(\boldsymbol{q}^- + z\left(\boldsymbol{q}^+ - \boldsymbol{q}^-\right)\right) dz\right| \tag{49}$$

or a simplified Osher–Solomon flux [15]:

$$\hat{M} = \int_0^1 \left|M\left(\boldsymbol{q}^- + z\left(\boldsymbol{q}^+ - \boldsymbol{q}^-\right)\right)\right| dz \tag{50}$$

$\hat{B}$ takes the following form:

$$\hat{B} = \int_0^1 B\left(\boldsymbol{q}^- + z\left(\boldsymbol{q}^+ - \boldsymbol{q}^-\right)\right) dz \tag{51}$$

It was found that the Osher-Solomon flux would often produce slightly less diffusive results, but that it was more computationally expensive, and also had a greater tendency to introduce numerical artifacts.

0.4.4 Time Step and Boundary Conditions

Let Λ_i^n be the set of eigenvalues of the HPR system evaluated at $\boldsymbol{Q}_i^n$. $C_{cfl} < 1$ is a constant (usually taken to be 0.9, unless the problem being simulated is particularly demanding, requiring a lower value). A semi-analytic form for Λ is given in Section B.2. The eigenvalues determine the speed of propagation of information in the solution to the Riemann Problem at the cell interfaces, and the time step is chosen to ensure that the characteristics do not enter into other cells between t_n and t_{n+1}:

$$\Delta t_n = \frac{C_{cfl} \cdot \Delta x}{\max_i \left|\Lambda_i^n\right|} \tag{52}$$

Transmissive boundary conditions (allowing material and heat to pass through) are implemented by setting the state variables in the boundary cells to the same value as their non-boundary neighbors. Reflective boundary conditions are implemented in the same way, except that the directions of the velocity and thermal impulse vectors in the boundary cells are reversed.

Chapter 1

Objective 1: Extending the GPR Model

1.1 Equations of State

1.1.1 Mie-Gruneisen Models

It is required to specify the microscale energy E_1 appearing in (6). In this study, several different possible choices for E_1 are put into the same framework by expressing them in the following Mie-Gruneisen form:

$$E_1(\rho, p) = e(\rho, p) = e_{ref}(\rho) + \frac{p - p_{ref}(\rho)}{\rho \Gamma(\rho)} \tag{1.1a}$$

$$T = T_{ref} + \frac{e - e_{ref}}{c_v} = T_{ref} + \frac{p - p_{ref}(\rho)}{c_V \rho \Gamma(\rho)} \tag{1.1b}$$

The forms taken by e_{ref}, p_{ref}, Γ for various different instances of this class are given in Table 1.1 on page 15. The first five entries in the table are standard results. The sixth is derived thus. The Godunov-Romenski hyperelastic EOS is given by:

$$E(\rho, S, A) = \frac{c_0^2}{2\alpha^2}\left(\left|A^T A\right|^{\alpha/2} - 1\right)^2 + c_v T_0 \left|A^T A\right|^{\gamma/2}\left(e^{S/c_v} - 1\right) + \frac{b_0^2}{4}\left|A^T A\right|^{\beta/2}\left\|\operatorname{dev}\left(A^T A\right)\right\|^2 \tag{1.2}$$

Using the relation $\det(A) = \frac{\rho}{\rho_0}$, this can be thought of as taking the form:

$$E_1(\rho, s) + \frac{c_s(\rho)^2}{4}\left\|\operatorname{dev}(G)\right\|_F^2 \tag{1.3}$$

where $c_s = b_0\left(\frac{\rho}{\rho_0}\right)^\beta$. Considering only the microscale energy component, note that we have:

$$p = \rho^2 \frac{\partial E_1}{\partial \rho} = \rho\left(\frac{c_0^2}{\alpha}\left(\left(\frac{\rho}{\rho_0}\right)^\alpha - 1\right)\left(\frac{\rho}{\rho_0}\right)^\alpha + \gamma c_v T_0 \left(\frac{\rho}{\rho_0}\right)^\gamma \left(e^{S/c_v} - 1\right)\right) \tag{1.4}$$

Therefore:

$$E_1 - \frac{c_0^2}{2\alpha^2}\left(\left(\frac{\rho}{\rho_0}\right)^\alpha - 1\right)^2 = \frac{p}{\gamma\rho} - \frac{c_0^2}{\gamma\alpha}\left(\left(\frac{\rho}{\rho_0}\right)^\alpha - 1\right)\left(\frac{\rho}{\rho_0}\right)^\alpha \tag{1.5}$$

Thus E_1 can be put in Mie-Gruneisen form:

$$E_1 = \frac{p - \frac{c_0^2 \rho}{\alpha}\left(\left(\frac{\rho}{\rho_0}\right)^{\alpha} - 1\right)\left(\frac{\rho}{\rho_0}\right)^{\alpha}}{\gamma \rho} + \frac{c_0^2}{2\alpha^2}\left(\left(\frac{\rho}{\rho_0}\right)^{\alpha} - 1\right)^2 \tag{1.6}$$

The following quantities are required when computing the eigenstructure of the system:

$$\frac{\partial T}{\partial \rho} = \frac{1}{c_v}\left(\frac{\partial e}{\partial \rho} - e_{ref}^{'}\left(\rho\right)\right) \tag{1.7a}$$

$$\frac{\partial T}{\partial p} = \frac{1}{c_v}\frac{\partial e}{\partial p} \tag{1.7b}$$

$$\frac{\partial e}{\partial \rho} = e_{ref}^{'}\left(\rho\right) - \frac{p_{ref}^{'}\left(\rho\right)\rho\Gamma\left(\rho\right) + \left(\Gamma\left(\rho\right) + \rho\Gamma^{'}\left(\rho\right)\right)\left(p - p_{ref}\left(\rho\right)\right)}{\left(\rho\Gamma\left(\rho\right)\right)^2} \tag{1.8a}$$

$$\frac{\partial e}{\partial p} = \frac{1}{\rho\Gamma\left(\rho\right)} \tag{1.8b}$$

The relevant functions for each of the EOSs used in this study are given in Table 1.2 on page 16.

Although this is a versatile class of equations of state - and it is fit for the purposes that the model is put to here - it should be noted that many other choices are available.

1.1.2 Variable Transverse Perturbation Speed

Taking (1.1a) and using the fact that $p = \rho^2 e_\rho$, we have:

$$e_\rho - \frac{\Gamma}{\rho} e = \frac{p_{ref}}{\rho^2} - \frac{\Gamma}{\rho} e_{ref} \tag{1.9}$$

The solutions to this equation for different forms of Γ, p_{ref}, e_{ref} take the form below, where f is an arbitrary function of s, g depends on the form of Γ, and $\hat{e}$ is a particular solution of the equation (which will be equal to e_{ref} if $p_{ref} = \rho^2 \frac{\partial e_{ref}}{\partial \rho}$).

$$e = f\left(s\right) g\left(\rho\right) + \hat{e}\left(\rho\right) \tag{1.10}$$

Equation of State	$p_{ref}(\rho)$	$e_{ref}(\rho)$	$\Gamma(\rho)$	T_{ref}
Ideal Gas	0	0	$\Gamma_0 (= \gamma - 1)$	0
Stiffened Gas	$-p_\infty$	$\frac{p_\infty}{\rho}$	$\Gamma_0 (= \gamma - 1)$	0
Shock Mie-Gruneisen	$\frac{c_0^2\left(\frac{1}{\rho_0}-\frac{1}{\rho}\right)}{\left(\frac{1}{\rho_0}-s\left(\frac{1}{\rho_0}-\frac{1}{\rho}\right)\right)^2}$	$\frac{p_{ref}}{2}\left(\frac{1}{\rho_0}-\frac{1}{\rho}\right)$	$\Gamma_0 \frac{\rho_0}{\rho}$	0
JWL	$Ae^{-\frac{R_1\rho_0}{\rho}} + Be^{-\frac{R_2\rho_0}{\rho}}$	$\frac{A}{\rho_0 R_1}e^{-\frac{R_1\rho_0}{\rho}} + \frac{B}{\rho_0 R_2}e^{-\frac{R_2\rho_0}{\rho}}$	Γ_0	0
Cochran-Chan	$A\left(\frac{\rho}{\rho_0}\right)^{\epsilon_1} - B\left(\frac{\rho}{\rho_0}\right)^{\epsilon_2}$	$\frac{A}{\rho_0(\epsilon_1-1)}\left(\left(\frac{\rho}{\rho_0}\right)^{\epsilon_1-1}-1\right) - \frac{B}{\rho_0(\epsilon_1-1)}\left(\left(\frac{\rho}{\rho_0}\right)^{\epsilon_2-1}-1\right)$	Γ_0	0
Godunov-Romenski	$\frac{c_0^2\rho}{\alpha}\left(\left(\frac{\rho}{\rho_0}\right)^{\alpha}-1\right)\left(\frac{\rho}{\rho_0}\right)^{\alpha}$	$\frac{c_0^2}{2\alpha^2}\left(\left(\frac{\rho}{\rho_0}\right)^{\alpha}-1\right)^2$	$\Gamma_0 (= \gamma)$	T_0

Table 1.1: e_{ref}, p_{ref}, Γ for different kinds of Mie-Gruneisen equations of state

Equation of State	$p'_{ref}(\rho)$	$e'_{ref}(\rho)$	$\Gamma'(\rho)$
Ideal Gas	0	0	0
Stiffened Gas	0	$-\frac{p_\infty}{\rho^2}$	0
Shock Mie-Gruneisen	$\frac{c_0^2\rho_0^2(s(\rho_0-\rho)-\rho)}{(s(\rho-\rho_0)-\rho)^3}$	$\frac{1}{2}\left(p'_{ref}\left(\frac{1}{\rho_0}-\frac{1}{\rho}\right)+\frac{p_{ref}}{\rho^2}\right)$	$-\Gamma_0\frac{\rho_0}{\rho^2}$
JWL	$\frac{AR_1\rho_0}{\rho^2}e^{-\frac{R_1\rho_0}{\rho}}+\frac{BR_2\rho_0}{\rho^2}e^{-\frac{R_2\rho_0}{\rho}}$	$\frac{A}{\rho^2}e^{-\frac{R_1\rho_0}{\rho}}+\frac{B}{\rho^2}e^{-\frac{R_2\rho_0}{\rho}}$	0
Cochran-Chan			0
Godunov-Romenski			0

Table 1.2: $e'_{ref}, p'_{ref}, \Gamma'$ for different kinds of Mie-Gruneisen equations of state

We have:

$$p = \rho^2 e_\rho = \rho^2 \left(f\left(s\right) g^{'}\left(\rho\right) + \hat{e}^{'}\left(\rho\right) \right) \tag{1.11}$$

Thus:

$$\frac{\frac{p}{\rho^2} - \hat{e}^{'}\left(\rho\right)}{g^{'}\left(\rho\right)} = f\left(s\right) = \frac{e - \hat{e}\left(\rho\right)}{g\left(\rho\right)} \tag{1.12}$$

Therefore:

$$E_1\left(\rho, p\right) = e\left(\rho, p\right) = \hat{e}\left(\rho\right) + \frac{g\left(\rho\right)}{g^{'}\left(\rho\right)} \left(\frac{p}{\rho^2} - \hat{e}^{'}\left(\rho\right) \right) \tag{1.13}$$

We now add another term to the energy, giving it the following form:

$$E\left(\rho, p\right) = e\left(\rho, p\right) = f\left(s\right) g\left(\rho\right) + \hat{e}\left(\rho\right) + B\left(\rho\right) h\left(A\right) \tag{1.14}$$

We then have:

$$p = \rho^2 \left(f\left(s\right) g^{'}\left(\rho\right) + \hat{e}^{'}\left(\rho\right) + B^{'}\left(\rho\right) h\left(A\right) \right) \tag{1.15}$$

Thus:

$$\frac{\frac{p}{\rho^2} - \hat{e}^{'}\left(\rho\right) - B^{'}\left(\rho\right) h\left(A\right)}{g^{'}\left(\rho\right)} = f\left(s\right) = \frac{e - \hat{e}\left(\rho\right) - B\left(\rho\right) h\left(A\right)}{g\left(\rho\right)} \tag{1.16}$$

Therefore:

$$e = \frac{g\left(\rho\right)}{g^{'}\left(\rho\right)} \left(\frac{p}{\rho^2} - \hat{e}^{'}\left(\rho\right) - B^{'}\left(\rho\right) h\left(A\right) \right) + \hat{e}\left(\rho\right) + B\left(\rho\right) h\left(A\right) \tag{1.17}$$

Noting that $\frac{g(\rho)}{g^{'}(\rho)} = \frac{\rho}{\Gamma(\rho)}$, this can be expressed as:

$$E\left(\rho, p\right) = e\left(\rho, p\right) = E_1\left(\rho, p\right) + \left(B\left(\rho\right) - \frac{\rho}{\Gamma\left(\rho\right)} B^{'}\left(\rho\right) \right) h\left(A\right) \tag{1.18}$$

If the EOS comprises a microscale energy component of Mie-Gruneisen type, and a mesoscale energy component with speed of transverse vibrations dependent upon ρ, then this provides a method to recover the EOS in terms of ρ and p (by substituting $B(\rho) = \frac{c_s^2(\rho)}{4}$ and $h(A) = \left\|\operatorname{dev}\left(A^T A\right)\right\|_F^2$).

1.2 Multiphase Reactive Materials

1.2.1 Extended Model

The GPR model is extended to account for multiphase materials thus:

$$\frac{\partial (z\rho_1)}{\partial t} + \frac{\partial (z\rho_1 v_k)}{\partial x_k} = 0 \tag{1.19a}$$

$$\frac{\partial (\rho v_i)}{\partial t} + \frac{\partial(\rho v_i v_k + p\delta_{ik} - \sigma_{ik})}{\partial x_k} = 0 \tag{1.19b}$$

$$\frac{\partial A_{ij}}{\partial t} + \frac{\partial (A_{ik} v_k)}{\partial x_j} + v_k \left(\frac{\partial A_{ij}}{\partial x_k} - \frac{\partial A_{ik}}{\partial x_j}\right) = -\frac{\psi_{ij}}{\theta_1(\tau_1)} \tag{1.19c}$$

$$\frac{\partial (\rho J_i)}{\partial t} + \frac{\partial (\rho J_i v_k + T\delta_{ik})}{\partial x_k} = -\frac{\rho H_i}{\theta_2(\tau_2)} \tag{1.19d}$$

$$\frac{\partial (\rho E)}{\partial t} + \frac{\partial (\rho E v_k + (p\delta_{ik} - \sigma_{ik}) v_i + q_k)}{\partial x_k} = 0 \tag{1.19e}$$

$$\frac{\partial ((1-z)\rho_2)}{\partial t} + \frac{\partial ((1-z)\rho_2 v_k)}{\partial x_k} = 0 \tag{1.19f}$$

$$\frac{\partial (z\rho)}{\partial t} + \frac{\partial (z\rho v_k)}{\partial x_k} = 0 \tag{1.19g}$$

$$\frac{\partial ((1-z)\rho_2\lambda)}{\partial t} + \frac{\partial ((1-z)\rho_2\lambda v_k)}{\partial x_k} = (1-z)\rho_2 K \tag{1.19h}$$

$$\rho = z\rho_1 + (1-z)\rho_2 \tag{1.20a}$$

$$e_i = e_i^0 + \frac{p - p_i^0}{\rho_i \Gamma_i} \tag{1.20b}$$

1.2.2 Mixture Rules

1.2.3 Reaction Rate Laws

1.3 Numerical Results

1.3.1 1D Tests

1.3.1.1 Copper-Detonation Products Shock Tube

1.3.1.2 Shock Initiation of LX-17

1.3.1.3 Nitromethane Ignition Pop-Plot

1.3.1.4 Nitromethane Steady ZND Detonation

1.3.1.5 Three-Component Inert Shock Wave

1.3.1.6 Three-Component Rate Stick

1.3.2 2D Tests

1.3.2.1 Confined Ideal-Gas Rate Stick

1.3.2.2 Confined JWL Rate Stick

1.3.2.3 Shock-Induced Void Collapse in Nitromethane

Chapter 2

Objective 2: Improved Numerical Methods

2.1 Extending the Montecinos-Balsara ADER Method

The material in this section is published in [25, 26].

[36] have proposed a new, more efficient class of basis polynomials. While the method was given for conservative, one-dimensional systems in the original paper, it is extended here to general non-conservative, multidimensional systems.

Take a non-homogeneous, non-conservative, hyperbolic system of the form:

$$\frac{\partial \boldsymbol{Q}}{\partial t} + \boldsymbol{\nabla} \cdot \overrightarrow{\boldsymbol{F}}\left(\boldsymbol{Q}\right) + \overrightarrow{\boldsymbol{B}}\left(\boldsymbol{Q}\right) \cdot \nabla \boldsymbol{Q} = \boldsymbol{S}\left(\boldsymbol{Q}\right) \tag{2.1}$$

where $\boldsymbol{Q}$ is the vector of conserved variables, $\overrightarrow{\boldsymbol{F}} = \left(\boldsymbol{F_1}, \boldsymbol{F_2}, \boldsymbol{F_3}\right)$ and $\overrightarrow{\boldsymbol{B}} = \left(B_1, B_2, B_3\right)$ are respectively the conservative nonlinear fluxes and matrices corresponding to the purely non-conservative components of the system, and $\boldsymbol{S}\left(\boldsymbol{Q}\right)$ is the algebraic source vector.

Define spatial variables $x^{(1)}, x^{(2)}, x^{(3)}$. Take the space-time cell $C = \left[x_{i_1}^{(1)}, x_{i_1+1}^{(1)}\right] \times \left[x_{i_2}^{(2)}, x_{i_2+1}^{(2)}\right] \times \left[x_{i_3}^{(3)}, x_{i_3+1}^{(3)}\right] \times \left[t_n, t_{n+1}\right]$. Define the scaled spatial and temporal variables:

$$\chi^{(k)} = \frac{x^{(k)} - x_{i_k}^{(k)}}{x_{i_k+1}^{(k)} - x_{i_k}^{(k)}} \tag{2.2a}$$

$$\tau = \frac{t - t_n}{t_{n+1} - t_n} \tag{2.2b}$$

Thus, C becomes:

$$\left(\chi^{(1)}, \chi^{(2)}, \chi^{(3)}, \tau\right) \in [0, 1]^4 \tag{2.3}$$

By rescaling $\vec{\boldsymbol{F}}, \vec{\boldsymbol{B}}, \boldsymbol{S}$ by the appropriate constant factors, and defining $\tilde{\nabla} = \left(\partial_{\chi^{(1)}}, \partial_{\chi^{(2)}}, \partial_{\chi^{(3)}}\right)$, within C equation (2.1) becomes:

$$\frac{\partial \boldsymbol{Q}}{\partial \tau} + \tilde{\boldsymbol{\nabla}} \cdot \vec{\boldsymbol{F}}\left(\boldsymbol{Q}\right) + \vec{\boldsymbol{B}}\left(\boldsymbol{Q}\right) \cdot \tilde{\nabla}\boldsymbol{Q} = \boldsymbol{S}\left(\boldsymbol{Q}\right) \tag{2.4}$$

A basis $\{\psi_0, ..., \psi_N\}$ of P_N and inner product $\langle \cdot, \cdot \rangle$ are now required to produce a polynomial reconstruction of $\boldsymbol{Q}$ within C. Traditionally, this basis has been chosen to be either nodal ($\psi_i\left(\alpha_j\right) = \delta_{ij}$ where $\{\alpha_0, \ldots, \alpha_N\}$ are a set of nodes, e.g. the Gauss-Legendre abscissae - see [10]), or modal (e.g. the Legendre polynomials - see [2]).

[36] take the following approach. $\langle \cdot, \cdot \rangle$ is taken to be the usual integral product on $[0, 1]$. Supposing that $N = 2n+1$ for some $n \in \mathbb{N}$, Gauss-Legendre nodes $\{\alpha_0, \ldots, \alpha_n\}$ are taken. The basis $\Psi = \{\psi_0, ..., \psi_N\} \subset P_N$ is taken with the following properties for $i = 0, \ldots, n$:

$$\begin{cases} \psi_i\left(\alpha_j\right) = \delta_{ij} & \psi_i'\left(\alpha_j\right) = 0 \\ \psi_{n+1+i}\left(\alpha_j\right) = 0 & \psi_{n+1+i}'\left(\alpha_j\right) = \delta_{ij} \end{cases} \tag{2.5}$$

Define the following subsets:

$$\Psi^0 = \{\psi_i : 0 \leq i \leq n\} \tag{2.6a}$$
$$\Psi^1 = \{\psi_i : n+1 \leq i \leq 2n+1\} \tag{2.6b}$$

The WENO method (as used in [18]) produces an order-N polynomial reconstruction $w\left(\chi^{(1)}, \chi^{(2)}, \chi^{(3)}\right)$ of the data at time t_n in $\left[x_{i_1}^{(1)}, x_{i_1+1}^{(1)}\right] \times \left[x_{i_2}^{(2)}, x_{i_2+1}^{(2)}\right] \times \left[x_{i_3}^{(3)}, x_{i_3+1}^{(3)}\right]$. It is used as initial data in the problem of finding the Galerkin predictor. Taking representation $w = w_{abc}\psi_a\left(\chi^{(1)}\right)\psi_b\left(\chi^{(2)}\right)\psi_c\left(\chi^{(3)}\right)$ we have for $0 \leq i, j, k \leq n$:

$$w_{ijk} = w\left(\alpha_i, \alpha_j, \alpha_k\right) \tag{2.7a}$$
$$w_{(n+i+1)jk} = \partial_{\chi^{(1)}} w\left(\alpha_i, \alpha_j, \alpha_k\right) \tag{2.7b}$$
$$w_{i(n+j+1)k} = \partial_{\chi^{(2)}} w\left(\alpha_i, \alpha_j, \alpha_k\right) \tag{2.7c}$$
$$w_{ij(n+k+1)} = \partial_{\chi^{(3)}} w\left(\alpha_i, \alpha_j, \alpha_k\right) \tag{2.7d}$$

Take the following temporal nodes, where $\tau_1, \ldots, \tau_N$ are the usual Legendre-Gauss nodes on $[0, 1]$ and $\tau_0 = 0$ or $\tau_0 = 1$ if we are performing a Continuous Galerkin / Discontinuous

Galerkin reconstruction, respectively:

$$\{\tau_0, \ldots, \tau_N\} \tag{2.8}$$

Define $\Phi = \{\phi_0, ..., \phi_N\} \subset P_N$ to be the set of Lagrange interpolating polynomials on the temporal nodes. We now define the spatio-temporal polynomial basis $\Theta = \Phi \otimes \Psi \otimes \Psi \otimes \Psi = \{\theta_\beta\}$ for $0 \leq \beta \leq (N+1)^4 - 1$. Define subsets $\Theta^{\iota\xi\kappa} = \Phi \otimes \Psi^\iota \otimes \Psi^\xi \otimes \Psi^\kappa = \left\{\theta_\mu^{\iota\xi\kappa}\right\}$ where $\iota, \xi, \kappa \in \{0, 1\}$ for $0 \leq \mu \leq (N+1)(n+1)^3 - 1$.

Denoting the Galerkin predictor by $\boldsymbol{q}$, take the following set of approximations:

$$\boldsymbol{Q} \approx \theta_\beta \boldsymbol{q}_\beta = \theta_\mu^{\iota\xi\kappa} \boldsymbol{q}_\mu^{\iota\xi\kappa} \tag{2.9a}$$
$$\overrightarrow{\boldsymbol{F}}(\boldsymbol{Q}) \approx \theta_\beta \overrightarrow{\boldsymbol{F}}_\beta = \theta_\mu^{\iota\xi\kappa} \overrightarrow{\boldsymbol{F}}_\mu^{\iota\xi\kappa} \tag{2.9b}$$
$$\overrightarrow{\boldsymbol{B}}(\boldsymbol{Q}) \cdot \tilde{\nabla} \boldsymbol{Q} \approx \theta_\beta \boldsymbol{B}_\beta = \theta_\mu^{\iota\xi\kappa} \boldsymbol{B}_\mu^{\iota\xi\kappa} \tag{2.9c}$$
$$\boldsymbol{S}(\boldsymbol{Q}) \approx \theta_\beta \boldsymbol{S}_\beta = \theta_\mu^{\iota\xi\kappa} \boldsymbol{S}_\mu^{\iota\xi\kappa} \tag{2.9d}$$

for some coefficients $\boldsymbol{q}_\beta, \overrightarrow{\boldsymbol{F}}_\beta, \boldsymbol{B}_\beta, \boldsymbol{S}_\beta$. The *nodal basis representation* is used for the coefficients of Θ^{000}:

$$\overrightarrow{\boldsymbol{F}}_\mu^{000} = \overrightarrow{\boldsymbol{F}}\left(\boldsymbol{q}_\mu^{000}\right) \tag{2.10a}$$
$$\boldsymbol{B}_\mu^{000} = B_1\left(\boldsymbol{q}_\mu^{000}\right) \boldsymbol{q}_\mu^{100} + B_2\left(\boldsymbol{q}_\mu^{000}\right) \boldsymbol{q}_\mu^{010} + B_3\left(\boldsymbol{q}_\mu^{000}\right) \boldsymbol{q}_\mu^{001} \tag{2.10b}$$
$$\boldsymbol{S}_\mu^{000} = \boldsymbol{S}\left(\boldsymbol{q}_\mu^{000}\right) \tag{2.10c}$$

In general, we have:

$$\overrightarrow{\boldsymbol{F}}_\mu^{\iota\xi\kappa} = \partial_\chi^\iota \partial_\upsilon^\xi \partial_\zeta^\kappa \left(\overrightarrow{\boldsymbol{F}}(\boldsymbol{Q})\right) \tag{2.11a}$$
$$\boldsymbol{B}_\mu^{\iota\xi\kappa} = \partial_\chi^\iota \partial_\upsilon^\xi \partial_\zeta^\kappa \left(\overrightarrow{\boldsymbol{B}}(\boldsymbol{Q}) \cdot \tilde{\nabla} \boldsymbol{Q}\right) \tag{2.11b}$$
$$\boldsymbol{S}_\mu^{\iota\xi\kappa} = \partial_\chi^\iota \partial_\upsilon^\xi \partial_\zeta^\kappa \left(\boldsymbol{S}(\boldsymbol{Q})\right) \tag{2.11c}$$

where the right-hand-side is evaluated at the nodal point corresponding to μ. The full expressions are omitted here for brevity's sake, but note that for a one-dimensional system:

$$\boldsymbol{F}_{1\mu}^{100} = \frac{\partial \boldsymbol{F}\left(\boldsymbol{q}_\mu^{000}\right)}{\partial \boldsymbol{Q}} \cdot \boldsymbol{q}_\mu^{100} \tag{2.12a}$$

$$\begin{aligned}\boldsymbol{B}_\mu^{100} = &\left(\frac{\partial B_1\left(\boldsymbol{q}_\mu^{000}\right)}{\partial \boldsymbol{Q}} \cdot \boldsymbol{q}_\mu^{100}\right) \cdot \boldsymbol{q}_\mu^{100} \\ &+ B_1\left(\boldsymbol{q}_\mu^{000}\right) \cdot \left(\frac{\partial^2 \theta_\kappa^{000}\left(\chi_\mu, \tau_\mu\right)}{\partial \chi^2} \boldsymbol{q}_\mu^{000} + \frac{\partial^2 \theta_\kappa^{100}\left(\chi_\mu, \tau_\mu\right)}{\partial \chi^2} \boldsymbol{q}_\mu^{100}\right)\end{aligned} \tag{2.12b}$$

$$\boldsymbol{S}_\mu^{100} = \frac{\partial \boldsymbol{S}\left(\boldsymbol{q}_\mu^{000}\right)}{\partial \boldsymbol{Q}} \cdot \boldsymbol{q}_\mu^{100} \tag{2.12c}$$

where χ_μ, τ_μ are the spatial and temporal coordinates where $\theta_\mu^{100} = 0$ and $\partial_\chi \theta_\mu^{100} = 1$. Note that $\frac{\partial B_1}{\partial \boldsymbol{Q}}$ is a rank 3 tensor.

Consider functions f, g of the following form:

$$f\left(\tau, \chi^{(1)}, \chi^{(2)}, \chi^{(3)}\right) = f_\tau(\tau)\, f_1\left(\chi^{(1)}\right) f_2\left(\chi^{(2)}\right) f_3\left(\chi^{(3)}\right) \tag{2.13a}$$

$$g\left(\tau, \chi^{(1)}, \chi^{(2)}, \chi^{(3)}\right) = g_\tau(\tau)\, g_1\left(\chi^{(1)}\right) g_2\left(\chi^{(2)}\right) g_3\left(\chi^{(3)}\right) \tag{2.13b}$$

Define the following integral operators:

$$[f, g]^t = f_\tau(t)\, g_\tau(t) \langle f_1, g_1\rangle \langle f_2, g_2\rangle \langle f_3, g_3\rangle \tag{2.14a}$$

$$\{f, g\} = \langle f_\tau, g_\tau\rangle \langle f_1, g_1\rangle \langle f_2, g_2\rangle \langle f_3, g_3\rangle \tag{2.14b}$$

Multiplying (2.9b) by test function θ_α, using the polynomial approximations for $\boldsymbol{Q}, \vec{\boldsymbol{F}}, \vec{\boldsymbol{B}}, \boldsymbol{S}$, and integrating over space and time gives:

$$\left\{\theta_\alpha, \frac{\partial \theta_\beta}{\partial \tau}\right\} \boldsymbol{q}_\beta = \{\theta_\alpha, \theta_\beta\}\left(\boldsymbol{S}_\beta - \boldsymbol{B}_\beta\right) - \left\{\theta_\alpha, \frac{\partial \theta_\beta}{\partial \chi^{(k)}}\right\} \boldsymbol{F}_{k\beta} \tag{2.15}$$

2.1.1 The Discontinuous Galerkin Method

This method of computing the Galerkin predictor allows solutions to be discontinuous at temporal cell boundaries, and is also suitable for stiff source terms. Integrating (2.15) by parts in time gives:

$$\left([\theta_\alpha,\theta_\beta]^1-\left\{\frac{\partial\theta_\alpha}{\partial\tau},\theta_\beta\right\}\right)\boldsymbol{q}_\beta=[\theta_\alpha,\boldsymbol{w}]^0+\{\theta_\alpha,\theta_\beta\}\left(\boldsymbol{S}_\beta-\boldsymbol{B}_\beta\right)-\left\{\theta_\alpha,\frac{\partial\theta_\beta}{\partial\chi^{(k)}}\right\}\boldsymbol{F}_{k\beta} \tag{2.16}$$

where $\boldsymbol{w}$ is the reconstruction obtained at the start of the time step with the WENO method. Take the following ordering:

$$\theta_{(N+1)^3h+(N+1)^2i+(N+1)j+k}\left(\tau,\chi,\upsilon,\zeta\right)=\phi_h\left(\tau\right)\psi_i\left(\chi\right)\psi_j\left(\upsilon\right)\psi_k\left(\zeta\right) \tag{2.17}$$

where $0\leq h,i,j,k\leq N$. Thus, define the following:

$$U_{\alpha\beta}=[\theta_\alpha,\theta_\beta]^1-\left\{\frac{\partial\theta_\alpha}{\partial\tau},\theta_\beta\right\}=\left(R^1-M^{\tau,1}\right)\otimes\left(M^\chi\right)^3 \tag{2.18a}$$

$$V^k_{\alpha\beta}=\left\{\theta_\alpha,\frac{\partial\theta_\beta}{\partial\chi^{(k)}}\right\}=M^\tau\otimes\left(M^\chi\right)^{k-1}\otimes M^{\chi,1}\otimes\left(M^\chi\right)^{3-k} \tag{2.18b}$$

$$\boldsymbol{W}_\alpha=[\theta_\alpha,\Psi_\gamma]^0\,\boldsymbol{w}_\gamma=R^0\otimes\left(M^\chi\right)^3 \tag{2.18c}$$

$$Z_{\alpha\beta}=\{\theta_\alpha,\theta_\beta\}=M^\tau\otimes\left(M^\chi\right)^3 \tag{2.18d}$$

where $\{\Psi_\gamma\}=\Psi\otimes\Psi\otimes\Psi$ and:

$$\begin{cases}M^\tau_{ij}=\langle\phi_i,\phi_j\rangle & M^{\tau,1}_{ij}=\left\langle\phi'_i,\phi_j\right\rangle\\ M^\chi_{ij}=\langle\psi_i,\psi_j\rangle & M^{\chi,1}_{ij}=\left\langle\psi_i,\psi'_j\right\rangle\\ R^1_{ij}=\phi_i\left(1\right)\phi_j\left(1\right) & \boldsymbol{R^0_i}=\phi_i\left(0\right)\end{cases} \tag{2.19}$$

Thus:

$$U_{\alpha\beta}\boldsymbol{q}_\beta=\boldsymbol{W}_\alpha+Z_{\alpha\beta}\left(\boldsymbol{S}_\beta-\boldsymbol{B}_\beta\right)-V^{(k)}_{\alpha\beta}\boldsymbol{F}_{k\beta} \tag{2.20}$$

Take the definitions:

$$\begin{cases}D &=\left(M^\chi\right)^{-1}M^{\chi,1}\\ E &=\left(R^1-M^{\tau,1}\right)\end{cases} \tag{2.21}$$

Noting that $E\mathbf{1}=\boldsymbol{R^0}$, we have, by inversion of U:

$$\begin{aligned}\boldsymbol{q} = &\left(\mathbf{1} \otimes I^3\right) \boldsymbol{w} + \left(E^{-1} M^\tau \otimes I^3\right) (\boldsymbol{S} - \boldsymbol{B}) \\ &- \left(E^{-1} M^\tau \otimes I^{k-1} \otimes D \otimes I^{3-k}\right) \boldsymbol{F}_k\end{aligned} \tag{2.22}$$

Thus, we have:

$$\begin{aligned}\boldsymbol{q}_{hijk} = &\boldsymbol{w}_{ijk} + \left(E^{-1} M^\tau\right)_{hm} (\boldsymbol{S}_{mijk} - \boldsymbol{B}_{mijk}) \\ &- \left(E^{-1} M^\tau\right)_{hm} \left(D_{in} (\boldsymbol{F}_1)_{mnjk} + D_{jn} (\boldsymbol{F}_2)_{mink} + D_{kn} (\boldsymbol{F}_3)_{mijn}\right)\end{aligned} \tag{2.23}$$

Note then that $\boldsymbol{q}^{\iota\xi\kappa}$ is a function of $\boldsymbol{S}^{\iota\xi\kappa}, \boldsymbol{B}^{\iota\xi\kappa}, \overrightarrow{\boldsymbol{F}}$:

$$\boldsymbol{q}^{\iota\xi\kappa} = \mathcal{F}\left(\boldsymbol{S}^{\iota\xi\kappa}\right) + \mathcal{F}\left(\boldsymbol{B}^{\iota\xi\kappa}\right) + \mathcal{G}_{\iota\xi\kappa}\left(\overrightarrow{\boldsymbol{F}}^{000}, \ldots, \overrightarrow{\boldsymbol{F}}^{111}\right) \tag{2.24}$$

where $\mathcal{F}, \mathcal{G}_{\iota\xi\kappa}$ are linear functions. Note in turn that, by (2.11c):

$$\boldsymbol{S}^{\iota\xi\kappa} = \mathcal{H}\left(\bigcup_{(0,0,0) \leq (a,b,c) \leq (\iota,\xi,\kappa)} \boldsymbol{q}^{abc}\right) \tag{2.25}$$

where $\mathcal{H}$ is a nonlinear function.

In the case of stiff source terms, the following Picard iteration procedure can be used to solve (2.23), as adapted from [36]:

$$\begin{aligned}\left(\boldsymbol{q}^{\iota\xi\kappa}\right)_{m+1} = &\mathcal{F}\left(\mathcal{H}\left(\left(\boldsymbol{q}^{\iota\xi\kappa}\right)_{m+1} \cup \bigcup_{\substack{(0,0,0) \leq (a,b,c) \leq (\iota,\xi,\kappa) \\ (a,b,c) \neq (\iota,\xi,\kappa)}} \left(\boldsymbol{q}^{abc}\right)_m\right)\right) \\ &+ \mathcal{F}\left(\left(\boldsymbol{B}^{\iota\xi\kappa}\right)_m\right) + \mathcal{G}_{\iota\xi\kappa}\left(\left(\overrightarrow{\boldsymbol{F}}^{000}\right)_m, \ldots, \left(\overrightarrow{\boldsymbol{F}}^{111}\right)_m\right)\end{aligned} \tag{2.26}$$

2.1.2 The Continuous Galerkin Method

This method of computing the Galerkin predictor is not suitable for stiff source terms, but is less computationally expensive and ensures continuity across temporal cell boundaries. The first $N+1$ elements of $\boldsymbol{q}$ are fixed by imposing the following condition:

$$\boldsymbol{q}(\chi, 0) = \boldsymbol{w}(\chi) \tag{2.27}$$

For $\boldsymbol{v} \in \mathbb{R}^{(N+1)^2}$ and $X \in M_{(N+1)^2,(N+1)^2}(\mathbb{R})$, let $\boldsymbol{v} = (\boldsymbol{v}^{\mathbf{0}}, \boldsymbol{v}^{\mathbf{1}})$ and $X = \begin{pmatrix} X^{00} & X^{01} \\ X^{10} & X^{11} \end{pmatrix}$ where $\boldsymbol{v}^{\mathbf{0}}, X^{00}$ are the components relating solely to the first $N+1$ components of $\boldsymbol{v}$. We only need to find the latter components of $\boldsymbol{q}$, and thus, from (2.15), we have:

$$\begin{aligned}\left\{\theta_\alpha, \frac{\partial \theta_\beta}{\partial \tau}\right\}^{11} \boldsymbol{q}_\beta^1 = \{\theta_\alpha, \theta_\beta\}^{11} \left(\boldsymbol{S}_\beta^1 - \boldsymbol{B}_\beta^1\right) - \left\{\theta_\alpha, \frac{\partial \theta_\beta}{\partial \chi^{(k)}}\right\}^{11} \boldsymbol{F}_{k\beta}^{\,1} \\ + \{\theta_\alpha, \theta_\beta\}^{10} \left(\boldsymbol{S}_\beta^0 - \boldsymbol{B}_\beta^0\right) - \left\{\theta_\alpha, \frac{\partial \theta_\beta}{\partial \chi^{(k)}}\right\}^{10} \boldsymbol{F}_{k\beta}^{\,0}\end{aligned} \tag{2.28}$$

Define the following:

$$U_{\alpha\beta} = \left\{\theta_\alpha, \frac{\partial \theta_\beta}{\partial \tau}\right\}^{11} \tag{2.29a}$$

$$V_{\alpha\beta}^k = \left\{\theta_\alpha, \frac{\partial \theta_\beta}{\partial \chi^{(k)}}\right\}^{11} \tag{2.29b}$$

$$\boldsymbol{W}_\alpha = \{\theta_\alpha, \theta_\beta\}^{10} \left(\boldsymbol{S}_\beta - \boldsymbol{B}_\beta\right)^0 - \left\{\theta_\alpha, \frac{\partial \theta_\beta}{\partial \chi^{(k)}}\right\}^{10} \boldsymbol{F}_{k\beta}^{\,0} \tag{2.29c}$$

$$Z_{\alpha\beta} = \{\theta_\alpha, \theta_\beta\}^{11} \tag{2.29d}$$

Thus:

$$U_{\alpha\beta} \boldsymbol{q}_\beta^1 = \boldsymbol{W}_\alpha + Z_{\alpha\beta} \left(\boldsymbol{S}_\beta^1 - \boldsymbol{B}_\beta^1\right) - V_{\alpha\beta}^k \boldsymbol{F}_{k\beta}^{\,1} \tag{2.30}$$

Note that, as with the discontinuous Galerkin method, $\boldsymbol{W}$ has no dependence on the degrees of freedom in $\boldsymbol{q}$. As the source terms are not stiff, the following iteration is used:

$$U_{\alpha\beta} \left(\boldsymbol{q}_\beta^1\right)_{m+1} = \boldsymbol{W}_\alpha + Z_{\alpha\beta} \left(\left(\boldsymbol{S}_\beta^1\right)_m - \left(\boldsymbol{B}_\beta^1\right)_m\right) - V_{\alpha\beta}^k \left(\boldsymbol{F}_{k\beta}^{\,1}\right)_m \tag{2.31}$$

2.1.3 Convergence Properties

In [25] it was proved that for traditional choices of polynomial bases, the eigenvalues of $U^{-1}V^i$ are all 0 for any $N \in \mathbb{N}$, for $i = 1, 2, 3$. This implies that in the conservative, homogeneous case ($\overrightarrow{\boldsymbol{B}} = \boldsymbol{S} = \mathbf{0}$), owing to the Banach Fixed Point Theorem, existence and uniqueness of a solution are established, and convergence to this solution is guaranteed. As noted in [17], in the linear case it is implied that the iterative procedure converges after at most $N+1$ iterations. A proof of this result for the Montecinos-Balsara polynomial basis class is now provided here. For the theory in linear algebra required for this section, please consult a standard textbook on the subject, such as [38].

Take the definitions (2.19), (2.21). Consider that:

$$U^{-1}V^k = E^{-1}M^\tau \otimes I^{k-1} \otimes D \otimes I^{3-k} \tag{2.32}$$

Therefore:

$$\left(U^{-1}V^k\right)^m = \left(E^{-1}M^\tau\right)^m \otimes \left(I^{k-1}\right)^m \otimes D^m \otimes \left(I^{3-k}\right)^m \tag{2.33}$$

A matrix X is nilpotent ($X^k = 0$ for some $k \in \mathbb{N}$) if and only if all its eigenvalues are 0. Note that $U^{-1}V^k$ is nilpotent if $D^m = 0$ for some $m \in \mathbb{N}$.

Note that if $p \in P_N$ then $p = a_j \psi_j$ for some unique coefficient vector $\boldsymbol{a}$. Thus, taking inner products with ψ_i, we have $\langle \psi_i, \psi_j \rangle a_j = \langle \psi_i, p \rangle$ for $i = 0, ..., N$. This produces the following result:

$$p = a_j \psi_j \Leftrightarrow \boldsymbol{a} = \left(M^\chi\right)^{-1} \boldsymbol{x},\ x_i = \langle \psi_i, p \rangle \tag{2.34}$$

Taking $\boldsymbol{a} \in \mathbb{R}^{N+1}$, define:

$$p = a_0\psi_0 + \ldots + a_N\psi_N \in P_N \tag{2.35}$$

Note that:

$$\left(M^{\chi,1}\boldsymbol{a}\right)_i = \left\langle \psi_i, \psi_0' \right\rangle a_0 + \ldots + \left\langle \psi_i, \psi_N' \right\rangle a_N = \left\langle \psi_i, p' \right\rangle \tag{2.36}$$

Thus, by (2.34):

$$\left(\left(M^\chi\right)^{-1} M^{\chi,1}\boldsymbol{a}\right)_i \psi_i = (D\boldsymbol{a})_i \psi_i = p' \tag{2.37}$$

By induction:

$$(D^m \boldsymbol{a})_i \psi_i = p^{(m)} \tag{2.38}$$

for any $m \in \mathbb{N}$. As $p \in P_N$, $D^{N+1}\boldsymbol{a} = \mathbf{0}$. As $\boldsymbol{a}$ was chosen arbitrarily, $D^{N+1} = 0$. No specific choice has been made for $N \in \mathbb{N}$ and thus the result holds in general.

Thus, in the case that $\overrightarrow{\boldsymbol{B}} = \boldsymbol{S} = \mathbf{0}$, existence and uniqueness of a solution are established, and convergence to this solution is guaranteed for the iterative solution to (2.20) in the Discontinuous Galerkin case, and (2.30) in the Continuous Galerkin case.

2.2 Operator Splitting Methods

The material in this section is published in [24].

Note that (1a), (1b), (1c), (1d), (3) can be written in the following form:

$$\frac{\partial \boldsymbol{Q}}{\partial t} + \boldsymbol{\nabla} \cdot \boldsymbol{F}(\boldsymbol{Q}) + \boldsymbol{B}(\boldsymbol{Q}) \cdot \nabla \boldsymbol{Q} = \boldsymbol{S}(\boldsymbol{Q}) \tag{2.39}$$

As described in [47], a viable way to solve inhomogeneous systems of PDEs is to employ an operator splitting. That is, the following subsystems are solved:

$$\frac{\partial \boldsymbol{Q}}{\partial t} + \boldsymbol{\nabla} \cdot \boldsymbol{F}(\boldsymbol{Q}) + \boldsymbol{B}(\boldsymbol{Q}) \cdot \nabla \boldsymbol{Q} = \mathbf{0} \tag{2.40a}$$

$$\frac{d\boldsymbol{Q}}{dt} = \boldsymbol{S}(\boldsymbol{Q}) \tag{2.40b}$$

The advantage of this approach is that specialized solvers can be employed to compute the results of the different subsystems. Let $H^{\delta t}, S^{\delta t}$ be the operators that take data $\boldsymbol{Q}(x,t)$ to $\boldsymbol{Q}(x, t+\delta t)$ under systems (2.40a) and (2.40b) respectively. A second-order scheme (in time) for solving the full set of PDEs over time step $[0, \Delta t]$ is obtained by calculating $\boldsymbol{Q}_{\boldsymbol{\Delta t}}$ using a Strang splitting:

$$\boldsymbol{Q}_{\boldsymbol{\Delta t}} = S^{\frac{\Delta t}{2}} H^{\Delta t} S^{\frac{\Delta t}{2}} \boldsymbol{Q}_{\mathbf{0}} \tag{2.41}$$

In the scheme proposed here, the homogeneous subsystem will be solved using a WENO reconstruction of the data, followed by a finite volume update, and the temporal ODEs will be solved with appropriate ODE solvers. This new scheme will be referred to here as *the Split-WENO method*.

Noting that $\frac{d\rho}{dt} = 0$ over the ODE time step, the operator S entails solving the following systems:

$$\frac{dA}{dt} = \frac{-3}{\tau_1} |A|^{\frac{5}{3}} A \operatorname{dev}(G) \tag{2.42a}$$
$$\frac{d\boldsymbol{J}}{dt} = -\frac{1}{\tau_2} \frac{T\rho_0}{T_0\rho} \boldsymbol{J} \tag{2.42b}$$

These systems can be solved concurrently with a stiff ODE solver. The Jacobians of these two systems to be used in an ODE solver are given in A.2 and A.2. However, these systems can also be solved separately, using the analytical results presented in Section **??**, under specific assumptions. The second-order Strang splitting is then:

$$\boldsymbol{Q_{\Delta t}} = D^{\frac{\Delta t}{2}} T^{\frac{\Delta t}{2}} H^{\Delta t} T^{\frac{\Delta t}{2}} D^{\frac{\Delta t}{2}} \boldsymbol{Q_0} \tag{2.43}$$

where $D^{\delta t}, T^{\delta t}$ are the operators solving the distortion and thermal impulse ODEs respectively, over time step δt. This allows us to bypass the relatively computationally costly process of solving these systems numerically.

2.2.1 The Homogeneous System

A WENO reconstruction of the cell-averaged data is performed at the start of the time step (as described in 0.4.1). Focusing on a single cell C_i at time t_n, we have $\boldsymbol{w}^n(\boldsymbol{x}) = \boldsymbol{w^n}_p \Psi_p(\boldsymbol{\chi}(\boldsymbol{x}))$ in C_i where Ψ_p is a tensor product of basis functions in each of the spatial dimensions. The flux in C is approximated by $\boldsymbol{F}(\boldsymbol{x}) \approx \boldsymbol{F}(\boldsymbol{w}_p)\Psi_p(\boldsymbol{\chi}(\boldsymbol{x}))$. $\boldsymbol{w}_p$ are stepped forwards half a time step using the update formula:

$$\frac{\boldsymbol{w_p^{n+\frac{1}{2}}} - \boldsymbol{w_p^n}}{\Delta t/2} + \boldsymbol{F}\left(\boldsymbol{w_k^n}\right) \cdot \nabla \Psi_k(\boldsymbol{\chi_p}) + \boldsymbol{B}\left(\boldsymbol{w_p^n}\right) \cdot \left(\boldsymbol{w_k^n} \nabla \Psi_k(\boldsymbol{\chi_p})\right) = \boldsymbol{0} \tag{2.44}$$

i.e.

$$\boldsymbol{w}_p^{n+\frac{1}{2}} = \boldsymbol{w}_p^n - \frac{\Delta t}{2\Delta x}\left(\boldsymbol{F}\left(\boldsymbol{w}_k^n\right)\cdot\nabla\Psi_k\left(\boldsymbol{\chi}_p\right) + \boldsymbol{B}\left(\boldsymbol{w}_p^n\right)\cdot\left(\boldsymbol{w}_k^n\nabla\Psi_k\left(\boldsymbol{\chi}_p\right)\right)\right) \tag{2.45}$$

where $\boldsymbol{\chi}_p$ is the node corresponding to Ψ_p. This evolution to the middle of the time step is similar to that used in the second-order MUSCL and SLIC schemes (see [47]) and, as with those schemes, it is integral to giving the method presented here its second-order accuracy.

Integrating (2.40a) over C gives:

$$\boldsymbol{Q}_i^{n+1} = \boldsymbol{Q}_i^n - \Delta t_n\left(\boldsymbol{P}_i^{n+\frac{1}{2}} + \boldsymbol{D}_i^{n+\frac{1}{2}}\right) \tag{2.46}$$

where

$$\boldsymbol{Q}_i^n = \frac{1}{V}\int_C \boldsymbol{Q}\left(\boldsymbol{x}, t_n\right) d\boldsymbol{x} \tag{2.47a}$$

$$\boldsymbol{P}_i^{n+\frac{1}{2}} = \frac{1}{V}\int_C \boldsymbol{B}\left(\boldsymbol{Q}\left(\boldsymbol{x}, t_{n+\frac{1}{2}}\right)\right)\cdot\nabla\boldsymbol{Q}\left(\boldsymbol{x}, t_{n+\frac{1}{2}}\right) d\boldsymbol{x} \tag{2.47b}$$

$$\boldsymbol{D}_i^{n+\frac{1}{2}} = \frac{1}{V}\oint_{\partial C} \boldsymbol{\mathcal{D}}\left(\boldsymbol{Q}^-\left(\boldsymbol{s}, t_{n+\frac{1}{2}}\right), \boldsymbol{Q}^+\left(\boldsymbol{s}, t_{n+\frac{1}{2}}\right)\right) d\boldsymbol{s} \tag{2.47c}$$

where V is the volume of C and $\boldsymbol{Q}^-, \boldsymbol{Q}^+$ are the interior and exterior extrapolated states at the boundary of C, respectively.

Note that (2.40a) can be rewritten as:

$$\frac{\partial\boldsymbol{Q}}{\partial t} + \boldsymbol{M}\left(\boldsymbol{Q}\right)\cdot\nabla\boldsymbol{Q} = \boldsymbol{0} \tag{2.48}$$

where $\boldsymbol{M} = \frac{\partial\boldsymbol{F}}{\partial\boldsymbol{Q}} + \boldsymbol{B}$. Let $\boldsymbol{n}$ be the normal to the boundary at point $\boldsymbol{s} \in \partial C$. For the GPR model, $\hat{M} = \boldsymbol{M}\left(\boldsymbol{Q}\left(\boldsymbol{s}\right)\right)\cdot\boldsymbol{n}$ is a diagonalizable matrix with decomposition $\hat{M} = \hat{R}\hat{\Lambda}\hat{R}^{-1}$ where the columns of $\hat{R}$ are the right eigenvectors and $\hat{\Lambda}$ is the diagonal matrix of eigenvalues. Define also $\hat{\boldsymbol{F}} = \boldsymbol{F}\cdot\boldsymbol{n}$ and $\hat{B} = \boldsymbol{B}\cdot\boldsymbol{n}$. Using these definitions, the interface terms arising in the FV formula have the following form:

$$\boldsymbol{\mathcal{D}}\left(\boldsymbol{Q}^-, \boldsymbol{Q}^+\right) = \frac{1}{2}\left(\hat{\boldsymbol{F}}\left(\boldsymbol{Q}^+\right) + \hat{\boldsymbol{F}}\left(\boldsymbol{Q}^-\right) + \tilde{B}\left(\boldsymbol{Q}^+ - \boldsymbol{Q}^-\right) + \tilde{M}\left(\boldsymbol{Q}^+ - \boldsymbol{Q}^-\right)\right) \tag{2.49}$$

$\tilde{M}$ is chosen to either correspond to a Rusanov/Lax-Friedrichs flux (see [47]):

$$\tilde{M} = \max\left(\max\left|\hat{\Lambda}\left(\boldsymbol{Q}^+\right)\right|, \max\left|\hat{\Lambda}\left(\boldsymbol{Q}^-\right)\right|\right) \tag{2.50}$$

or a simplified Osher–Solomon flux (see [15, 16]):

$$\tilde{M} = \int_0^1 \left|\hat{M}\left(\boldsymbol{Q}^- + z\left(\boldsymbol{Q}^+ - \boldsymbol{Q}^-\right)\right)\right| dz \tag{2.51}$$

where

$$\left|\hat{M}\right| = \hat{R}\left|\hat{\Lambda}\right|\hat{R}^{-1} \tag{2.52}$$

$\tilde{B}$ takes the following form:

$$\tilde{B} = \int_0^1 \hat{B}\left(\boldsymbol{Q}^- + z\left(\boldsymbol{Q}^+ - \boldsymbol{Q}^-\right)\right) dz \tag{2.53}$$

It was found that the Osher-Solomon flux would often produce slightly less diffusive results, but that it was more computationally expensive, and also had a greater tendency to introduce numerical artefacts.

$\boldsymbol{P}_i^{n+\frac{1}{2}}, \boldsymbol{D}_i^{n+\frac{1}{2}}$ are calculated using an $N+1$-point Gauss-Legendre quadrature, replacing $\boldsymbol{Q}\left(\boldsymbol{x}, t_{n+\frac{1}{2}}\right)$ with $\boldsymbol{w}^{n+\frac{1}{2}}\left(\boldsymbol{x}\right)$.

2.2.2 The Thermal Impulse ODEs

Taking the EOS for the GPR model (6) and denoting by $E_2^{(A)}, E_2^{(J)}$ the components of E_2 depending on A and $\boldsymbol{J}$ respectively, we have:

$$\begin{aligned} T &= \frac{E_1}{c_v} \\ &= \frac{E - E_2^{(A)}\left(\rho, s, A\right) - E_3\left(\boldsymbol{v}\right)}{c_v} - \frac{1}{c_v} E_2^{(J)}\left(\boldsymbol{J}\right) \\ &= c_1 - c_2\left\|\boldsymbol{J}\right\|^2 \end{aligned} \tag{2.54}$$

where:

$$c_1 = \frac{E - E_2^{(A)}(A) - E_3(\boldsymbol{v})}{c_v} \tag{2.55a}$$

$$c_2 = \frac{\alpha^2}{2c_v} \tag{2.55b}$$

Over the time period of the ODE (2.42b), $c_1, c_2 > 0$ are constant. We have:

$$\frac{dJ_i}{dt} = -\left(\frac{1}{\tau_2}\frac{\rho_0}{T_0\rho}\right) J_i \left(c_1 - c_2 \|\boldsymbol{J}\|^2\right) \tag{2.56}$$

Therefore:

$$\frac{d}{dt}\left(J_i^2\right) = J_i^2\left(-a + b\left(J_1^2 + J_2^2 + J_3^2\right)\right) \tag{2.57}$$

where

$$a = \frac{2\rho_0}{\tau_2 T_0 \rho c_v}\left(E - E_2^{(A)}(A) - E_3(\boldsymbol{v})\right) \tag{2.58a}$$

$$b = \frac{\rho_0 \alpha^2}{\tau_2 T_0 \rho c_v} \tag{2.58b}$$

Note that this is a generalized Lotka-Volterra system in $\{J_1^2, J_2^2, J_3^2\}$. It has the following analytical solution:

$$\boldsymbol{J}(t) = \boldsymbol{J}(0)\sqrt{\frac{1}{e^{at} - \frac{b}{a}\left(e^{at} - 1\right)\|\boldsymbol{J}(0)\|^2}} \tag{2.59}$$

2.2.3 The Distortion ODEs

Let $k_0 = \frac{3}{\tau_1}\left(\frac{\rho}{\rho_0}\right)^{\frac{5}{3}} > 0$ and let A have singular value decomposition $U\Sigma V^T$. Then:

$$G = \left(U\Sigma V^T\right)^T U\Sigma V^T = V\Sigma^2 V^T \tag{2.60}$$

$$\operatorname{tr}(G) = \operatorname{tr}\left(V\Sigma^2 V^T\right) = \operatorname{tr}\left(\Sigma^2 V^T V\right) = \operatorname{tr}\left(\Sigma^2\right) \tag{2.61}$$

Therefore:

$$\frac{dA}{dt} = -k_0 U \Sigma V^T \left(V \Sigma^2 V^T - \frac{\mathrm{tr}\left(\Sigma^2\right)}{3} I \right) \tag{2.62}$$
$$= -k_0 U \Sigma \left(\Sigma^2 - \frac{\mathrm{tr}\left(\Sigma^2\right)}{3} \right) V^T$$
$$= -k_0 U \Sigma \, \mathrm{dev}\left(\Sigma^2\right) V^T$$

It is a common result (see [21]) that:

$$d\Sigma = U^T dA V \tag{2.63}$$

and thus:

$$\frac{d\Sigma}{dt} = -k_0 \Sigma \, \mathrm{dev}\left(\Sigma^2\right) \tag{2.64}$$

Using a fast 3×3 SVD algorithm (such as in [34]), U, V, Σ can be obtained, after which the following procedure is applied to Σ, giving $A(t) = U \Sigma(t) V^T$.

Denote the singular values of A by a_1, a_2, a_3. Then:

$$\Sigma \, \mathrm{dev}\left(\Sigma^2\right) = \begin{pmatrix} a_1 \left(a_1^2 - \frac{a_1^2 + a_2^2 + a_3^2}{3} \right) & 0 & 0 \\ 0 & a_1 \left(a_1^2 - \frac{a_1^2 + a_2^2 + a_3^2}{3} \right) & 0 \\ 0 & 0 & a_1 \left(a_1^2 - \frac{a_1^2 + a_2^2 + a_3^2}{3} \right) \end{pmatrix} \tag{2.65}$$

Letting $x_i = \frac{a_i^2}{\det(A)^{\frac{2}{3}}} = \frac{a_i^2}{\left(\frac{\rho}{\rho_0}\right)^{\frac{2}{3}}}$ we have:

$$\frac{dx_i}{d\tau} = -3 x_i \left(x_i - \bar{x} \right) \tag{2.66}$$

where $\tau = \frac{2}{\tau_1} \left(\frac{\rho}{\rho_0}\right)^{\frac{7}{3}} t$ and $\bar{x}$ is the arithmetic mean of x_1, x_2, x_3. This ODE system travels along the surface $\Psi = \{x_1, x_2, x_3 > 0, x_1 x_2 x_3 = 1\}$ to the point $x_1, x_2, x_3 = 1$. This surface is symmetrical in the planes $x_1 = x_2$, $x_1 = x_3$, $x_2 = x_3$. As such, given that the system is autonomous, the paths of evolution of the x_i cannot cross the intersections of these planes with Ψ. Thus, any non-strict inequality of the form $x_i \geq x_j \geq x_k$ is maintained for the whole history of the system. By considering (2.66) it is clear that in this case x_i is monotone decreasing, x_k is monotone increasing, and the time derivative of x_j may switch sign.

Note that we have:

$$\begin{cases} \frac{dx_i}{d\tau} = -x_i\left(2x_i - x_j - x_k\right) = -x_i\left(2x_i - x_j - \frac{1}{x_i x_j}\right) \\ \frac{dx_j}{d\tau} = -x_j\left(2x_j - x_k - x_i\right) = -x_j\left(2x_j - x_i - \frac{1}{x_i x_j}\right) \end{cases} \tag{2.67}$$

Thus, an ODE solver can be used on these two equations to effectively solve the ODEs for all 9 components of A. Note that:

$$\frac{dx_j}{dx_i} = \frac{x_j}{x_i}\frac{2x_j - x_i - \frac{1}{x_i x_j}}{2x_i - x_j - \frac{1}{x_i x_j}} \tag{2.68}$$

This has solution:

$$x_j = \frac{c + \sqrt{c^2 + 4\left(1 - c\right)x_i^3}}{2x_i^2} \tag{2.69}$$

where

$$c = -\frac{x_{i,0}\left(x_{i,0}x_{j,0}^2 - 1\right)}{x_{i,0} - x_{j,0}} \in \left(-\infty, 0\right] \tag{2.70}$$

In the case that $x_{i,0} = x_{j,0}$, we have $x_i = x_j$ for all time. Thus, the ODE system for A has been reduced to a single ODE, as $x_j\left(x_i\right)$ can be inserted into the RHS of the equation for $\frac{dx_i}{d\tau}$. However, it is less computationally expensive to evolve the system presented in (2.67).

2.2.3.1 Bounds on the Solutions

If any of the relations in $x_i \geq x_j \geq x_k$ are in fact equalities, equality is maintained throughout the history of the system. This can be seen by noting that the time derivatives of the equal variables are in this case equal. If $x_j = x_k$ then $x_i = \frac{1}{x_j^2}$. Combining these results, the path of the system in $\left(x_i, x_j\right)$ coordinates is in fact confined to the curved triangular region:

$$\left\{\left(x_i, x_j\right) : x_i \leq x_i^0 \,\cap\, x_i \geq x_j \,\cap\, x_i \geq \frac{1}{x_j^2}\right\} \tag{2.71}$$

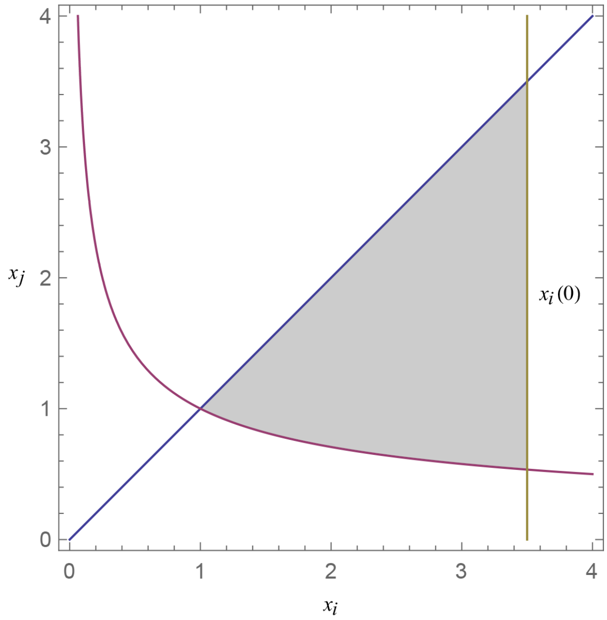

Figure 2.1: The (shaded) region to which x_i, x_j are confined in the evolution of the distortion ODEs

This is demonstrated in Figure 2.1 on page 35. By (2.67), the rate of change of x_i at a particular value $x_i = x_i^*$ is given by:

$$-x_i^* \left(2x_i^* - x_j - \frac{1}{x_i^* x_j}\right) \tag{2.72}$$

Note that:

$$\begin{aligned} \frac{d}{dx_j}\left(2x_i^* - x_j - \frac{1}{x_i^* x_j}\right) &= -1 + \frac{1}{x_i^* x_j^2} = 0 \\ \Rightarrow x_j &= \frac{1}{\sqrt{x_i^*}} \end{aligned} \tag{2.73}$$

$$\frac{d^2}{dx_j^2}\left(2x_i^* - x_j - \frac{1}{x_i^* x_j}\right) = \frac{-2}{x_i^* x_j^3} < 0 \tag{2.74}$$

Thus, x_i decreases fastest on the line $x_i = \frac{1}{x_j^2}$ (the bottom boundary of the region given in Figure 2.1 on page 35), and slowest on the line $x_i = x_j$. The rates of change of x_i along these two lines are given respectively by:

$$\frac{dx_i}{d\tau} = -2x_i\left(x_i - \sqrt{\frac{1}{x_i}}\right) \tag{2.75a}$$

$$\frac{dx_i}{d\tau} = -x_i\left(x_i - \frac{1}{x_i^2}\right) \tag{2.75b}$$

These have implicit solutions:

$$\tau = \left(f\left(\sqrt{x_i}\right) + g\left(\sqrt{x_i}\right)\right) - \left(f\left(\sqrt{x_i^0}\right) + g\left(\sqrt{x_i^0}\right)\right) \equiv F_1\left(x_i; x_i^0\right) \tag{2.76a}$$

$$\tau = \left(f\left(x_i\right) - g\left(x_i\right)\right) - \left(f\left(x_i^0\right) - g\left(x_i^0\right)\right) \equiv F_2\left(x_i; x_i^0\right) \tag{2.76b}$$

where

$$f\left(x_i\right) = \frac{1}{6}\log\left(\frac{x_i^2 + x_i + 1}{\left(x_i - 1\right)^2}\right) \tag{2.77a}$$

$$g\left(x_i\right) = \frac{1}{\sqrt{3}}\tan^{-1}\left(\frac{2x_i + 1}{\sqrt{3}}\right) \tag{2.77b}$$

As (2.66) is an autonomous system of ODEs, it has the property that its limit $x_1 = x_2 = x_3 = 1$ is never obtained in finite time, in precise arithmetic. In floating point arithmetic we may say that the system has converged when $x_i - 1 < \epsilon$ (machine epsilon) for each i. This happens when:

$$\tau > F_2\left(1 + \epsilon; x_i^0\right) \tag{2.78}$$

This provides a quick method to check whether it is necessary to run the ODE solver in a particular cell. If the following condition is satisfied then we know the system in that cell converges to the ground state over the time interval in which the ODE system is calculated:

$$\frac{2}{\tau_1}\left(\frac{\rho}{\rho_0}\right)^{\frac{7}{3}}\Delta t > F_2\left(1 + \epsilon; \max\left\{x_i^0\right\}\right) \tag{2.79}$$

If the fluid is very inviscid, resulting in a stiff ODE, the critical time is lower, and there is more chance that the ODE system in the cell reaches its limit in Δt. This check potentially saves a lot of computationally expensive stiff ODE solves. The same goes for if the flow is slow-moving, as the system will be closer to its ground state at the start of the time step and is more likely to converge over Δt. Similarly, if the following condition is satisfied then we know for sure that an ODE solver is necessary, as the system certainly will not have converged over the timestep:

$$\frac{2}{\tau_1}\left(\frac{\rho}{\rho_0}\right)^{\frac{7}{3}}\Delta t < F_1\left(1+\epsilon;\max\left\{x_i^0\right\}\right) \tag{2.80}$$

2.2.3.2 Newontian Fluids

We now explore cases when even the reduced ODE system (2.67) need not be solved numerically. Define the following variables:

$$m = \frac{x_1 + x_2 + x_3}{3} \tag{2.81a}$$

$$u = \frac{(x_1 - x_2)^2 + (x_2 - x_3)^2 + (x_3 - x_1)^2}{3} \tag{2.81b}$$

It is a standard result that $m \geq \sqrt[3]{x_1 x_2 x_3}$. Thus, $m \geq 1$. Note that u is proportional to the internal energy contribution from the distortion. From (2.66) we have:

$$\frac{du}{d\tau} = -18\left(1 - m\left(m^2 - \frac{5}{6}u\right)\right) \tag{2.82a}$$

$$\frac{dm}{d\tau} = -u \tag{2.82b}$$

Combining these equations, we have:

$$\frac{d^2m}{d\tau^2} = -\frac{du}{d\tau} = 18\left(1 - m\left(m^2 - \frac{5}{6}u\right)\right) \tag{2.83}$$

Therefore:

$$\begin{cases} \frac{d^2m}{d\tau^2} + 15m\frac{dm}{d\tau} + 18\left(m^3 - 1\right) = 0 \\ m(0) = m_0 \\ m'(0) = -u_0 \end{cases} \tag{2.84}$$

We make the following assumption, noting that it is true in all physical situations tested in this study:

$$m(t) = 1 + \eta(t), \quad \eta \ll 1 \; \forall t \geq 0 \tag{2.85}$$

Thus, we have the linearized ODE:

$$\begin{cases} \frac{d^2\eta}{d\tau^2} + 15\frac{d\eta}{d\tau} + 54\eta = 0 \\ \eta(0) = m_0 - 1 \\ \eta'(0) = -u_0 \end{cases} \tag{2.86}$$

This is a Sturm-Liouville equation with solution:

$$\eta(\tau) = \frac{e^{-9\tau}}{3}\Big((9m_0 - u_0 - 9)\, e^{3\tau} - (6m_0 - u_0 - 6)\Big) \tag{2.87}$$

Thus, we also have:

$$u(\tau) = e^{-9\tau}\Big(e^{3\tau}(18m_0 - 2u_0 - 18) - (18m_0 - 3u_0 - 18)\Big) \tag{2.88}$$

Once $m_{\Delta t} = 1 + \eta\left(\frac{2}{\tau_1}\left(\frac{\rho}{\rho_0}\right)^{\frac{7}{3}}\Delta t\right)$ and $u_{\Delta t} = u\left(\frac{2}{\tau_1}\left(\frac{\rho}{\rho_0}\right)^{\frac{7}{3}}\Delta t\right)$ have been found, we have:

$$\frac{x_i + x_j + x_k}{3} = m_{\Delta t} \tag{2.89a}$$

$$\frac{(x_i - x_j)^2 + (x_j - x_k)^2 + (x_k - x_i)^2}{3} = u_{\Delta t} \tag{2.89b}$$

$$x_i x_j x_k = 1 \tag{2.89c}$$

This gives:

$$x_i = \frac{\sqrt[3]{6\left(\sqrt{81\Delta^2 - 6u_{\Delta t}^3} + 9\Delta\right)}}{6} + \frac{u_{\Delta t}}{\sqrt[3]{6\left(\sqrt{81\Delta^2 - 6u_{\Delta t}^3} + 9\Delta\right)}} + m_{\Delta t} \tag{2.90a}$$

$$x_j = \frac{1}{2}\left(\sqrt{\frac{x_i(3m_{\Delta t} - x_i)^2 - 4}{x_i}} + 3m_{\Delta t} - x_i\right) \tag{2.90b}$$

$$x_k = \frac{1}{x_i x_j} \tag{2.90c}$$

where

$$\Delta = -2m_{\Delta t}^3 + m_{\Delta t}u_{\Delta t} + 2 \tag{2.91}$$

Note that taking the real parts of the above expression for x_i gives:

$$x_i = \frac{\sqrt{6u_{\Delta t}}}{3}\cos\left(\frac{\theta}{3}\right) + m_{\Delta t} \tag{2.92a}$$

$$\theta = \tan^{-1}\left(\frac{\sqrt{6u_{\Delta t}^3 - 81\Delta^2}}{9\Delta}\right) \tag{2.92b}$$

At this point it is not clear which values of $\{x_i, x_j, x_k\}$ are taken by x_1, x_2, x_3. However, this can be inferred from the fact that any relation $x_i \geq x_j \geq x_k$ is maintained over the lifetime of the system. Thus, the stiff ODE solver has been obviated by a few arithmetic operations.

2.2.3.3 Power Law Materials

Take the singular value decomposition $A = U\Sigma V^T$ as in 2.2.3. Note that:

$$\sigma = -\rho c_s^2 A^T A \operatorname{dev}\left(A^T A\right) = -\rho c_s^2 V \Sigma^2 \operatorname{dev}\left(\Sigma^2\right) V^T \tag{2.93}$$

Thus:

$$\|\operatorname{dev}(\sigma)\|_F^n = \rho^n c_s^{2n} \left\|\operatorname{dev}\left(\Sigma^2 \operatorname{dev}\left(\Sigma^2\right)\right)\right\|_F^n \tag{2.94}$$

Using this result, for elastoplastic materials governed by the power law described in (12a):

$$\frac{d\Sigma}{dt} = -\frac{3}{\tau_0}\left(\frac{\rho}{\rho_0}\right)^{\frac{5}{3}} \frac{\left(\frac{3}{2}\right)^{\frac{n}{2}} \rho^n c_s^{2n} \|\operatorname{dev}(\Sigma^2 \operatorname{dev}(\Sigma^2))\|_F^n}{\sigma_0^n} \Sigma \operatorname{dev}\left(\Sigma^2\right) \tag{2.95}$$

Letting $x_i = \frac{a_i^2}{\det(A)^{\frac{2}{3}}} = \frac{a_i^2}{\left(\frac{\rho}{\rho_0}\right)^{\frac{2}{3}}}$ then $\Sigma^2 = \det(A)^{\frac{2}{3}} X$ where $X = \operatorname{diag}(x_1, x_2, x_3)$. Thus, we have:

$$\frac{dx_i}{d\tilde{t}} = -3\|\operatorname{dev}(X \operatorname{dev}(X))\|_F^n x_i (x_i - \bar{x}) \tag{2.96}$$

where:

$$\tilde{t} = \frac{2}{\tau_0} \left(\frac{\rho}{\rho_0}\right)^{\frac{4n+7}{3}} \left(\sqrt{\frac{3}{2}} \frac{\rho c_s^2}{\sigma_0}\right)^n t \tag{2.97}$$

Note that:

$$\begin{aligned} \frac{27}{2} \left\|\operatorname{dev}\left(X \operatorname{dev}\left(X\right)\right)\right\|_F^2 = {} & 3\left(x_2 x_3 x_1^2 + x_2 x_3^2 x_1 + x_2^2 x_3 x_1\right) \\ & - 3\left(x_1^2 x_2^2 + x_3^2 x_2^2 + x_1^2 x_3^2\right) \\ & - 2\left(x_2 x_1^3 + x_3 x_1^3 + x_2^3 x_1 + x_3^3 x_1 + x_2 x_3^3 + x_2^3 x_3\right) \\ & + 4\left(x_1^4 + x_2^4 + x_3^4\right) \end{aligned} \tag{2.98}$$

Define the following quantities:

$$m = \frac{x_1 + x_2 + x_3}{3} \tag{2.99a}$$

$$u = \frac{\left(x_1 - x_2\right)^2 + \left(x_2 - x_3\right)^2 + \left(x_3 - x_1\right)^2}{3} \tag{2.99b}$$

Then we have:

$$\left\|\operatorname{dev}\left(X \operatorname{dev}\left(X\right)\right)\right\|_F^2 = \frac{1}{6}u^2 + 4m^2 u - 6m^4 + 6m \tag{2.100}$$

This leads to the following coupled system of ODEs:

$$\frac{du}{d\tilde{t}} = -18\left(\frac{1}{6}u^2 + 4m^2 u - 6m^4 + 6m\right)^{\frac{n}{2}} \left(1 - m\left(m^2 - \frac{5}{6}u\right)\right) \tag{2.101a}$$

$$\frac{dm}{d\tilde{t}} = -\left(\frac{1}{6}u^2 + 4m^2 u - 6m^4 + 6m\right)^{\frac{n}{2}} u \tag{2.101b}$$

Define the the variable τ by:

$$\frac{d\tau}{d\tilde{t}} = \left(\frac{1}{6}u^2 + 4m^2 u - 6m^4 + 6m\right)^{\frac{n}{2}} \tag{2.102}$$

Then we have:

$$\frac{du}{d\tau} = -18\left(1 - m\left(m^2 - \frac{5}{6}u\right)\right) \tag{2.103a}$$
$$\frac{dm}{d\tau} = -u \tag{2.103b}$$

Using the approximate solution from before:

$$m(\tau) = 1 + \frac{e^{-9\tau}}{3}\left((9m_0 - u_0 - 9)\,e^{3\tau} - (6m_0 - u_0 - 6)\right) \tag{2.104a}$$
$$u(\tau) = e^{-9\tau}\left(e^{3\tau}(18m_0 - 2u_0 - 18) - (18m_0 - 3u_0 - 18)\right) \tag{2.104b}$$

Denoting $a = 9m_0 - u_0 - 9$, $b = 6m_0 - u_0 - 6$, it is straightforward to verify that:

$$\frac{d\tau}{d\tilde{t}} = \frac{1}{54^{\frac{n}{2}}}\begin{pmatrix} 108ae^{-6\tau} - 324be^{-9\tau} + 108a^2e^{-12\tau} \\ -396abe^{-15\tau} + 297b^2e^{-18\tau} - 24a^2be^{-21\tau} \\ +\left(48ab^2 - 4a^4\right)e^{-24\tau} + \left(16a^3b - 24b^3\right)e^{-27\tau} \\ -24a^2b^2e^{-30\tau} + 16ab^3e^{-33\tau} - 4b^4e^{-36\tau} \end{pmatrix}^{\frac{n}{2}} \equiv \frac{f(\tau)^{\frac{n}{2}}}{54^{\frac{n}{2}}} \tag{2.105}$$

$f(\tau)$ is approximated by $g(\tau) \equiv ce^{-\lambda\tau}$, where:

$$c = 108a - 324b + 108a^2 - 396ab + 297b^2 - 24\left(a^2b - 2ab^2 + b^3\right) - 4(a-b)^4 \tag{2.106a}$$
$$\lambda = \frac{c}{18a - 36b + 9a^2 - \frac{132ab}{5} + \frac{33b^2}{2} - \frac{8a^2b}{7} + 2ab^2 - \frac{8b^3}{9} - \frac{a^4}{6} + \frac{16a^3b}{27} - \frac{4a^2b^2}{5} + \frac{16ab^3}{33} - \frac{b^4}{9}} \tag{2.106b}$$

Note that $f(0) = g(0)$ and $\int_0^\infty (f(\tau) - g(\tau))\,d\tau = 0$. Thus, we have:

$$\frac{d\tau}{d\tilde{t}} \approx \left(\frac{c}{54}\right)^{\frac{n}{2}} e^{-\frac{n\lambda}{2}\tau} \tag{2.107}$$

Therefore:

$$\begin{aligned} \tau &\approx \frac{2}{n\lambda}\log\left(\frac{n\lambda}{2}\left(\frac{c}{54}\right)^{\frac{n}{2}}\tilde{t} + 1\right) \\ &= \frac{2}{n\lambda}\log\left(\frac{n\lambda}{\tau_0}\left(\frac{\rho}{\rho_0}\right)^{\frac{4n+7}{3}}\left(\frac{\sqrt{c}}{6}\frac{\rho c_s^2}{\sigma_0}\right)^n t + 1\right) \end{aligned} \tag{2.108}$$

Thus, the value of A at time Δt is found by substituting $\tau = \frac{2}{n\lambda} \log \left(\frac{n\lambda}{\tau_0} \left(\frac{\rho}{\rho_0} \right)^{\frac{4n+7}{3}} \left(\frac{\sqrt{c}}{6} \frac{\rho c_s^2}{\sigma_0} \right)^n \Delta t + 1 \right)$ into (2.104a),(2.104b), and in turn substituting the values obtained into (2.92a), (2.90b), (2.90c).

2.2.3.4 Bingham Plastics

For a Bingham plastic:

$$\dot{\gamma} = \begin{cases} 0 & \sigma \leq \sigma_0 \\ \frac{1}{\mu_\infty} (\sigma - \sigma_0) & \sigma \geq \sigma_0 \end{cases} \tag{2.109}$$

Define:

$$\theta_1 = \frac{\tau_1 c_s^2}{3 |A|^{\frac{5}{3}} \phi} \tag{2.110}$$

$$\phi = \begin{cases} 0 & \sigma \leq \sigma_0 \\ 1 - \frac{\sigma_0}{|\sigma|} & \sigma \geq \sigma_0 \end{cases} \tag{2.111}$$

We have:

$$\dot{G} = -\left(G \nabla v + \nabla v^T G \right) + \frac{2}{\rho \theta_1} \sigma \tag{2.112}$$

Take the asymptotic expansion:

$$G = G_0 + \tau_1 G_1 + \tau_1^2 G_2 + \cdots \tag{2.113}$$

$$\begin{aligned} \therefore \sigma &= -\rho c_s^2 \left(G_0 + \tau_1 G_1 + \cdots \right) \left(\operatorname{dev} G_0 + \tau_1 \operatorname{dev} G_1 + \right) \\ &= -\rho c_s^2 \left(G_0 \operatorname{dev} G_0 + \tau_1 \left(G_1 \operatorname{dev} G_0 + G_0 \operatorname{dev} G_1 \right) + \cdots \right) \end{aligned} \tag{2.114}$$

Then:

$$\begin{aligned} \frac{D}{Dt} \left(G_0 + \tau_1 G_1 + \cdots \right) = &- \left(G_0 + \tau_1 G_1 + \cdots \right) \nabla v - \nabla v^T \left(G_0 + \tau_1 G_1 + \cdots \right) \\ &- \frac{6\phi}{\tau_1} \left| G_0 + \tau_1 G_1 + \cdots \right|^{\frac{5}{6}} \left(G_0 \operatorname{dev} G_0 + \tau_1 \left(G_1 \operatorname{dev} G_0 + G_0 \operatorname{dev} G_1 \right) + \cdots \right) \end{aligned} \tag{2.115}$$

This can be approximated using some analytical function f:

$$\dot{\gamma} = \frac{\sigma - f(\sigma)}{\mu_\infty} \tag{2.116}$$

where $f(\sigma) \sim \sigma$ for $\sigma < \sigma_0$, $f(\sigma) \sim \sigma_0$ for $\sigma > \sigma_0$.

f will take the form of the generalized logistic function:

$$f(\sigma) = \frac{a}{(1 + be^{-c\sigma})^d} + g \tag{2.117}$$

We require:

$$f(\infty) = a + g = \sigma_0 \tag{2.118}$$

Thus:

$$f(\sigma) = \frac{a}{(1 + be^{-c\sigma})^d} + \sigma_0 - a \tag{2.119}$$

We also require:

$$f(0) = \frac{a}{(1 + b)^d} + \sigma_0 - a = 0 \tag{2.120}$$

$$f'(0) = abcd\,(1 + b)^{-(d+1)} = \frac{(a - \sigma_0)\,bcd}{1 + b} = 1 \tag{2.121}$$

$$f'(\sigma) = abcd\left(1 + be^{-c\sigma}\right)^{-(d+1)} e^{-c\sigma} \leq 1 \tag{2.122}$$

$$\left(1 + be^{-c\sigma}\right)^{-(d+1)} e^{-c\sigma} \leq \frac{1}{abcd} \tag{2.123}$$

$$\frac{d}{d\sigma}\left(\left(1+be^{-c\sigma}\right)^{-(d+1)}e^{-c\sigma}\right) = bc\left(d+1\right)\left(1+be^{-c\sigma}\right)^{-(d+2)}e^{-2c\sigma} - c\left(1+be^{-c\sigma}\right)^{-(d+1)}e^{-c\sigma} \tag{2.124}$$

$$= c\left(1+be^{-c\sigma}\right)^{-(d+1)}e^{-c\sigma}\left(b\left(d+1\right)\left(1+be^{-c\sigma}\right)^{-1}e^{-c\sigma}-1\right) \tag{2.125}$$

$$= 0 \tag{2.126}$$

$$\Rightarrow b\left(d+1\right)e^{-c\sigma} = 1+be^{-c\sigma} \tag{2.127}$$

$$\Rightarrow e^{-c\sigma} = \frac{1}{bd} \tag{2.128}$$

Thus, the maximum of $\left(1+be^{-c\sigma}\right)^{-(d+1)}e^{-c\sigma}$ is:

$$\left(1+\frac{1}{d}\right)^{-(d+1)}\frac{1}{bd} = \frac{1}{abcd} \tag{2.129}$$

So we have:

$$\left(1+\frac{1}{d}\right)^{d+1} = ac \tag{2.130}$$

$$\frac{a}{\left(1+b\right)^{d}} = a-\sigma_0 \tag{2.131}$$

$$\left(a-\sigma_0\right)bcd = 1+b \tag{2.132}$$

2.3 Numerical Results

2.3.1 Newtonian Fluids & Elastic Solids

2.3.1.1 Strain Relaxation

In this section, the approximate analytic solver for the distortion ODEs, presented in 2.2.3.2, is compared with a numerical ODE solver. Initial data was taken from [3]:

$$A = \begin{pmatrix} 1 & 0 & 0 \\ -0.01 & 0.95 & 0.02 \\ -0.015 & 0 & 0.9 \end{pmatrix}^{-1} \tag{2.133}$$

	ρ	p	$\boldsymbol{v}$	A	$\boldsymbol{J}$
$x < 0$	1	$1/\gamma$	$(0, -0.1, 0)$	I_3	$\mathbf{0}$
$x \geq 0$	1	$1/\gamma$	$(0, 0.1, 0)$	I_3	$\mathbf{0}$

Table 2.1: Initial conditions for the slow opposing shear flow test

Additionally, the following parameter values were used: $\rho_0 = 1, c_s = 1, \mu = 10^{-2}$, giving $\tau_1 = 0.06$. As can be seen in Figure 2.2 on page 46, Figure 2.3 on page 46, and Figure 2.4 on page 46, the approximate analytic solver compares well with the numerical solver in its results for the distortion tensor A, and thus also the internal energy and stress tensor. The numerical ODE solver was the odeint solver from SciPy 0.18.1, based on the LSODA solver from the FORTRAN library ODEPACK (see [39]).

2.3.1.2 Stokes' First Problem

This problem is one of the few test cases with an analytic solution for the Navier-Stokes equations. It consists of two ideal gases in an infinite domain, meeting at the plane $x = 0$, initially flowing with equal and opposite velocity ± 0.1 in the y-axis. The initial conditions are given in Table 2.1 on page 45.

The flow has a low Mach number of 0.1, and this test case is designed to demonstrate the efficacy of the numerical methods in this flow regime. The exact solution to the Navier-Stokes equations is given by[1]:

$$v = v_0 \operatorname{erf}\left(\frac{x}{2\sqrt{\mu t}}\right) \tag{2.134}$$

Heat conduction is neglected, and $\gamma = 1.4$, $c_v = 1$, $\rho_0 = 1$, $c_s = 1$. The viscosity is variously taken to be $\mu = 10^{-2}$, $\mu = 10^{-3}$, $\mu = 10^{-4}$ (resulting in $\tau_1 = 0.06$, $\tau_1 = 0.006$, $\tau_1 = 0.0006$, respectively). Due to the stiffness of the source terms in the equations governing A in the case that $\mu = 10^{-4}$, the step (2.45) in the WENO reconstruction under the Split-WENO method was not performed, and $\boldsymbol{w}_{\boldsymbol{p}}^{\boldsymbol{n}+\frac{1}{2}} \equiv \boldsymbol{w}_{\boldsymbol{p}}^{\boldsymbol{n}}$ was taken instead. This avoided the numerical diffusion that otherwise would have emerged at the interface at $x = 0$.

[1] In this problem, the Navier-Stokes equations reduce to $v_t = \mu v_{xx}$. Defining $\eta = \frac{x}{2\sqrt{\mu t}}$, and assuming $v = f(\eta)$, this becomes $f'' + 2\eta f' = 0$. The result follows by solving this equation with the boundary conditions $v(\pm\infty) = \pm v_0$.

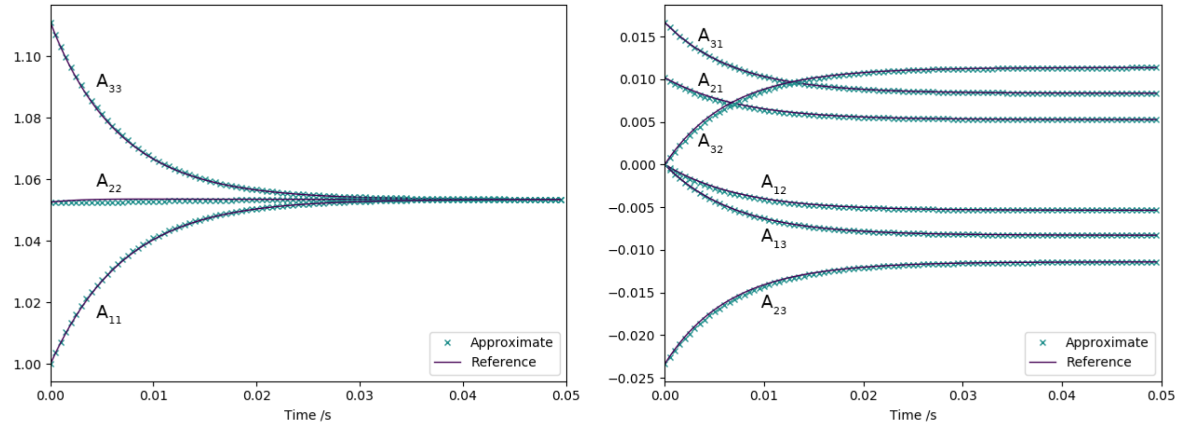

Figure 2.2: The components of the distortion tensor in the Strain Relaxation Test

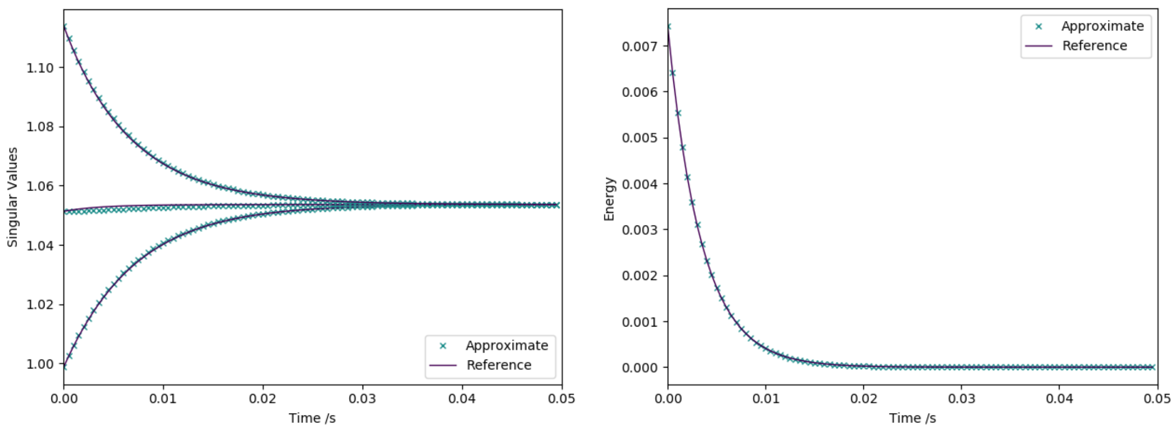

Figure 2.3: The singular values of the distortion tensor and the energy in the Strain Relaxation Test

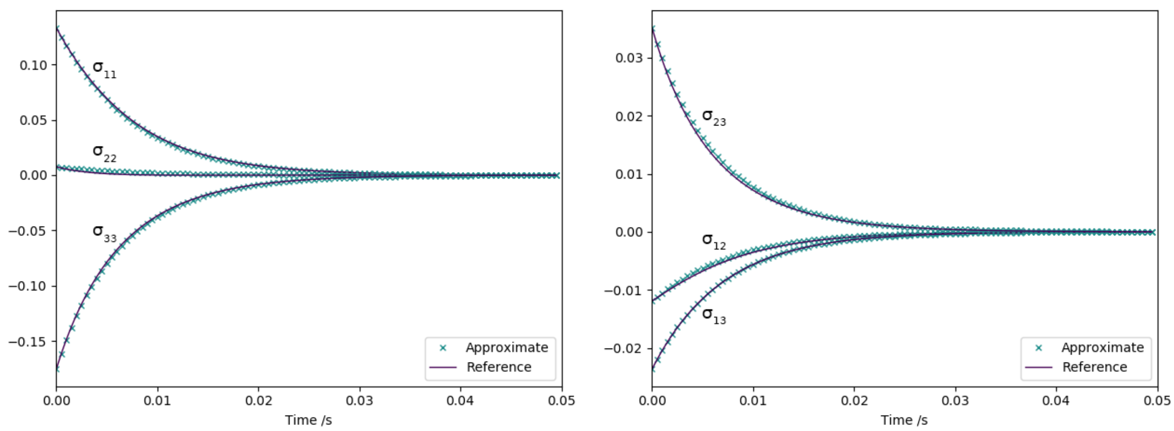

Figure 2.4: The components of the stress tensor in the Strain Relaxation Test

The results of simulations with 200 cells at time $t = 1$, using reconstruction polynomials of order $N = 2$, are presented in Figure 2.5 on page 48. The GPR model solved with both the ADER-WENO and Split-WENO methods closely matches the exact Navier-Stokes solution. Note that at $\mu = 10^{-2}$ and $\mu = 10^{-3}$, the ADER-WENO and Split-WENO methods are almost indistinguishable. At $\mu = 10^{-4}$ the Split-WENO method matches the curve of the velocity profile more closely, but overshoots slightly at the boundaries of the center region. This overshoot phenomenon is not visible in the ADER-WENO results.

2.3.1.3 Viscous Shock

This test is designed to demonstrate that the numerical methods used are also able to cope with fast flows. First demonstrated by Becker [7], the Navier-Stokes equations have an analytic solution for $P_r = 0.75$ (see Johnson [28] for a full analysis). As noted by Dumbser [14], if the wave has nondimensionalised upstream velocity $\bar{v} = 1$ and Mach number M_c, then its nondimensionalised downstream velocity is:

$$a = \frac{1 + \frac{\gamma-1}{2} M_c^2}{\frac{\gamma+1}{2} M_c^2} \tag{2.135}$$

The wave's velocity profile $\bar{v}(x)$ is given by the roots of the following equation:

$$\frac{1 - \bar{v}}{(\bar{v} - a)^a} = c_1 \exp(-c_2 x) \tag{2.136a}$$

$$c_1 = \left(\frac{1-a}{2}\right)^{1-a} \tag{2.136b}$$

$$c_2 = \frac{3}{4} R_e \frac{M_c^2 - 1}{\gamma M_c^2} \tag{2.136c}$$

c_1, c_2 are constants that affect the position of the center of the wave, and its stretch factor, respectively. Following the analysis of Morduchow and Libby [37], the nondimensional pressure and density profiles are given by:

$$\bar{p} = \frac{1}{\bar{v}} \left(1 + \frac{\gamma - 1}{2} M_c^2 \left(1 - \bar{v}^2\right)\right) \tag{2.137}$$

$$\bar{\rho} = \frac{1}{\bar{v}} \tag{2.138}$$

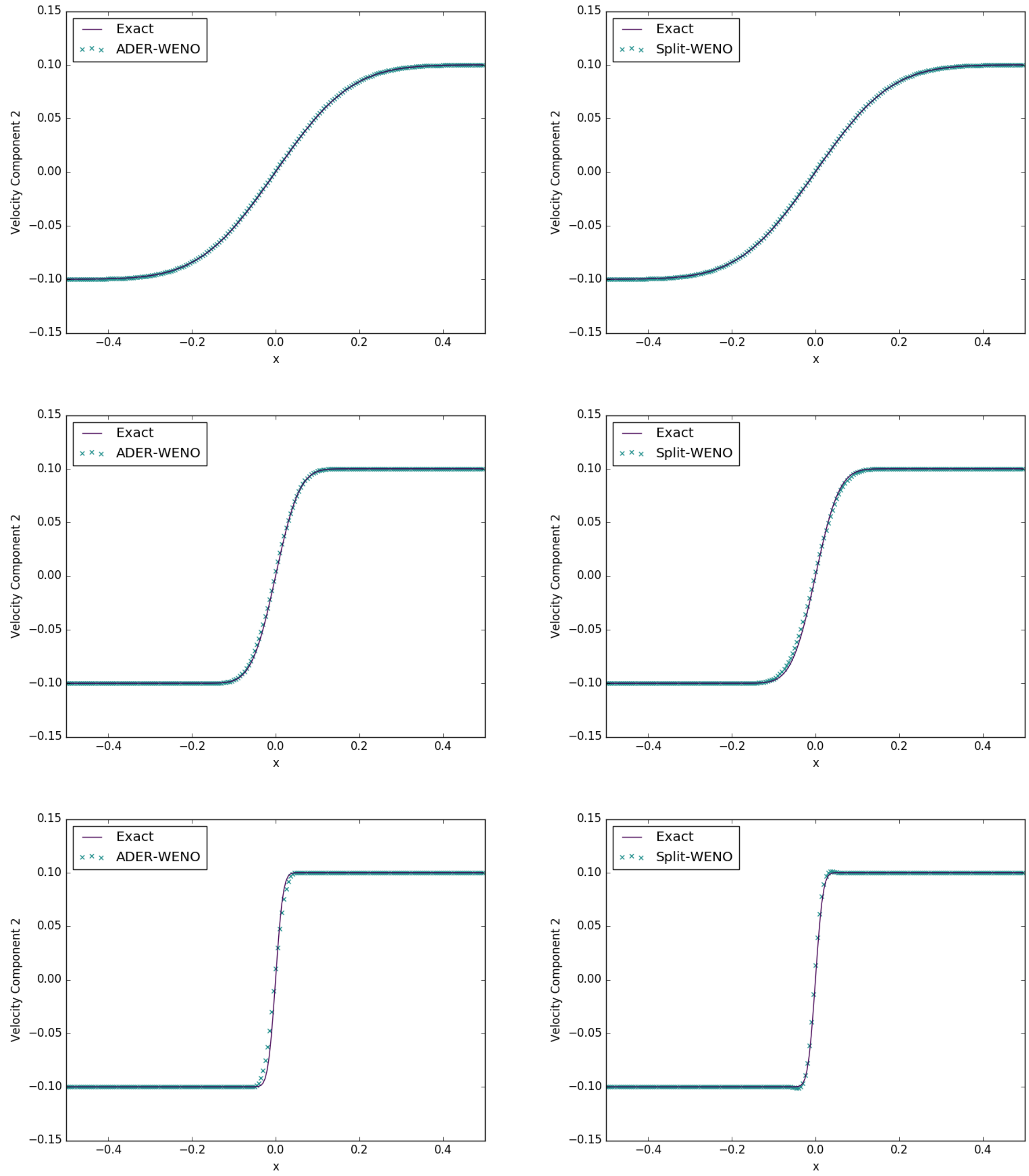

Figure 2.5: Results of solving Stokes' First Problem ($\mu = 10^{-2}, \mu = 10^{-3}, \mu = 10^{-4}$) with an ADER-WENO scheme and a Split-WENO scheme ($N = 2$)

	ρ	p	$\boldsymbol{v}$	A	$\boldsymbol{J}$
$x < 0$	2	1	$\mathbf{0}$	$\sqrt[3]{2} \cdot I_3$	$\mathbf{0}$
$x \geq 0$	0.5	1	$\mathbf{0}$	$\frac{1}{\sqrt[3]{2}} \cdot I_3$	$\mathbf{0}$

Table 2.2: Initial conditions for the heat conduction test

To obtain an unsteady shock traveling into a region at rest, a constant velocity field $v = M_c c_0$ is imposed on the traveling wave solution presented here (where c_0 is the adiabatic sound speed). Thus, if p_0, ρ_0 are the downstream (reference) values for pressure and density:

$$v = Mc_0 (1 - \bar{v}) \tag{2.139a}$$

$$p = p_0 \bar{p} \tag{2.139b}$$

$$\rho = \rho_0 \bar{\rho} \tag{2.139c}$$

These functions are used as initial conditions, along with $A = \sqrt[3]{\bar{\rho}} I$ and $\boldsymbol{J} = \mathbf{0}$. The downstream density and pressure are taken to be $\rho_0 = 1$ and $p_0 = \frac{1}{\gamma}$ (so that $c_0 = 1$). $M_c = 2$ and $R_e = 100$. The material parameters are taken to be: $\gamma = 1.4$, $p_\infty = 0$, $c_v = 2.5$, $c_s = 5$, $\alpha = 5$, $\mu = 2 \times 10^{-2}$, $\kappa = \frac{28}{3} \times 10^{-2}$ (resulting in $\tau_1 = 0.0048$, $\tau_2 = 0.00522\dot{6}$).

The results of a simulation with 200 cells at time $t = 0.2$, using reconstruction polynomials of order $N = 2$, are presented in Figure 2.6 on page 50 and Figure 2.7 on page 52. The shock was initially centered at $x = 0.25$, reaching $x = 0.65$ at the final time. Note that the density, velocity, and pressure results for both methods match the exact solution well, with the ADER-WENO method appearing to produce a slightly more accurate solution. The results for the two methods for the stress tensor and heat flux are close.

2.3.1.4 Heat Conduction in a Gas

This is a simple test case to ensure that the heat transfer terms in the implementation are working correctly. Two ideal gases at different temperatures are initially in contact at position $x = 0$. The initial conditions for this problem are given in Table 2.2 on page 49.

The material parameters are taken to be: $\gamma = 1.4$, $c_v = 2.5$, $\rho_0 = 1$, $p_0 = 1$, $c_s = 1$, $\alpha = 2$, $\mu = 10^{-2}$, $\kappa = 10^{-2}$ (resulting in $\tau_1 = 0.06$, $\tau_2 = 0.0025$). The results of a

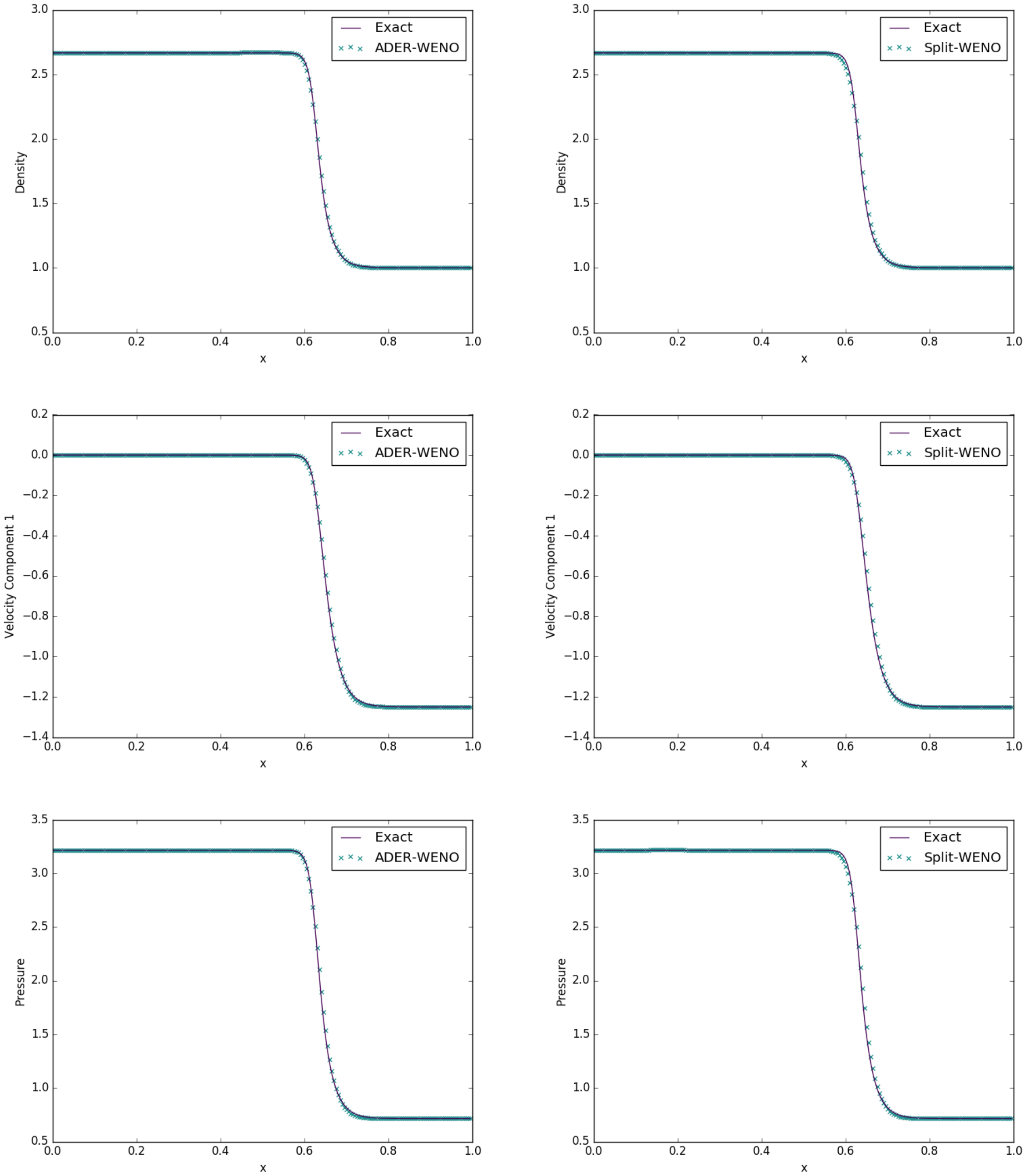

Figure 2.6: Density, velocity, and pressure for the Viscous Shock problem, solved with an ADER-WENO scheme and a Split-WENO scheme ($N = 2$)

simulation with 200 cells at time $t = 1$, using reconstruction polynomials of order $N = 2$, are presented in Figure 2.8 on page 52. The ADER-WENO and Split-WENO methods are in perfect agreement for both the temperature and heat flux profiles. As demonstrated in [14], this means that they in turn agree very well with a reference Navier-Stokes-Fourier solution.

2.3.1.5 Speed

Both the ADER-WENO scheme and the Split-WENO scheme used in this study were implemented in Python3. All array functions were precompiled with Numba's JIT capabilities and the root-finding procedure in the Galerkin predictor was performed using SciPy's Newton-Krylov solver, compiled against the Intel MKL. Clear differences in computational cost between the ADER-WENO and Split-WENO methods were apparent, as is to be expected, owing to the lack of Galerkin method in the Split-WENO scheme. The wall times for the various tests undertaken in this study are given in Table 2.3 on page 52, comparing the combined WENO and Galerkin methods of the ADER-WENO scheme to the combined WENO and ODE methods of the Split-WENO scheme. All computations were performed using an Intel Core i7-4910MQ, on a single core. The number of time steps taken are given in Table 2.4 on page 54. The differences between the methods in terms of the number of time steps taken in each test result from the fact that, for numerical stability, CFL numbers of 0.8 and 0.7 were required by the ADER-WENO method and the Split-WENO method, respectively.

Note that, unlike with the ADER-WENO scheme, the wall time for the Split-WENO scheme is unaffected by a decrease in the viscosity in Stokes' First Problem (and the corresponding increase in the stiffness of the source terms). This is because the analytic approximation to the distortion ODEs obviates the need for a stiff solver. The large difference in ADER-WENO solver times between the $\mu = 10^{-3}$ and $\mu = 10^{-4}$ cases is due to the fact that, in the latter case, a stiff solver must be employed for the initial guess to the root of the nonlinear system produced by the Discontinuous Galerkin method (as described in [23]).

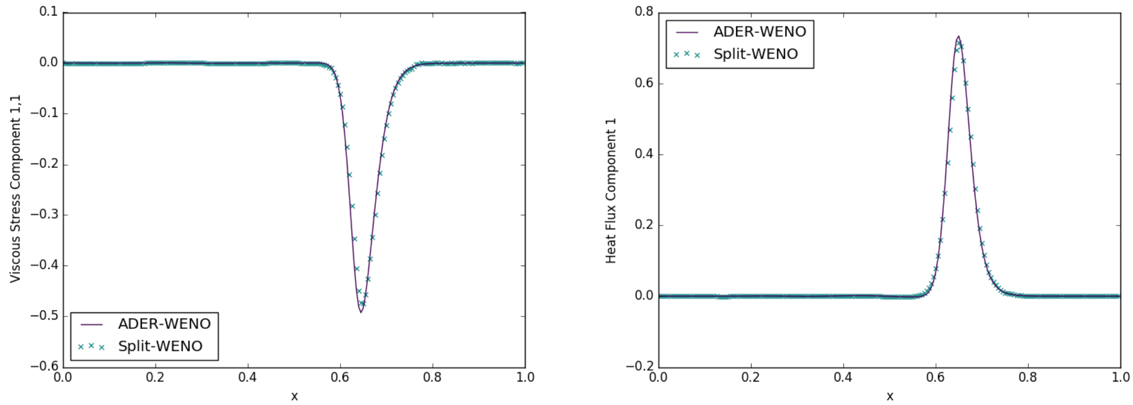

Figure 2.7: Viscous stress and heat flux for the Viscous Shock problem, solved with both an ADER-WENO scheme and a Split-WENO scheme ($N = 2$)

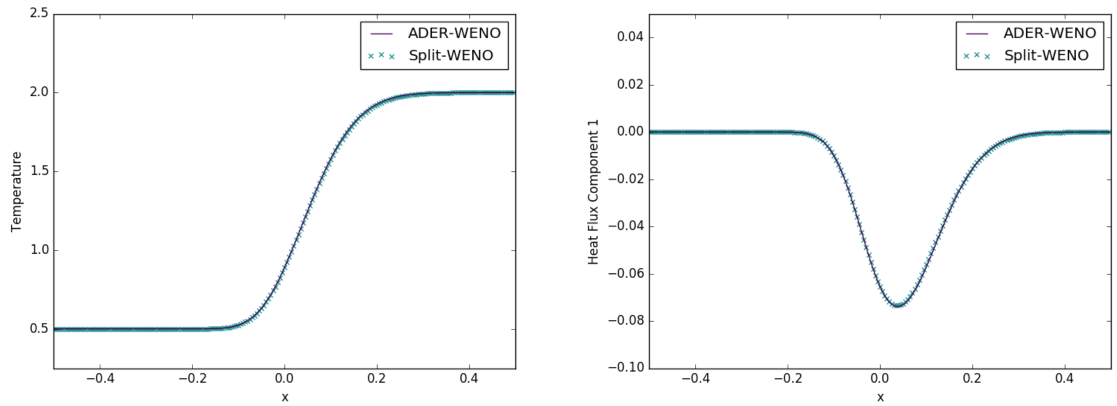

Figure 2.8: Results of solving the problem of Heat Conduction in Gas with both an ADER-WENO scheme and a Split-WENO scheme ($N = 2$)

	ADER-WENO	Split-WENO	Speed-up
Stokes' First Problem ($\mu = 10^{-2}$)	265s	38s	7.0
Stokes' First Problem ($\mu = 10^{-3}$)	294s	38s	7.7
Stokes' First Problem ($\mu = 10^{-4}$)	536s	38s	14.1
Viscous Shock	297s	56s	5.3
Heat Conduction in a Gas	544s	94s	5.8

Table 2.3: Wall time for various tests (all with 200 cells) under the ADER-WENO method and the Split-WENO method

2.3.1.6 Purely Elastic Riemann Problems

2.3.1.7 Convergence

To assess the rate of convergence of the Split-WENO method, the convected isentropic vortex convergence study from [14] was performed. The initial conditions are given as $\rho = 1 + \delta\rho$, $p = 1 + \delta p$, $\boldsymbol{v} = (1, 1, 0) + \delta\boldsymbol{v}$, $A = \sqrt[3]{\rho} I$, $\boldsymbol{J} = \boldsymbol{0}$, where:

$$\delta T = -\frac{(\gamma - 1)\,\epsilon^2}{8\gamma\pi^2} e^{1-r^2} \tag{2.140a}$$

$$\delta\rho = (1 + \delta T)^{\frac{1}{\gamma-1}} - 1 \tag{2.140b}$$

$$\delta p = (1 + \delta T)^{\frac{\gamma}{\gamma-1}} - 1 \tag{2.140c}$$

$$\delta\boldsymbol{v} = \frac{\epsilon}{2\pi} e^{\frac{1-r^2}{2}} \begin{pmatrix} -(y-5) \\ x-5 \\ 0 \end{pmatrix} \tag{2.140d}$$

The 2D domain is taken to be $[0, 10]^2$. ϵ is taken to be 5. The material parameters are taken to be: $\gamma = 1.4$, $c_v = 2.5$, $\rho_0 = 1$, $p_0 = 1$, $c_s = 0.5$, $\alpha = 1$, $\mu = 10^{-6}$, $\kappa = 10^{-6}$ (resulting in $\tau_1 = 2.4 \times 10^{-5}$, $\tau_2 = 10^{-6}$). Thus, this can be considered to be a stiff test case.

The convergence rates in the L_1, L_2, L_∞ norms for the density variable are given in Table 2.5 on page 54 and Table 2.6 on page 54 for WENO reconstruction polynomial orders of $N = 2$ and $N = 3$, respectively. As expected, both sets of tests attain roughly second order convergence. For comparison, the corresponding results for this test from [14] - solved using a third-order P2P2 scheme - are given in Table 2.7 on page 54 for comparison.

2.3.2 Non-Newtonian Fluids & Elastoplastic Solids

2.3.2.1 Strain Relaxation Test

Take initial data used by Barton:

$$A = \begin{pmatrix} 1 & 0 & 0 \\ -0.01 & 0.95 & 0.02 \\ -0.015 & 0 & 0.9 \end{pmatrix}^{-1} \tag{2.141}$$

	Timesteps (ADER-WENO)	Timesteps (Split-WENO)
Stokes' First Problem ($\mu = 10^{-2}$)	385	442
Stokes' First Problem ($\mu = 10^{-3}$)	386	443
Stokes' First Problem ($\mu = 10^{-4}$)	385	442
Viscous Shock	562	645
Heat Conduction in a Gas	942	1077

Table 2.4: Time steps taken for various tests (all with 200 cells) under the ADER-WENO method and the Split-WENO method

Grid Size	$\epsilon(L_1)$	$\epsilon(L_2)$	$\epsilon(L_\infty)$	$\mathcal{O}(L_1)$	$\mathcal{O}(L_2)$	$\mathcal{O}(L_\infty)$
20	2.87×10^{-3}	7.15×10^{-3}	6.21×10^{-2}			
40	5.81×10^{-4}	1.62×10^{-3}	1.73×10^{-2}	2.30	2.14	1.85
60	1.98×10^{-4}	5.39×10^{-4}	5.94×10^{-3}	2.65	2.70	2.63
80	1.23×10^{-4}	3.47×10^{-4}	3.41×10^{-3}	1.67	1.52	1.92

Table 2.5: Convergence rates for the Split-WENO method ($N = 2$)

Grid Size	$\epsilon(L_1)$	$\epsilon(L_2)$	$\epsilon(L_\infty)$	$\mathcal{O}(L_1)$	$\mathcal{O}(L_2)$	$\mathcal{O}(L_\infty)$
10	1.01×10^{-2}	2.58×10^{-2}	1.27×10^{-1}			
20	1.68×10^{-3}	4.02×10^{-3}	2.93×10^{-2}	2.59	2.68	2.11
30	5.34×10^{-4}	1.57×10^{-3}	1.70×10^{-2}	2.83	2.32	1.34
40	3.32×10^{-4}	8.94×10^{-4}	7.55×10^{-3}	1.65	1.95	2.82

Table 2.6: Convergence rates for the Split-WENO method ($N = 3$)

Grid Size	$\epsilon(L_1)$	$\epsilon(L_2)$	$\epsilon(L_\infty)$	$\mathcal{O}(L_1)$	$\mathcal{O}(L_2)$	$\mathcal{O}(L_\infty)$
20	9.44×10^{-3}	2.20×10^{-3}	2.16×10^{-3}			
40	1.95×10^{-3}	4.50×10^{-4}	4.27×10^{-4}	2.27	2.29	2.34
60	7.52×10^{-4}	1.74×10^{-4}	1.48×10^{-4}	2.35	2.35	2.61
80	3.72×10^{-4}	8.66×10^{-5}	7.40×10^{-5}	2.45	2.42	2.41

Table 2.7: Convergence rates for the ADER-DG PNPM method ($N, M = 2$)

The following parameter values were used: $\rho_0 = 1, c_s = 0.219, n = 4, \sigma_0 = 9 \times 10^{-4}, \tau_0 = 0.1$. As can be seen in Figure 2.9 on page 56, Figure 2.10 on page 56, and Figure 2.11 on page 56, the approximate analytic solver compares well with the exact solution for the distortion tensor A, and thus also the stress tensor and the energy.

2.3.2.2 Prandtl Boundary Layer

2.3.2.3 Poiseuille Flow

2.3.2.4 Elastoplastic Piston Test

In this test, a piston with speed 0.002 is driven into copper initially at rest. An elastic shock wave develops, followed by a plastic shock wave. The following parameters were used: $\rho_0 = 8.93, c_s = 0.219, n = 10, \sigma_0 = 9 \times 10^{-4}, \tau_0 = 0.1$. The shock Mie-Gruneisen EOS is used for the internal energy, with $p_0 = 0, c_0 = 0.394, \Gamma_0 = 2, s = 1.48$. Figure 2.12 on page 58 demonstrates the results using the split solver, compared with the ADER-WENO solution.

[RESULTS AS $n \to \infty$]

2.3.2.5 2D Elastoplastic Test

2.3.2.6 Convergence

2.4 Conclusions

In summary, a new numerical method based on an operator splitting, and including some analytical results, has been proposed for the GPR model of continuum mechanics. It has been demonstrated that this method is able to match current ADER-WENO methods in terms of accuracy on a range of test cases. It is significantly faster than the other currently available methods, and it is easier to implement. The author would recommend that if very high order-of-accuracy is required, and computational cost is not important, then ADER-WENO methods may present a better option, as by design the new method cannot achieve better than second-order accuracy. This new method clearly has applications in which it will prove useful, however.

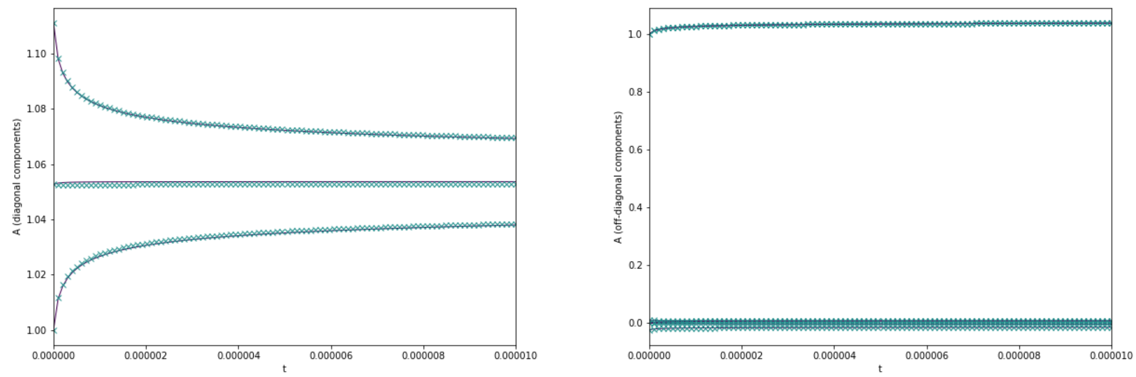

Figure 2.9: The distortion tensor during the Strain Relaxation Test

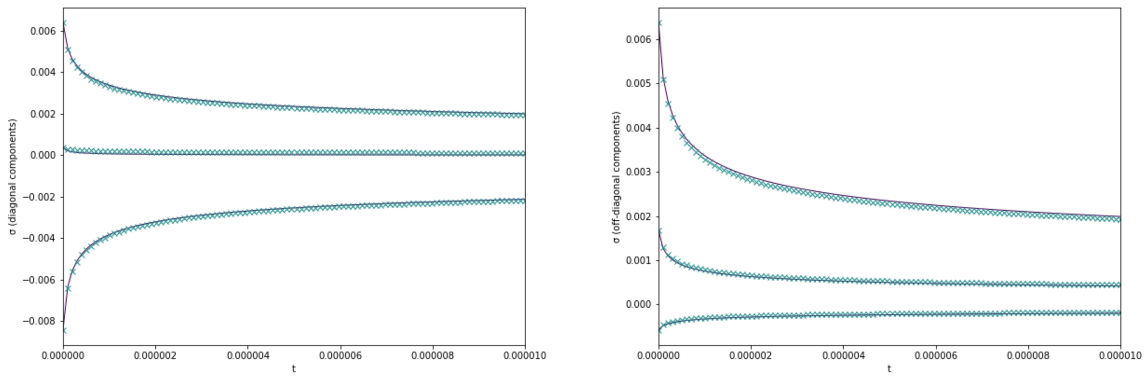

Figure 2.10: The stress tensor during the Strain Relaxation Test

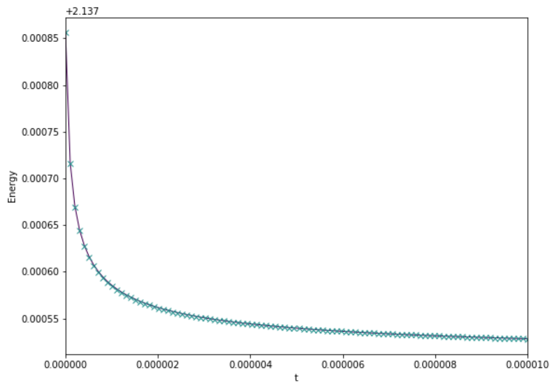

Figure 2.11: The total energy during the Strain Relaxation Test

In a similar manner to the operator splitting method presented in [29], the Split-WENO method is second-order accurate and stable even for very stiff problems (in particular, the reader is referred to the results of the $\mu = 10^{-4}$ variation of Stokes' First Problem in 2.3.1.2 and the convergence study in 2.3.1.7). However, it will inevitably suffer from the incorrect speed of propagation of discontinuities on regular, structured grids. This is due to a lack of spatial resolution in evaluating the source terms, as detailed in [29]. This issue can be rectified by the use of some form of shock tracking or mesh refinement, as noted in the cited paper. It is noted in [12] that operator splitting-based methods can result in schemes that are neither well-balanced nor asymptotically consistent. The extent to which these two conditions are violated by the Split-WENO method - and the severity in practice of any potential violation - is a topic of further research.

It should be noted that the assumption (2.85) used to derive the approximate analytical solver may break down for situations where the flow is compressed heavily in one direction but not the others. The reason for this is that one of the singular values of the distortion tensor will be much larger than the others, and the mean of the squares of the singular values will not be close to its geometric mean, meaning that the subsequent linearization of the ODE governing the mean of the singular values fails. It should be noted that none of the situations covered in this study presented problems for the approximate analytical solver, and situations which may be problematic are in some sense unusual. In any case, a stiff ODE solver can be used to solve the system (2.67) if necessary, utilizing the Jacobians derived in the appendix, and so the Split-WENO method is still very much usable in these situations, albeit slightly slower.

It should be noted that both the ADER-WENO and Split-WENO methods, as described in this study, are trivially parallelizable on a cell-wise basis. Thus, given a large number of computational cores, deficiencies in the Split-WENO method in terms of its order of accuracy may be overcome by utilizing a larger number of computational cells and cores. The computational cost of each time step is significantly smaller than with the ADER-WENO method, and the number of grid cells that can be used scales roughly linearly with number of cores, at constant time per iteration.

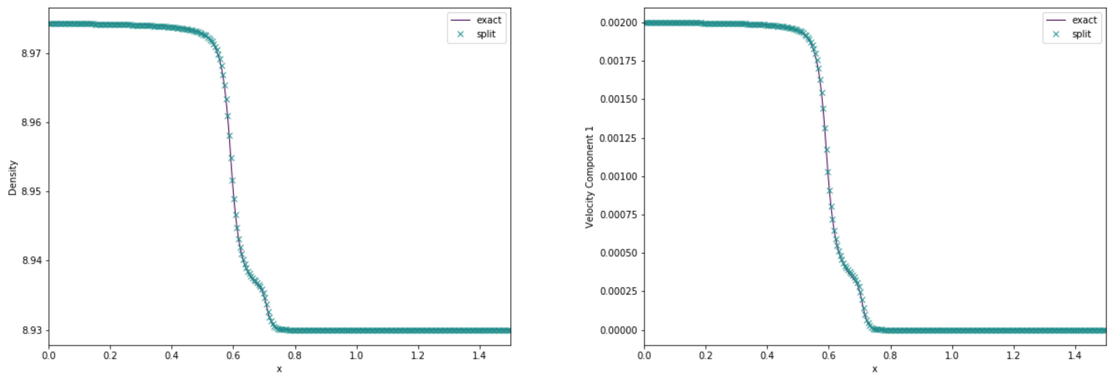

Figure 2.12: Density and velocity in the elastoplastic piston test

Chapter 3

Objective 3: Simulating Material Interfaces

3.1 Ghost Fluid Methods

3.1.1 Level Set Methods

Given a function $\phi : \mathbb{R}^n \to \mathbb{R}$, the level set of ϕ at level c is defined as:

$$\Gamma_c = \{\boldsymbol{x} : \phi(\boldsymbol{x}) = c\} \tag{3.1}$$

In this study, problems involving m different materials were assigned the functions $\phi_1, \ldots, \phi_{m-1} : \mathbb{R}^n \to \mathbb{R}$, such that the region occupied by material i is considered to be exactly that in which $\phi_1, \ldots, \phi_{i-1} > 0$, $\phi_i, \ldots, \phi_{m-1} < 0$. The locations of the zero level sets correspond to the locations of the interfaces.

Given the local velocity field $\boldsymbol{v} : \mathbb{R}^n \to \mathbb{R}^3$, the functions ϕ are advected according to the level set equation [40]:

$$\frac{\partial \phi}{\partial t} = \boldsymbol{v} \cdot \nabla \phi \tag{3.2}$$

$\phi_1, \ldots, \phi_{m-1}$ are renormalized to resemble a straight line at every time step, to avoid unwanted distortions such as becoming a multivalued function.

3.1.2 The Original Ghost Fluid Method

The Original Ghost Fluid Method of Fedkiw et al. [19] (an adaptation of the work of Glimm et al. [22]) is a numerical method for the Euler equations for simulating interfaces between multiple materials. The primitive variables for the Euler equations in 1D are given by $\boldsymbol{P} = \begin{pmatrix} \rho & v & p \end{pmatrix}^T$.

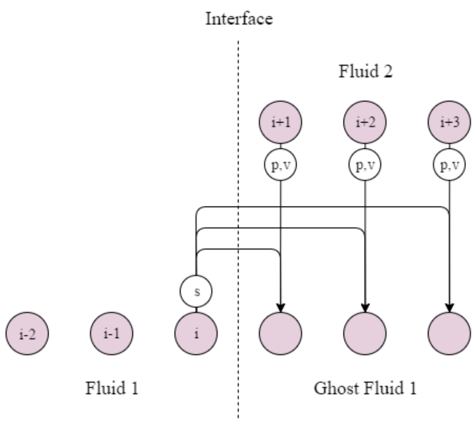

Figure 3.1: The Original Ghost Fluid Method

Suppose the interface between two fluids is modeled on spatial domain $[0, 1]$, divided into N cells with width $\Delta x = \frac{1}{N}$. Let the time step be Δt and let $\boldsymbol{P}_i^n$ be the set of primitive variables in cell i at time $t_n = n\Delta t$. Let the level set function f have root x_n where $x_n \in \left[\left(i + \frac{1}{2}\right)\Delta x, \left(i + \frac{3}{2}\right)\Delta x\right]$. Thus, at time t_n the interface lies between the cells with primitive variables $\boldsymbol{P}_i^n, \boldsymbol{P}_{i+1}^n$. Define two sets of primitive variables:

$$\boldsymbol{P}_j^{(1)} = \begin{cases} \boldsymbol{P}_j^n & j \leq i \\ \left(\rho\left(s_i^n, p_j^n, \gamma_i^n\right) \; v_j^n \; p_j^n\right) & j > i \end{cases} \tag{3.3}$$

$$\boldsymbol{P}_j^{(2)} = \begin{cases} \boldsymbol{P}_j^n & j \geq i+1 \\ \left(\rho\left(s_{i+1}^n, p_j^n, \gamma_{i+1}^n\right) \; v_j^n \; p_j^n\right) & j < i+1 \end{cases} \tag{3.4}$$

where:

$$\rho\left(s, p, \gamma\right) = \left(\frac{p}{s}\right)^{\frac{1}{\gamma}} \tag{3.5}$$

All cells in $\boldsymbol{P}^{(1)}$ to the left of the interface have the same state variables as those of $\boldsymbol{P}^n$. All cells to the right have the same pressure and velocity as their counterparts in $\boldsymbol{P}^n$, but the same entropy as $\boldsymbol{P}_i^n$. This affects their density. The situation is analogous for $\boldsymbol{P}^{(2)}$. This is demonstrated in Figure 3.1 on page 60.

$\boldsymbol{P}^{(1)}, \boldsymbol{P}^{(2)}$ are stepped forward by time step Δt using a standard Eulerian method. f is advected using (3.2), taking the velocity in each cell to be that of $\boldsymbol{P}^n$. Now let $f\left(x_{n+1}\right) = 0$

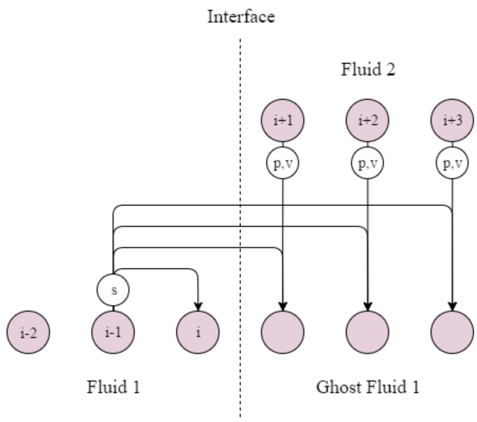

Figure 3.2: The Original Ghost Fluid Method, with the isobaric fix

where $x_{n+1} \in \left[\left(k+\frac{1}{2}\right)\Delta x, \left(k+\frac{3}{2}\right)\Delta x\right]$ for some k. Define:

$$\boldsymbol{P}_j^{n+1} = \begin{cases} \boldsymbol{P}_j^{(1)} & j \leq k \\ \boldsymbol{P}_j^{(2)} & j > k \end{cases} \tag{3.6}$$

The rationale behind the original GFM is that in most applications, pressure and velocity are continuous across the interface, and thus the ghost cells may take the real pressure and velocity values. Entropy is generally discontinuous at a contact discontinuity, resulting in large truncation errors if a standard finite difference scheme is used to solve the system. Thus, entropy is extrapolated as a constant from the interface boundary cell into the ghost region.

Fedkiw et al. advised to use the *isobaric fix* technique. This involves setting the entropy of cell i, and all cells in the right ghost region, to that of cell $i-1$, and setting the entropy of cell $i+1$, and all cells in the left ghost region, to that of cell $i+2$. This is demonstrated in Figure 3.2 on page 61.

Effectively, the ghost regions behave like they are composed of the same fluid as the regions they extend (as they have the same entropy), facilitating calculation of the next time step, but they have the same pressure and velocity profiles as the real fluids they replace, meaning the boundary conditions at the interface are upheld.

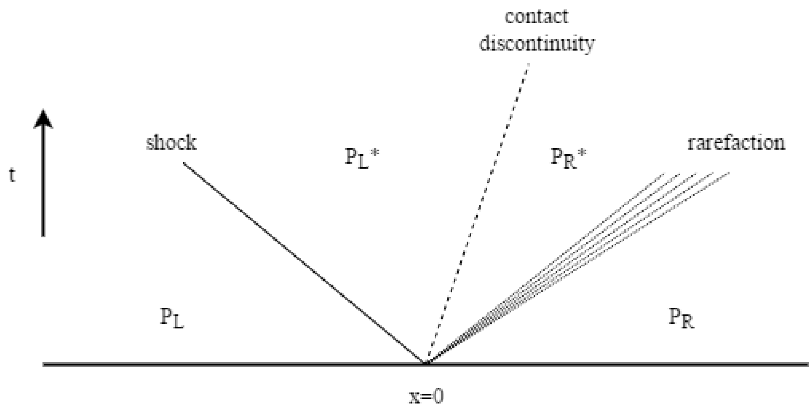

Figure 3.3: The qualitative structure of the solution to the Riemann Problem, showing the different possible types of waves

3.1.3 The Riemann Ghost Fluid Method

The Riemann Problem in its general form is the solution of the following initial value problem. Given a set of variables $\boldsymbol{P}$ dependent on space and time, and a hyperbolic set of equations which govern their spatio-temporal evolution, $\boldsymbol{P}(x,t)$ is sought for $t > 0$, given the initial condition:

$$\boldsymbol{P}(x,0) = \begin{cases} \boldsymbol{P_L} & x < 0 \\ \boldsymbol{P_R} & x > 0 \end{cases} \tag{3.7}$$

This problem is denoted by $RP(\boldsymbol{P_L}, \boldsymbol{P_R})$. Exact solvers exist for the Riemann Problem for various sets of governing equations, such as the Euler equations [47], the equations of non-linear elasticity [4], or the shallow water equations [1], among others. There also exist approximate solvers for general conservative [31, 35] or non-conservative [8] hyperbolic systems of PDEs. The references given here form a very small sample of the work that has been done in this area.

The solution of the Riemann Problem usually takes the form of a set of waves, between which $\boldsymbol{P}$ is constant. The waves can either be a contact discontinuity (across which pressure and velocity are continuous), a shock (across which all variables may be discontinuous), or a rarefaction (along which the variables vary continuously between their values on either side of the wave). The number and form of the waves are determined by the governing equations and the initial conditions. The states of the variables either side of the contact discontinuity

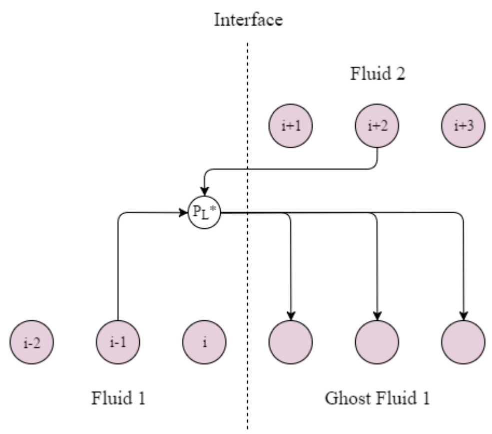

Figure 3.4: The Riemann Ghost Fluid Method

in the middle are known as the *star states*. This qualitative description is depicted in Figure 3.3 on page 62.

Liu et al. [30] demonstrated that the original GFM fails to resolve strong shocks at material interfaces. This is because the method effectively solves two separate single-fluid Riemann problems. The waves present in these Riemann problems do not necessarily correspond to those in the real Riemann problem across the interface. The Riemann Ghost Fluid Method of Sambasivan et al. [45, 46] aims to rectify this.

Given $\boldsymbol{P}^n$ and $x_n \in \left[\left(i+\frac{1}{2}\right)\Delta x, \left(i+\frac{3}{2}\right)\Delta x\right]$, the ghost cells for fluid 1 are populated with the left star state of $RP\left(\boldsymbol{P}_{i-1}^n, \boldsymbol{P}_{i+2}^n\right)$, and the ghost cells for fluid 2 are populated with the right star state. $RP\left(\boldsymbol{P}_{i-1}^n, \boldsymbol{P}_{i+2}^n\right)$ is solved rather than $RP\left(\boldsymbol{P}_{i}^n, \boldsymbol{P}_{i+1}^n\right)$, as $\boldsymbol{P}_{i}^n, \boldsymbol{P}_{i+1}^n$ often contain errors generated by the fact that they lie on the material interface. $\boldsymbol{P}^{n+1}$ is then generated as before from the newly formed $\boldsymbol{P}^{(1)}, \boldsymbol{P}^{(2)}$. This process is demonstrated in Figure 3.4 on page 63.

3.2 A Riemann Ghost Fluid Method for the GPR Model

3.2.1 Solving the Riemann Problem

Barton et al. have presented an RGFM for the equations of non-linear elasticity [3, 6]. Owing to the similarity of the structure of the non-linear elasticity equations to those of the GPR model (differing only in the presence of source terms and the form of the shear stress tensor,

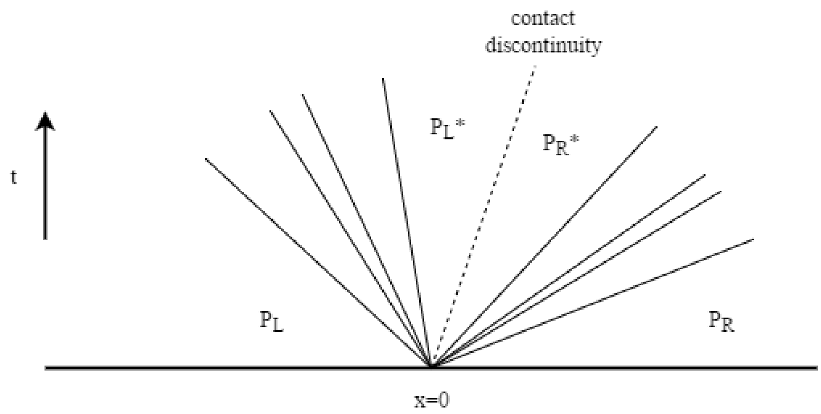

Figure 3.5: The Riemann Problem for the GPR model, assuming all waves are distinct

and possibly the EOS), their method is built upon here. The resulting method is named *the GPR-RGFM*.

The Riemann Problem of the GPR model takes the form demonstrated in Figure 3.5 on page 64. Assuming all waves are distinct, there are four waves on either side of the contact discontinuity. On each side, one wave corresponds to the thermal impulse (manifesting as a heat wave) and the other three correspond to the distortion components in the axis in which the Riemann Problem is considered (manifesting as two shear waves and one longitudinal pressure wave). In the following the effect of the source terms on the solution to the RP is neglected. This is thought to be a reasonable assumption for the problem at hand, as only the star states are required, and the time step over which the RP is taken is very small. The method is presented here along the first spatial axis. It can easily be adapted along any axis.

Denote the vector of primitive variables by $\boldsymbol{P}$. Take the set of left eigenvectors L (B.25) with eigenvalues $\{\lambda_i\}$. We have the standard set of relations along characteristics (curves along which $\frac{dx}{dt} = \lambda_i$):[1]

$$L \cdot d\boldsymbol{P} = dt \cdot L \cdot \boldsymbol{S} \tag{3.8}$$

[1]Take the hyperbolic system $\frac{\partial \boldsymbol{P}}{\partial t} + M \frac{\partial \boldsymbol{P}}{\partial x} = \boldsymbol{S}$. Let ${\boldsymbol{l_i}}^T M = \lambda_i {\boldsymbol{l_i}}^T$. Along characteristics corresponding to λ_i:

$$\begin{aligned} \boldsymbol{l_i^T} \left(\frac{\partial \boldsymbol{P}}{\partial t} + M \frac{\partial \boldsymbol{P}}{\partial x} \right) &= \boldsymbol{l_i^T} \left(\frac{\partial \boldsymbol{P}}{\partial t} + \frac{dx}{dt} \frac{\partial \boldsymbol{P}}{\partial x} \right) \\ &= \boldsymbol{l_i^T} \frac{d\boldsymbol{P}}{dt} = \boldsymbol{l_i^T} \boldsymbol{S} \end{aligned}$$

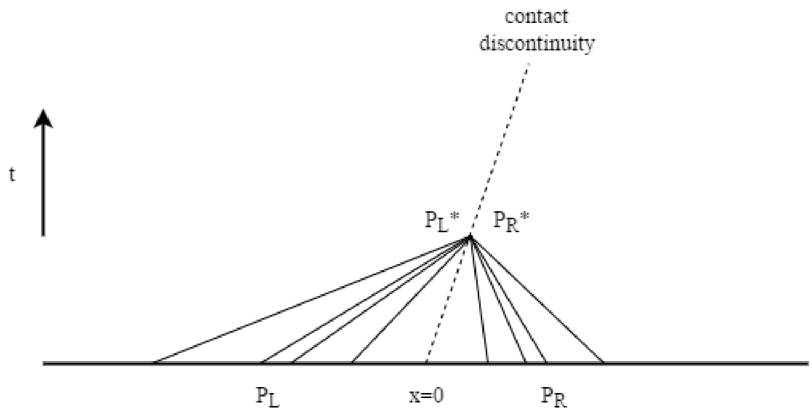

Figure 3.6: Different sets of characteristic curves, traveling from their respective initial points to the star region

$\boldsymbol{P_K^*}$ is now sought, where $K = L$ or $K = R$, denoting the left or right sides of the interface, respectively. Take the following linearization:

$$d\boldsymbol{P} \approx \boldsymbol{P_K^*} - \boldsymbol{P_K} \tag{3.9}$$

13 relations from (3.8) are taken: four regarding the 4 sets of characteristics traveling into the contact discontinuity from side K (with speeds greater or less than v for $K = L$ or $K = R$, respectively), and nine relating to the contact discontinuity itself. This is demonstrated in Figure 3.6 on page 65. Four more relations must be derived to solve the system for $\boldsymbol{P_K^*}$. Expanding the Taylor series of $\boldsymbol{\Sigma}^*, T^*$:

$$\Sigma^* = \Sigma + (\rho^* - \rho)\frac{\partial \Sigma}{\partial \rho} + (p^* - p)\frac{\partial \Sigma}{\partial p} + (A_{mn}^* - A_{mn})\frac{\partial \Sigma}{\partial A_{mn}} + O\left(d\boldsymbol{P}^2\right) \tag{3.10a}$$

$$T^* = T + (\rho^* - \rho)\frac{\partial T}{\partial \rho} + (p^* - p)\frac{\partial T}{\partial p} + O\left(d\boldsymbol{P}^2\right) \tag{3.10b}$$

Thus, we have:

$$\Sigma^* - \Sigma \approx -(\rho^* - \rho)\frac{\partial \sigma}{\partial \rho} + (p^* - p)\, I - (A_{mn}^* - A_{mn})\frac{\partial \sigma}{\partial A_{mn}} \tag{3.11a}$$

$$T^* - T \approx (\rho^* - \rho)\frac{\partial T}{\partial \rho} + (p^* - p)\frac{\partial T}{\partial p} \tag{3.11b}$$

These are the extra required relations. Let $\boldsymbol{n}$ be the normal to the boundary. Then we have:

$$\hat{L}_K \cdot \left(\boldsymbol{P_K^*} - \boldsymbol{P_K}\right) = \boldsymbol{c_K} \tag{3.12}$$

where $\hat{L}_K$ takes the form found in (3.17), with $\xi = -1$ for $K = R$ and $\xi = 1$ for $K = L$, and:

$$\boldsymbol{c_K} = \begin{pmatrix} \left(\Sigma_K^* - \Sigma_K\right) \cdot \boldsymbol{n} \\ T_K^* - T_K \\ dt \cdot \left(L_K \cdot \boldsymbol{S_K}\right)_{5:17} \end{pmatrix} \tag{3.13}$$

The inverse of $\hat{L}_K$ takes the form found in (3.18).

$\hat{L}_K, \hat{L}_K^{-1}$ are evaluated at $\boldsymbol{P_K}$. It remains to find expressions for $\Sigma^* \cdot \boldsymbol{n}$ and T^* in terms of $\boldsymbol{P_L}, \boldsymbol{P_R}$ to close the system. The following boundary conditions are used:

$$\Sigma_L^* \cdot \boldsymbol{n} = \Sigma_R^* \cdot \boldsymbol{n} \tag{3.14a}$$
$$T_L^* = T_R^* \tag{3.14b}$$
$$\boldsymbol{v_L^*} = \boldsymbol{v_R^*} \tag{3.14c}$$
$$\alpha^2 \boldsymbol{J}_L^* \cdot \boldsymbol{n} = \alpha^2 \boldsymbol{J}_R^* \cdot \boldsymbol{n} \tag{3.14d}$$

Taking the relevant rows of $\boldsymbol{P_K^*} = \boldsymbol{P_K} + \hat{L}_K^{-1} \boldsymbol{c_K}$:

$$\begin{aligned} \begin{pmatrix} \boldsymbol{v}^* \\ \boldsymbol{J}^* \cdot \boldsymbol{n} \end{pmatrix} = \begin{pmatrix} \boldsymbol{v_K} \\ \boldsymbol{J}_K \cdot \boldsymbol{n} \end{pmatrix} &+ Y_K \left(\begin{pmatrix} \Sigma^* \cdot \boldsymbol{n} \\ T^* \end{pmatrix} - \begin{pmatrix} \Sigma_K \cdot \boldsymbol{n} \\ T_K \end{pmatrix} \right) \\ &+ dt \cdot \xi_K \cdot Q_K^{-1} \left(L_K \cdot \boldsymbol{S_K}\right)_{5:8} \end{aligned} \tag{3.15}$$

Thus, using the boundary conditions:

$$\begin{pmatrix} \Sigma^* \cdot \boldsymbol{n} \\ T^* \end{pmatrix} = \left(Y_L - Y_R\right)^{-1} \begin{pmatrix} \begin{pmatrix} \boldsymbol{v_R} \\ \boldsymbol{J}_R \cdot \boldsymbol{n} \end{pmatrix} - \begin{pmatrix} \boldsymbol{v_L} \\ \boldsymbol{J}_L \cdot \boldsymbol{n} \end{pmatrix} \\ +dt \left(Q_R^{-1} \left(L_R \cdot \boldsymbol{S_R}\right)_{5:8} + Q_L^{-1} \left(L_L \cdot \boldsymbol{S_L}\right)_{5:8} \right) \\ +Y_L \begin{pmatrix} \Sigma_L \cdot \boldsymbol{n} \\ T_L \end{pmatrix} - Y_R \begin{pmatrix} \Sigma_R \cdot \boldsymbol{n} \\ T_R \end{pmatrix} \end{pmatrix} \tag{3.16}$$

Thus, $\boldsymbol{P_L^*}, \boldsymbol{P_R^*}$ are obtained with (3.12) and used in the RGFM, as described in Section 3.1.

It may be necessary to iterate this process a few times to ensure convergence to star states for which the boundary conditions hold.

3.2.2 Linear Conditions

Replacing the first four lines of (B.25) with the conditions

$$\hat{L}_K = \left\{ \begin{matrix} \begin{pmatrix} -\frac{\partial \boldsymbol{\sigma_d}}{\partial \rho} & \boldsymbol{e_d} & -\Pi_1 & -\Pi_2 & -\Pi_3 & 0_{3,6} \\ \frac{\partial T}{\partial \rho} & \frac{\partial T}{\partial p} & 0_{1,3} & 0_{1,3} & 0_{1,3} & 0_{1,6} \end{pmatrix} \\ \begin{pmatrix} Q\Xi_1 & -\frac{1}{\rho}Q_{:,1:3}\Pi_2 & -\frac{1}{\rho}Q_{:,1:3}\Pi_3 & \xi DQ & 0_{4,2} \end{pmatrix} \\ \begin{pmatrix} -\frac{1}{\rho} & 0 & \boldsymbol{e_d^T} A^{-1} & \boldsymbol{e_d^T} A^{-1}\Pi_1^{-1}\Pi_2 & \boldsymbol{e_d^T} A^{-1}\Pi_1^{-1}\Pi_3 & 0_{1,6} \end{pmatrix} \\ \begin{pmatrix} 0_{3,5} & I_3 & 0_{3,3} & 0_{3,6} \\ 0_{3,5} & 0_{3,3} & I_3 & 0_{3,6} \end{pmatrix} \\ \begin{pmatrix} 0_{2,15} & I_2 \end{pmatrix} \end{matrix} \right\} \tag{3.17}$$

$$\hat{L}_K^{-1} = \left\{ \begin{pmatrix} X \\ 0_{6,4} \\ Y \\ 0_{2,4} \end{pmatrix}, \begin{pmatrix} 0_{11,4} \\ \xi (DQ)^{-1} \\ 0_{2,4} \end{pmatrix}, \begin{pmatrix} -cT_p \\ cT_\rho \\ c\Pi_d^{-1}\boldsymbol{w} \\ 0_{12,1} \end{pmatrix}, \begin{pmatrix} 0_{2,3} & 0_{2,3} \\ -\Pi_1^{-1}\Pi_2 & -\Pi_1^{-1}\Pi_3 \\ I_3 & 0_{3,3} \\ 0_{3,3} & I_3 \\ 0_{6,3} & 0_{6,3} \end{pmatrix}, \begin{pmatrix} 0_{15,2} \\ I_2 \end{pmatrix} \right\} \tag{3.18}$$

where:

$$X = \begin{pmatrix} \vdots & \vdots & \ddots & \vdots & \iddots \\ -\frac{\partial \boldsymbol{\sigma_d}}{\partial \rho} & \boldsymbol{e_d} & \cdots & -\Pi_1 & \cdots \\ \vdots & \vdots & \iddots & \vdots & \ddots \\ \frac{\partial T}{\partial \rho} & \frac{\partial T}{\partial p} & 0 & 0 & 0 \\ -\frac{1}{\rho} & 0 & \cdots & \boldsymbol{e_d^T} A^{-1} & \cdots \end{pmatrix}^{-1} \begin{pmatrix} 1 & 0 & 0 & 0 \\ 0 & 1 & 0 & 0 \\ 0 & 0 & 1 & 0 \\ 0 & 0 & 0 & 1 \\ 0 & 0 & 0 & 0 \end{pmatrix} \tag{3.19a}$$

$$Y = -\xi Q^{-1} D^{-1} Q \Xi_1 X \tag{3.19b}$$

By inversion of block matrices[2]:

$$\begin{pmatrix} \vdots & \vdots & \ddots & \vdots & \cdots \\ -\frac{\partial \boldsymbol{\sigma_d}}{\partial \rho} & \boldsymbol{e_d} & \cdots & -\Pi_1 & \cdots \\ \vdots & \vdots & \cdots & \vdots & \ddots \\ \frac{\partial T}{\partial \rho} & \frac{\partial T}{\partial p} & 0 & 0 & 0 \\ -\frac{1}{\rho} & 0 & \cdots & \boldsymbol{e_d^T} A^{-1} & \cdots \end{pmatrix}^{-1} = \begin{pmatrix} D^{-1}CZ^{-1} & D^{-1}\left(I - CZ^{-1}BD^{-1}\right) \\ -Z^{-1} & Z^{-1}BD^{-1} \end{pmatrix} \tag{3.20}$$

where

$$B = \begin{pmatrix} \vdots & \vdots \\ -\frac{\partial \boldsymbol{\sigma_d}}{\partial \rho} & \boldsymbol{e_d} \\ \vdots & \vdots \end{pmatrix} \tag{3.21a}$$

$$C = \begin{pmatrix} 0 & 0 & 0 \\ \cdots & \boldsymbol{e_d^T} A^{-1} & \cdots \end{pmatrix} \tag{3.21b}$$

$$D = \begin{pmatrix} \frac{\partial T}{\partial \rho} & \frac{\partial T}{\partial p} \\ -\frac{1}{\rho} & 0 \end{pmatrix} \tag{3.21c}$$

$$Z = \Pi_1 + \frac{\rho}{T_p}\left(T_p \frac{\partial \boldsymbol{\sigma_d}}{\partial \rho} + T_\rho \boldsymbol{e_d}\right) \boldsymbol{e_d^T} A^{-1} \tag{3.21d}$$

3.2.3 The Case without Heat Conduction

If the heat conduction terms are dropped from the GPR model, the eigenstructure of the system changes, along with the solution of the linear conditions. Ξ retains the same definition, but is now a 3×3 matrix (comprising the top-left corner of Ξ under heat conduction). Thus,

[2] $\begin{pmatrix} A & B \\ C & D \end{pmatrix}^{-1} = \begin{pmatrix} \left(A - BD^{-1}C\right)^{-1} & -\left(A - BD^{-1}C\right)^{-1} BD^{-1} \\ -D^{-1}C\left(A - BD^{-1}C\right)^{-1} & D^{-1}\left(I + C\left(A - BD^{-1}C\right)^{-1} BD^{-1}\right) \end{pmatrix}$

Q, D are also 3×3 matrices. Taking the eigenvectors (B.38), the linear conditions become:

$$
\hat{L}_K = \left\{ \begin{array}{c}
\begin{pmatrix} -\frac{\partial \boldsymbol{\sigma_d}}{\partial \rho} & \boldsymbol{e_d} & -\Pi_1 & -\Pi_2 & -\Pi_3 \end{pmatrix} \\
\begin{pmatrix} Q\Xi_1 & -\frac{1}{\rho} Q\Pi_2 & -\frac{1}{\rho} Q\Pi_3 & \xi DQ \end{pmatrix} \\
\left(I - BA^{-1}C\right)^{-1} \begin{pmatrix} I_2 & -BA^{-1} & -BA^{-1}\Pi_1^{-1}\Pi_2 & -BA^{-1}\Pi_1^{-1}\Pi_3 & 0_{2,3} \end{pmatrix} \\
\begin{pmatrix} 0_{3,5} & I_3 & 0_{3,3} & 0_{3,3} \\ 0_{3,5} & 0_{3,3} & I_3 & 0_{3,3} \end{pmatrix}
\end{array} \right\} \tag{3.22}
$$

$$
\hat{L}_K^{-1} = \left\{ \begin{pmatrix} X \\ 0_{6,3} \\ Y \end{pmatrix}, \begin{pmatrix} 0_{11,3} \\ \xi \left(DQ\right)^{-1} \end{pmatrix}, \begin{pmatrix} 1 & 0 \\ 0 & 1 \\ -\Pi_1^{-1} \frac{\partial \boldsymbol{\sigma_1}}{\partial \rho} & \Pi_1^{-1} \boldsymbol{e_1} \\ \boldsymbol{0_9} & \boldsymbol{0_9} \end{pmatrix}, \begin{pmatrix} 0_{2,3} & 0_{2,3} \\ -\Pi_1^{-1}\Pi_2 & -\Pi_1^{-1}\Pi_3 \\ I_3 & 0_{3,3} \\ 0_{3,3} & I_3 \\ 0_{3,3} & 0_{3,3} \end{pmatrix} \right\} \tag{3.23}
$$

where:

$$
X = \begin{pmatrix}
\vdots & \vdots \ \ddots & \vdots & \iddots \\
-\frac{\partial \boldsymbol{\sigma_d}}{\partial \rho} & \boldsymbol{e_d} \ \cdots & -\Pi_1 & \cdots \\
\vdots & \vdots \ \iddots & \vdots & \ddots \\
\vdots & \iddots \ \ddots & \vdots & \iddots \\
\left(I - BA^{-1}C\right)^{-1} & \cdots \ \cdots & -\left(I - BA^{-1}C\right)^{-1} BA^{-1} & \cdots
\end{pmatrix}^{-1}
\begin{pmatrix} 1 & 0 & 0 & 0 \\ 0 & 1 & 0 & 0 \\ 0 & 0 & 1 & 0 \\ 0 & 0 & 0 & 1 \\ 0 & 0 & 0 & 0 \end{pmatrix} \tag{3.24a}
$$

$$
Y = -\xi Q^{-1} D^{-1} Q \Xi_1 X \tag{3.24b}
$$

By inversion of block matrices:

$$
\begin{pmatrix}
\vdots & \vdots \ \ddots & \vdots & \iddots \\
-\frac{\partial \boldsymbol{\sigma_d}}{\partial \rho} & \boldsymbol{e_d} \ \cdots & -\Pi_1 & \cdots \\
\vdots & \vdots \ \iddots & \vdots & \ddots \\
\vdots & \iddots \ \ddots & \vdots & \iddots \\
\left(I - BA^{-1}C\right)^{-1} & \cdots \ \cdots & -\left(I - BA^{-1}C\right)^{-1} BA^{-1} & \cdots
\end{pmatrix}^{-1}
= \left(\begin{array}{cc} -BA^{-1}\left(\Pi_1 - \tilde{B}BA^{-1}\right)^{-1} & \left(I + BA^{-1} \right. \\ -\left(\Pi_1 - \tilde{B}BA^{-1}\right)^{-1} & \left(\Pi_1 - \right. \end{array} \right. \tag{3.25}
$$

where

$$\tilde{B} = \begin{pmatrix} \cdots & -\frac{\partial \boldsymbol{\sigma_1}}{\partial \rho} & \cdots \\ \cdots & \boldsymbol{e_1} & \cdots \end{pmatrix}^T \tag{3.26a}$$

$$B = \begin{pmatrix} \rho & 0 & 0 \\ \left(\rho c_0^2 + \sigma_{11} - \rho \frac{\partial \sigma_{11}}{\partial \rho}\right) & \left(\sigma_{21} - \rho \frac{\partial \sigma_{21}}{\partial \rho}\right) & \left(\sigma_{31} - \rho \frac{\partial \sigma_{31}}{\partial \rho}\right) \end{pmatrix} \tag{3.26b}$$

3.3 Numerical Results

The GPR-RGFM is now assessed. The first two tests in this chapter are standard Riemann problems, exact solutions to which exist for the Euler equations. The viscosity of the GPR model smears the solutions in areas in which the solutions to the Euler equations are discontinuous or not smooth. This smearing is not the result of using a low-order solver (all results in these sections being calculated to third order). The last two tests assess the ability of the GPR-RGFM to correctly model heat conduction across interfaces.

3.3.1 Helium Bubble

The interface between two different gases is now modeled. As in Test B of Wang et al. [48], a bubble of helium - surrounded by air - initially occupies the region $x \in [0.4, 0.6]$. A shock front in the air, initially at $x = 0.05$, travels towards the helium bubble. The initial conditions are given in Table 3.1 on page 72. Realistic material parameters are taken for the helium: $\gamma = 1.66$, $c_v = 3127$, $\rho_0 = 0.163$, $\mu = 1.99 \times 10^{-5}$, $P_r = 0.688$, and for the air: $\gamma = 1.4$, $c_v = 721$, $\rho_0 = 1.18$, $\mu = 1.85 \times 10^{-5}$, $P_r = 0.714$. In both cases, $p_0 = 101325$, $c_s = 55$, and $\alpha = 500$.

200 cells are used. The results for times $t = 7 \times 10^{-4}$ and $t = 14 \times 10^{-4}$ are displayed in Figure 3.7 on page 71. In the former, the shock is about to hit the helium bubble (corresponding to the region of low density). In the latter, the shock has traveled through the helium bubble, compressing it slightly, and the bubble itself has moved almost 0.1 spatial units to the right. There is good correspondence with the results in [48] and the sharp discontinuity in density is maintained.

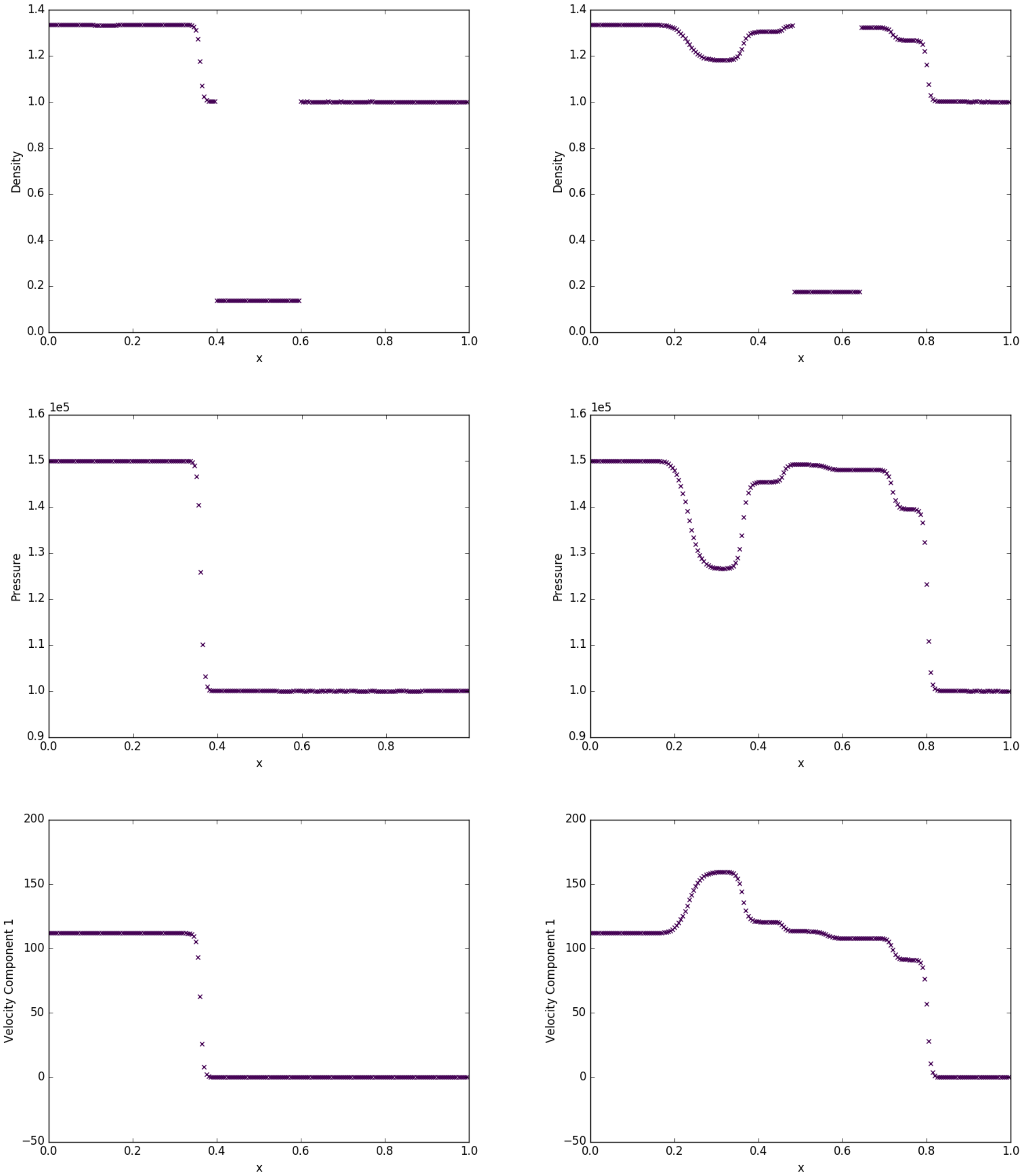

Figure 3.7: Density, pressure, and velocity for the helium bubble test with GPR-RGFM at times $t = 7 \times 10^{-4}$ (left) and $t = 14 \times 10^{-4}$ (right)

	ρ	p	$\boldsymbol{v}$	A	$\boldsymbol{J}$
$x < 0.05$	1.3333	1.5×10^5	$\begin{pmatrix} 35.35\sqrt{10} & 0 & 0 \end{pmatrix}$	$\left(\frac{1.3333}{1.18}\right)^{\frac{1}{3}} I_3$	$\mathbf{0}$
$0.05 \leq x < 0.4$	1	10^5	$\mathbf{0}$	$\left(\frac{1}{1.18}\right)^{\frac{1}{3}} I_3$	$\mathbf{0}$
$0.4 \leq x < 0.6$	0.1379	10^5	$\mathbf{0}$	$\left(\frac{0.1379}{0.163}\right)^{\frac{1}{3}} I_3$	$\mathbf{0}$
$0.6 \leq x \leq 1$	1	10^5	$\mathbf{0}$	$\left(\frac{1}{1.18}\right)^{\frac{1}{3}} I_3$	$\mathbf{0}$

Table 3.1: Initial conditions for the helium bubble test

	ρ	p	$\boldsymbol{v}$	A	$\boldsymbol{J}$
$0 \leq x < 0.7$	1000	10^9	$\mathbf{0}$	I_3	$\mathbf{0}$
$0.7 \leq x \leq 1$	50	10^5	$\mathbf{0}$	$\sqrt[3]{50} \cdot I_3$	$\mathbf{0}$

Table 3.2: Initial conditions for the water-air shock tube test

3.3.2 Water-Air Shock Tube

This test comprises an interface between water and air, with initial data taken from Chinnayya et al. [REF]. Due to the large difference in state variables are qualitative characteristics of the two fluids, this is an example of a test with which the original GFM does not perform well. The results using the GPR-RGFM are shown, along with the exact solution to the Euler equations.

3.3.3 Copper-PBX Impact

3.3.4 Aluminium in Vacuum

3.3.5 Heat Conduction in a Gas

This test is based on the Heat Conduction in a Gas Test of Dumbser et al. [14]. Two ideal gases at different temperatures are initially in contact at position $x = 0$. The initial conditions for this problem are given in Table 3.3 on page 73.

The material parameters are taken to be: $\gamma = 1.4$, $c_v = 2.5$, $\rho_0 = 1$, $p_0 = 1$, $c_s = 1$, $\alpha = 2$, $\mu = 10^{-2}$, $\kappa = 10^{-2}$. An interface is initially placed between the two volumes of air at $x = 0.5$. The final time is taken to be $t = 1$, and 200 cells are used. Results are displayed

	ρ	p	$\boldsymbol{v}$	A	$\boldsymbol{J}$
$x < 0$	2	1	$\mathbf{0}$	$\sqrt[3]{2} \cdot I_3$	$\mathbf{0}$
$x \geq 0$	0.5	1	$\mathbf{0}$	$\frac{1}{\sqrt[3]{2}} \cdot I_3$	$\mathbf{0}$

Table 3.3: Initial conditions for the heat conduction test

in Figure 3.8 on page 74, using the results from [9] as a reference. The material interface is denoted by a dashed vertical line.

The temperature curve generated using the GPR-RGFM matches very well the reference solution. The interface has moved to $x = 0.53756$, as is to be expected, as the cooler gas on the left expands as it heats up, and the hotter gas on the right contracts as it cools. Initially, the mass of the left volume is 1 and the right volume is 0.25. At $t = 1$, these masses are 0.9997 and 0.2503, respectively. Thus, mass on either side is conserved to a good approximation. Although the GPR-RGFM results for the heat flux match the reference solution well over most of the domain, there are aberrations in a small region around the interface. Although this doesn't affect the temperature curve, these discrepancies are undesirable, and possible methods to rectify them are discussed in Chapter 5.

3.3.6 Intermaterial Heating-Induced Acoustic Wave

The test assesses the ability of the GPR-RGFM to conduct heat between two different materials. Take the material parameters for air and helium from Section 3.3.1. Take the scaled spatial variable x^* defined by:

$$x = \frac{\mu^{air} c_0^{air}}{p_0 \gamma^{air}} x^* \tag{3.27}$$

The domain $x^* \in [0, 90]$ is used. Thermal energy is added at the left boundary at a high power of $\frac{\gamma^{air} p_0 c_0^{air}}{P_r^{air}(\gamma^{air}-1)}$ (around $1.7 \times 10^8 W m^{-2}$). Three scenarios are tested:

1. The domain is filled with air.
2. The domain comprises two volumes of air, initially separated at $x^* = 22.5$.
3. The domain comprises a volume of air (left) and a volume of helium (right), initially separated at $x^* = 22.5$.

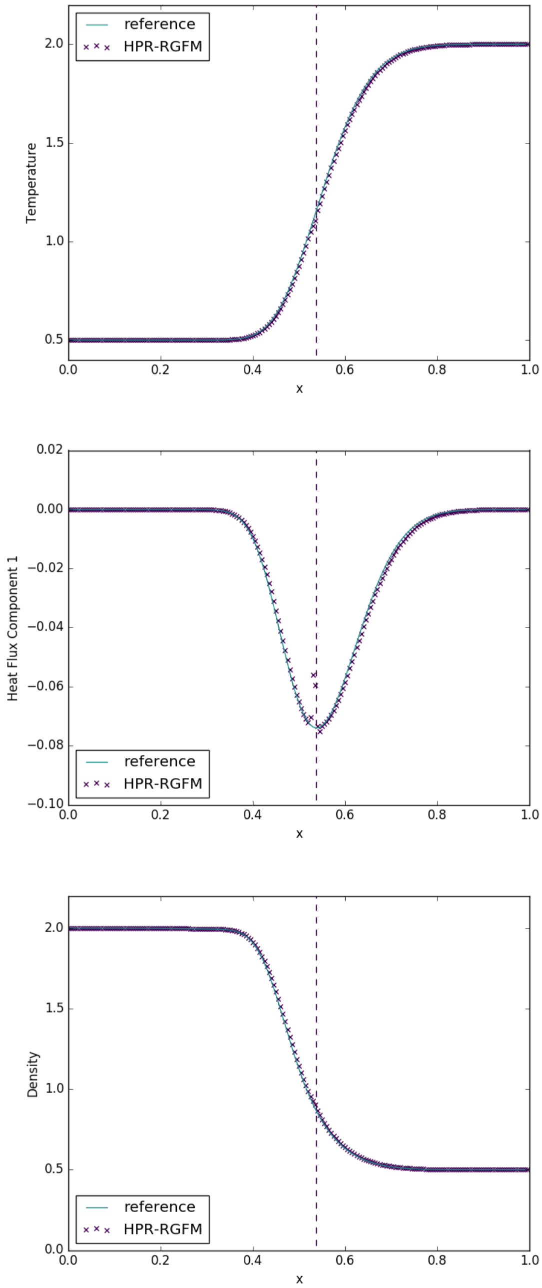

Figure 3.8: Temperature, heat flux, and density for the intermaterial heat conduction test with GPR-RGFM

	ρ	p	$\boldsymbol{v}$	A	$\boldsymbol{J}$
air	1.18	101325	$\mathbf{0}$	I_3	$\mathbf{0}$
helium	0.164	101325	$\mathbf{0}$	I_3	$\mathbf{0}$

Table 3.4: Initial conditions for the intermaterial heating-induced acoustic wave test

The initial conditions for the two gases in all scenarios are given in Table 3.4 on page 75. The results of the test are shown in Figure 3.9 on page 76 and Figure 3.10 on page 77 for various times. The material interface is represented by a dashed vertical line in scenarios 2 and 3. All simulations used 400 cells.

As the left wall heats up, a temperature gradient develops and the acoustic wave described appears. The results for scenarios 1 and 2 are indistinguishable, as they should be, and there are no aberrations around the material interface in scenario 2. In scenario 3, the acoustic wave hits the interface at around $t = 2 \times 10^{-9}$ and then speeds up (as it should, the speed of sound in helium being around three times that of air). The heat flux wave increases in intensity after passing into the helium, owing to the fact that the wave is traveling faster. As expected, all variables displayed are continuous across the interface.

In scenarios 2 and 3 the interface moves to the right as the air heats up and expands. The masses of the air volumes in these two scenarios at various times are given in Table 3.5 on page 75, demonstrating that mass is conserved well as the interface moves.

Time ($\times 10^{-9}$)	0	1	2	3	4	5
Mass in Scenario 2 ($\times 10^{-6}$)	1.254	1.255	1.253	1.252	1.252	1.253
Mass in Scenario 3 ($\times 10^{-6}$)	1.254	1.253	1.248	1.254	1.255	1.255

Table 3.5: Mass of the air volume in scenarios 2 and 3 at various times

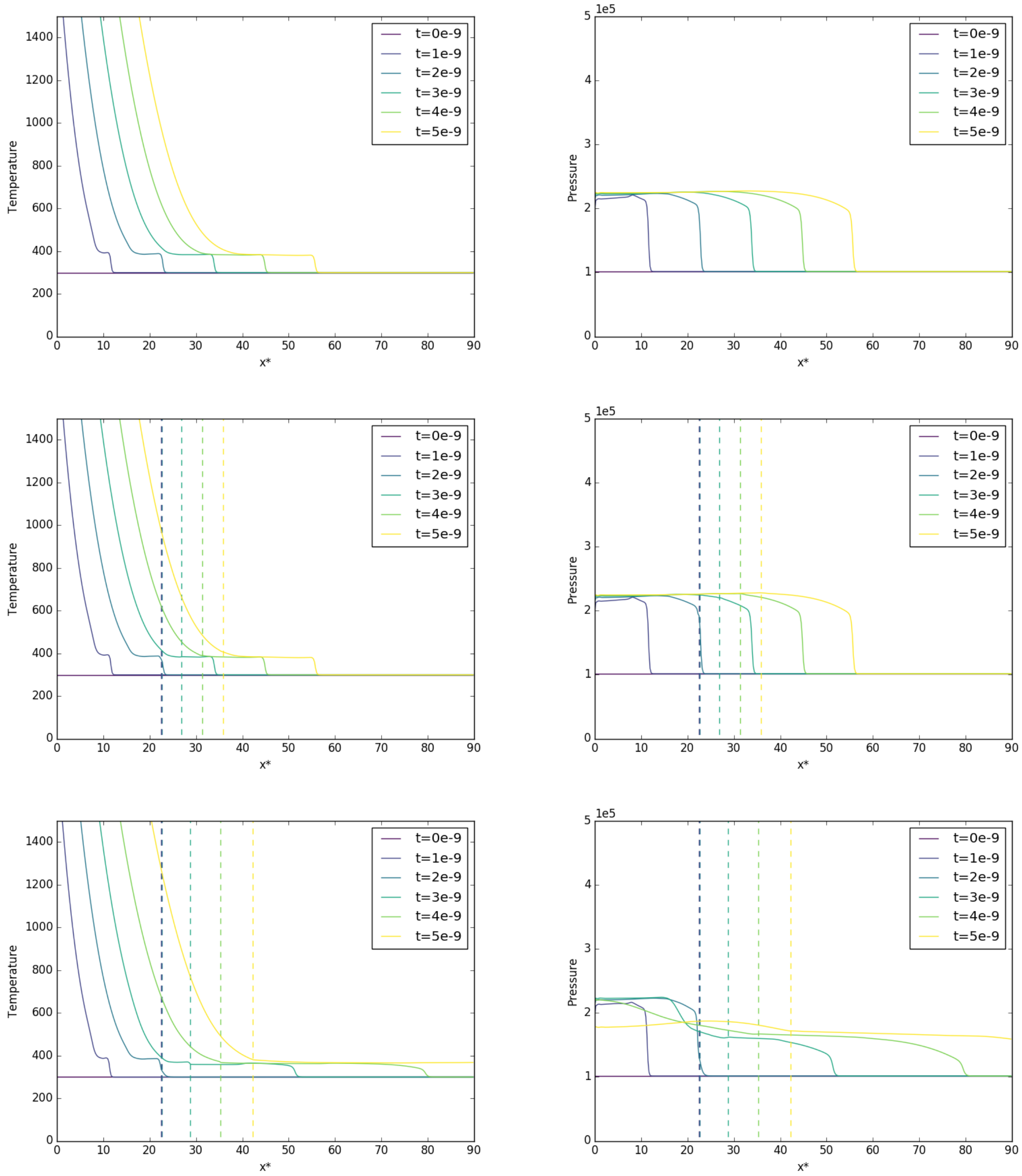

Figure 3.9: Temperature and pressure for the intermaterial heating-induced acoustic wave test with: a single volume of air (top); two volumes of air initially separated at $x^* = 22.5$ (middle); air and helium initially separated at $x^* = 22.5$ (bottom).

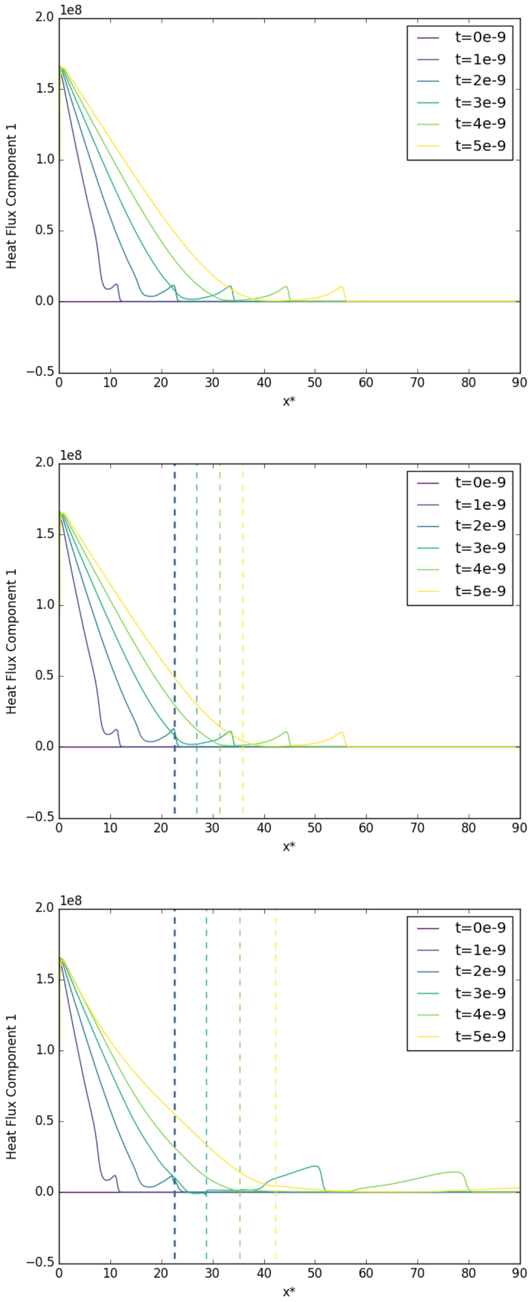

Figure 3.10: Heat flux for the intermaterial heating-induced acoustic wave test with: a single volume of air (top); two volumes of air initially separated at $x^* = 22.5$ (middle); air and helium initially separated at $x^* = 22.5$ (bottom).

Chapter 4

Impact-Induced Detonation in an Elasto-Plastic Confiner

4.1 Impact

4.1.1 Aluminium Plates

4.1.2 Taylor Bar

4.1.3 Rod Penetration

4.1.4 Inert Detasheet Confined by Steel

4.2 Detonation

4.2.1 Reactive C4 Confined by Steel

4.2.2 Reactive C4 Confined by Steel with Air Gap

4.2.3 Rod Impact on Copper Vessel

4.2.4 Rod Impact on Car Fuel Tank

4.3 Conclusions

Chapter 5

Conclusions & Discussion

References

[1] F. Alcrudo and F. Benkhaldoun, *Exact solutions to the Riemann problem of the shallow water equations with a bottom step*, Computers & Fluids, 30 (2001), pp. 643–671.

[2] D. S. Balsara, T. Rumpf, M. Dumbser, and C. D. Munz, *Efficient, high accuracy ADER-WENO schemes for hydrodynamics and divergence-free magnetohydrodynamics*, Journal of Computational Physics, 228 (2009), pp. 2480–2516.

[3] P. T. Barton and D. Drikakis, *An Eulerian method for multi-component problems in non-linear elasticity with sliding interfaces*, Journal of Computational Physics, 229 (2010), pp. 5518–5540.

[4] P. T. Barton, D. Drikakis, E. Romenski, and V. a. Titarev, *Exact and approximate solutions of Riemann problems in non-linear elasticity*, Journal of Computational Physics, 228 (2009), pp. 7046–7068.

[5] P. T. Barton, D. Drikakis, and E. I. Romenski, *An Eulerian finite-volume scheme for large elastoplastic deformations in solids*, International Journal for Numerical Methods in Engineering, 81 (2011), pp. 453–484.

[6] P. T. Barton, B. Obadia, and D. Drikakis, *A conservative level-set based method for compressible solid/fluid problems on fixed grids*, Journal of Computational Physics, 230 (2011), pp. 7867–7890.

[7] R. Becker, *Impact Waves and Detonation*, Zeitschrift f{ü}r Physik, 8 (1929), p. 381.

[8] M. Dumbser and D. S. Balsara, *A new efficient formulation of the HLLEM Riemann solver for general conservative and non-conservative hyperbolic systems*, Journal of Computational Physics, 304 (2016), pp. 275–319.

[9] M. Dumbser and D. S. Balsara, *A new efficient formulation of the HLLEM Riemann solver for general conservative and non-conservative hyperbolic systems*, Journal of Computational Physics, 304 (2016), pp. 275–319.

[10] M. Dumbser, D. S. Balsara, E. F. Toro, and C. D. Munz, *A unified framework for the construction of one-step finite volume and discontinuous Galerkin schemes on unstructured meshes*, Journal of Computational Physics, 227 (2008), pp. 8209–8253.

[11] M. Dumbser, M. Castro, C. Pares, and E. F. Toro, *ADER schemes on unstructured meshes for nonconservative hyperbolic systems: Applications to geophysical flows*, Computers & Fluids, 38 (2009), pp. 1731–1748.

[12] M. Dumbser, C. Enaux, and E. F. Toro, *Finite volume schemes of very high order of accuracy for stiff hyperbolic balance laws*, Journal of Computational Physics, 227 (2008), pp. 3971–4001.

[13] M. Dumbser, A. Hidalgo, and O. Zanotti, *High order space-time adaptive ADER-WENO finite volume schemes for non-conservative hyperbolic systems*, Computer Methods in Applied Mechanics and Engineering, 268 (2014), pp. 359–387.

[14] M. Dumbser, I. Peshkov, E. Romenski, and O. Zanotti, *High order ADER schemes for a unified first order hyperbolic formulation of continuum mechanics: Viscous heat-conducting fluids and elastic solids*, Journal of Computational Physics, 314 (2016), pp. 824–862.

[15] M. Dumbser and E. F. Toro, *A simple extension of the Osher Riemann solver to non-conservative hyperbolic systems*, Journal of Scientific Computing, 48 (2011), pp. 70–88.

[16] ——, *On universal Osher-type schemes for general nonlinear hyperbolic conservation laws*, Communications in Computational Physics, 10 (2011), pp. 635–671.

[17] M. Dumbser and O. Zanotti, *Very high order PNPM schemes on unstructured meshes for the resistive relativistic MHD equations*, Journal of Computational Physics, 228 (2009), pp. 6991–7006.

[18] M. Dumbser, O. Zanotti, A. Hidalgo, and D. S. Balsara, *ADER-WENO finite volume schemes with space-time adaptive mesh refinement*, Journal of Computational Physics, 248 (2013), pp. 257–286.

[19] R. Fedkiw, T. Aslam, B. Merriman, and S. Osher, *A Non-oscillatory Eulerian Approach to Interfaces in Multimaterial Flows (the Ghost Fluid Method)*, Journal of Computational Physics, 152 (1999), pp. 457–492.

[20] J. Frenkel, *Kinetic Theory of Liquids*, Oxford University Press, 1947.

[21] M. B. Giles, *An extended collection of matrix derivative results for forward and reverse mode algorithmic differentiation*, tech. rep., University of Oxford, 2008.

[22] J. Glimm and D. Marchesin, *A Numerical Method for Two Phase Flow with an Unstable Interface*, Journal of Computational Physics, 39 (1981), pp. 179–200.

[23] A. Hidalgo and M. Dumbser, *ADER schemes for nonlinear systems of stiff advection-diffusion-reaction equations*, Journal of Scientific Computing, 48 (2011), pp. 173–189.

[24] H. Jackson, *A Fast Numerical Scheme for the Godunov-Peshkov-Romenski Model of Continuum Mechanics*, Journal of Computational Physics, 348 (2017), pp. 514–533.

[25] ——, *On the Eigenvalues of the ADER-WENO Galerkin Predictor*, Journal of Computational Physics, 333 (2017), pp. 409–413.

[26] ——, *The Montecinos-Balsara ADER-FV Polynomial Basis: Convergence Properties & Extension to Non-Conservative Multidimensional Systems*, Computers and Fluids, 163 (2017), pp. 50–53.

[27] G. S. Jiang and C. W. Shu, *Efficient implementation of weighted WENO schemes*, Journal of Computational Physics, 126 (1996), pp. 202–228.

[28] B. M. Johnson, *Analytical shock solutions at large and small Prandtl number*, eprint arXiv:1305.7132, 726 (2013), pp. 1–12.

[29] R. Leveque and H. Yee, *A Study of Numerical Methods for Hyperbolic Conservation Laws with Stiff Source Terms*, Journal of Computational Physics, 86 (1990), pp. 187–210.

[30] T. G. Liu, B. C. Khoo, and K. S. Yeo, *Ghost fluid method for strong shock impacting on material interface*, Journal of Computational Physics, 190 (2003), pp. 651–681.

[31] T.-P. Liu, *The Riemann problem for general systems of conservation laws*, Journal of Differential Equations, 18 (1975), pp. 218–234.

[32] X.-D. Liu, S. Osher, and T. Chan, *Weighted Essentially Non-oscillatory Schemes*, Journal of Computational Physics, 115 (1994), pp. 200–212.

[33] A. N. Malyshev and E. I. Romenskii, *Hyperbolic equations for heat transfer. Global solvability of the Cauchy problem*, Siberian Mathematical Journal, 27 (1986), pp. 734–740.

[34] A. McAdams, A. Selle, R. Tamstorf, J. Teran, and E. Sifakis, *Computing the Singular Value Decomposition of 3 x 3 matrices with minimal branching and elementary floating point operations*, University of Wisconsin Madison, (2011).

[35] G. H. Miller, *An iterative Riemann solver for systems of hyperbolic conservation laws, with application to hyperelastic solid mechanics*, Journal of Computational Physics, 193 (2004), pp. 198–225.

[36] G. I. Montecinos and D. S. Balsara, *A cell-centered polynomial basis for efficient Galerkin predictors in the context of ADER finite volume schemes. The one-dimensional case*, Computers & Fluids, 156 (2017), pp. 220–238.

[37] M. Morduchow and P. A. Libby, *On a Complete Solution of the One-Dimensional Flow Equations of a Viscous, Heat-Conducting, Compressible Gas*, tech. rep., Polytechnic Institute of Brooklyn, 1949.

[38] E. D. Nering, *Linear Algebra and Matrix Theory*, 1970.

[39] T. E. Oliphant, *SciPy: Open source scientific tools for Python*, 2007.

[40] S. Osher and R. Fedkiw, *Level Set Methods and Dynamic Implicit Surfaces*, Springer, 2002.

[41] I. Peshkov and E. Romenski, *A hyperbolic model for viscous Newtonian flows*, Continuum Mechanics and Thermodynamics, 28 (2016), pp. 85–104.

[42] E. Romenski, D. Drikakis, and E. Toro, *Conservative models and numerical methods for compressible two-phase flow*, Journal of Scientific Computing, 42 (2010), pp. 68–95.

[43] E. Romenski, A. D. Resnyansky, and E. F. Toro, *Conservative hyperbolic model for compressible two-phase flow with different phase pressures and temperatures*, Quarterly of applied mathematics, 65(2) (2007), pp. 259–279.

[44] E. I. Romenski, *Hyperbolic equations of Maxwell's nonlinear model of elastoplastic heat-conducting media*, Siberian Mathematical Journal, 30 (1989), pp. 606–625.

[45] S. K. Sambasivan and H. S. UdayKumar, *Ghost Fluid Method for Strong Shock Interactions Part 1: Fluid-Fluid Interfaces*, AIAA Journal, 47 (2009), pp. 2907–2922.

[46] ——, *Ghost Fluid Method for Strong Shock Interactions Part 2: Immersed Solid Boundaries*, AIAA Journal, 47 (2009), pp. 2923–2937.

[47] E. Toro, *Riemann solvers and numerical methods for fluid dynamics: a practical introduction*, Springer, 2009.

[48] S. P. Wang, M. H. Anderson, J. G. Oakley, M. L. Corradini, and R. Bonazza, *A thermodynamically consistent and fully conservative treatment of contact discontinuities for compressible multicomponent flows*, Journal of Computational Physics, 195 (2004), pp. 528–559.

Appendix A

System Matrices

A.1 Fluxes, Sources, and Non-Conservative Terms

The GPR model takes the form $\frac{\partial \boldsymbol{Q}}{\partial t} + \frac{\partial \boldsymbol{F}(\boldsymbol{Q})}{\partial x} + B(\boldsymbol{Q}) \cdot \frac{\partial \boldsymbol{Q}}{\partial x} = \boldsymbol{S}(\boldsymbol{Q})$ where $\boldsymbol{Q}, \boldsymbol{F}, B, \boldsymbol{S}$ are given below.

A.2 Jacobians

Jacobian of the Conserved System

Define the following variables:

$$\tilde{\psi} = \left.\frac{\partial E}{\partial A}\right|_{\rho,p} \tag{A.1a}$$

$$\Psi_{ij} = \rho v_i v_j - \sigma_{ij} \tag{A.1b}$$

$$\Phi_{ij} = v_i v_j - \frac{\partial \sigma_{ij}}{\partial \rho} \tag{A.1c}$$

$$\Omega_{ij}^k = \rho v_k \tilde{\psi}_{ij} - v_m \frac{\partial \sigma_{mk}}{\partial A_{ij}} \tag{A.1d}$$

$$\Delta_i = v_i \left(E + \rho \left.\frac{\partial E}{\partial \rho}\right|_{p,A} \right) - \frac{\partial \sigma_{im}}{\partial \rho} v_m + \frac{\partial T}{\partial \rho} H_i \tag{A.1e}$$

$$\Pi_i = v_i \left(\rho \frac{\partial E}{\partial p} + 1 \right) + \frac{\partial T}{\partial p} H_i \tag{A.1f}$$

$$\Upsilon = \Gamma \left(\|\boldsymbol{v}\|^2 + \alpha^2 \|\boldsymbol{J}\|^2 - \left(E + \rho \left.\frac{\partial E}{\partial \rho}\right|_{p,A} \right) \right) \tag{A.1g}$$

The Jacobians of the GPR system are given on the following pages.

$$
\boldsymbol{Q} = \begin{pmatrix} \rho \\ \rho E \\ \rho v_1 \\ \rho v_2 \\ \rho v_3 \\ A_{11} \\ A_{12} \\ A_{13} \\ A_{21} \\ A_{22} \\ A_{23} \\ A_{31} \\ A_{32} \\ A_{33} \\ \rho J_1 \\ \rho J_2 \\ \rho J_3 \end{pmatrix}
\quad
\boldsymbol{F_1} = \begin{pmatrix} \rho v_1 \\ \rho v_1 E + v_1 p - v_m \sigma_{m1} + q_1 \\ \rho v_1^2 + p - \sigma_{11} \\ \rho v_1 v_2 - \sigma_{21} \\ \rho v_1 v_3 - \sigma_{31} \\ A_{1m} v_m \\ 0 \\ 0 \\ A_{2m} v_m \\ 0 \\ 0 \\ A_{3m} v_m \\ 0 \\ 0 \\ \rho J_1 v_1 + T \\ \rho J_2 v_1 \\ \rho J_3 v_1 \end{pmatrix}
\quad
\boldsymbol{F_2} = \begin{pmatrix} \rho v_2 \\ \rho v_2 E + v_2 p - v_m \sigma_{m2} + q_2 \\ \rho v_1 v_2 - \sigma_{12} \\ \rho v_2^2 + p - \sigma_{22} \\ \rho v_2 v_3 - \sigma_{32} \\ 0 \\ A_{1m} v_m \\ 0 \\ 0 \\ A_{2m} v_m \\ 0 \\ 0 \\ A_{3m} v_m \\ 0 \\ \rho J_1 v_2 \\ \rho J_2 v_2 + T \\ \rho J_3 v_2 \end{pmatrix}
\quad
\boldsymbol{F_3} = \begin{pmatrix} \rho v_3 \\ \rho v_3 E + v_3 p - v_m \sigma_{m3} + q_3 \\ \rho v_1 v_3 - \sigma_{13} \\ \rho v_2 v_3 - \sigma_{23} \\ \rho v_3^2 + p - \sigma_{33} \\ 0 \\ 0 \\ A_{1m} v_m \\ 0 \\ 0 \\ A_{2m} v_m \\ 0 \\ 0 \\ A_{3m} v_m \\ \rho J_1 v_3 \\ \rho J_2 v_3 \\ \rho J_3 v_3 + T \end{pmatrix}
$$

$$B_1 = \begin{pmatrix}
0&0&0&0&0&0&0&0&0&0&0&0&0&0&0&0&0\\
0&0&0&0&0&0&0&0&0&0&0&0&0&0&0&0&0\\
0&0&0&0&0&0&0&0&0&0&0&0&0&0&0&0&0\\
0&0&0&0&0&0&0&0&0&0&0&0&0&0&0&0&0\\
0&0&0&0&0&0&0&0&0&0&0&0&0&0&0&0&0\\
0&0&0&0&0&0&0&0&-v_2&0&0&-v_3&0&0&0&0&0\\
0&0&0&0&0&0&0&0&0&-v_2&0&0&-v_3&0&0&0&0\\
0&0&0&0&0&0&0&0&0&0&-v_2&0&0&-v_3&0&0&0\\
0&0&0&0&0&0&0&0&v_1&0&0&0&0&0&0&0&0\\
0&0&0&0&0&0&0&0&0&v_1&0&0&0&0&0&0&0\\
0&0&0&0&0&0&0&0&0&0&v_1&0&0&0&0&0&0\\
0&0&0&0&0&0&0&0&0&0&0&v_1&0&0&0&0&0\\
0&0&0&0&0&0&0&0&0&0&0&0&v_1&0&0&0&0\\
0&0&0&0&0&0&0&0&0&0&0&0&0&v_1&0&0&0\\
0&0&0&0&0&0&0&0&0&0&0&0&0&0&0&0&0\\
0&0&0&0&0&0&0&0&0&0&0&0&0&0&0&0&0\\
0&0&0&0&0&0&0&0&0&0&0&0&0&0&0&0&0
\end{pmatrix}$$

$$B_2 = \begin{pmatrix}
0&0&0&0&0&0&0&0&0&0&0&0&0&0&0&0&0\\
0&0&0&0&0&0&0&0&0&0&0&0&0&0&0&0&0\\
0&0&0&0&0&0&0&0&0&0&0&0&0&0&0&0&0\\
0&0&0&0&0&0&0&0&0&0&0&0&0&0&0&0&0\\
0&0&0&0&0&0&0&0&0&0&0&0&0&0&0&0&0\\
0&0&0&0&0&v_2&0&0&0&0&0&0&0&0&0&0&0\\
0&0&0&0&0&0&v_2&0&0&0&0&0&0&0&0&0&0\\
0&0&0&0&0&0&0&v_2&0&0&0&0&0&0&0&0&0\\
0&0&0&0&0&-v_1&0&0&0&0&0&-v_3&0&0&0&0&0\\
0&0&0&0&0&0&-v_1&0&0&0&0&0&-v_3&0&0&0&0\\
0&0&0&0&0&0&0&-v_1&0&0&0&0&0&-v_3&0&0&0\\
0&0&0&0&0&0&0&0&0&0&0&v_2&0&0&0&0&0\\
0&0&0&0&0&0&0&0&0&0&0&0&v_2&0&0&0&0\\
0&0&0&0&0&0&0&0&0&0&0&0&0&v_2&0&0&0\\
0&0&0&0&0&0&0&0&0&0&0&0&0&0&0&0&0\\
0&0&0&0&0&0&0&0&0&0&0&0&0&0&0&0&0\\
0&0&0&0&0&0&0&0&0&0&0&0&0&0&0&0&0
\end{pmatrix}$$

$$B_3 = \begin{pmatrix}
0&0&0&0&0&0&0&0&0&0&0&0&0&0&0&0&0\\
0&0&0&0&0&0&0&0&0&0&0&0&0&0&0&0&0\\
0&0&0&0&0&0&0&0&0&0&0&0&0&0&0&0&0\\
0&0&0&0&0&0&0&0&0&0&0&0&0&0&0&0&0\\
0&0&0&0&0&0&0&0&0&0&0&0&0&0&0&0&0\\
0&0&0&0&0&v_3&0&0&0&0&0&0&0&0&0&0&0\\
0&0&0&0&0&0&v_3&0&0&0&0&0&0&0&0&0&0\\
0&0&0&0&0&0&0&v_3&0&0&0&0&0&0&0&0&0\\
0&0&0&0&0&0&0&0&v_3&0&0&0&0&0&0&0&0\\
0&0&0&0&0&0&0&0&0&v_3&0&0&0&0&0&0&0\\
0&0&0&0&0&0&0&0&0&0&v_3&0&0&0&0&0&0\\
0&0&0&0&0&-v_1&0&0&-v_2&0&0&0&0&0&0&0&0\\
0&0&0&0&0&0&-v_1&0&0&-v_2&0&0&0&0&0&0&0\\
0&0&0&0&0&0&0&-v_1&0&0&-v_2&0&0&0&0&0&0\\
0&0&0&0&0&0&0&0&0&0&0&0&0&0&0&0&0\\
0&0&0&0&0&0&0&0&0&0&0&0&0&0&0&0&0\\
0&0&0&0&0&0&0&0&0&0&0&0&0&0&0&0&0
\end{pmatrix}$$

$$\boldsymbol{S} = \frac{1}{\theta_1(\tau_1)} \begin{pmatrix} 0\\0\\0\\0\\0\\-\psi_{11}\\-\psi_{21}\\-\psi_{31}\\-\psi_{12}\\-\psi_{22}\\-\psi_{32}\\-\psi_{13}\\-\psi_{23}\\-\psi_{33}\\0\\0\\0 \end{pmatrix} + \frac{1}{\theta_2(\tau_2)} \begin{pmatrix} 0\\0\\0\\0\\0\\0\\0\\0\\0\\0\\0\\0\\0\\0\\-\rho H_1\\-\rho H_2\\-\rho H_3 \end{pmatrix}$$

$$
\frac{\partial \boldsymbol{Q}}{\partial \boldsymbol{P}} =
\begin{pmatrix}
1 & 0 & 0 & 0 & 0 & 0 & 0 & 0 & 0 & 0 & 0 & 0 & 0 & 0 & 0 & 0 & 0 \\
\left(E + \rho\frac{\partial E}{\partial \rho}\right) & \frac{1}{\Gamma} & \rho v_1 & \rho v_2 & \rho v_3 & \rho\tilde{\psi}_{11} & \rho\tilde{\psi}_{12} & \rho\tilde{\psi}_{13} & \rho\tilde{\psi}_{21} & \rho\tilde{\psi}_{22} & \rho\tilde{\psi}_{23} & \rho\tilde{\psi}_{31} & \rho\tilde{\psi}_{32} & \rho\tilde{\psi}_{33} & \rho H_1 & \rho H_2 & \rho H_3 \\
v_1 & 0 & \rho & 0 & 0 & 0 & 0 & 0 & 0 & 0 & 0 & 0 & 0 & 0 & 0 & 0 & 0 \\
v_2 & 0 & 0 & \rho & 0 & 0 & 0 & 0 & 0 & 0 & 0 & 0 & 0 & 0 & 0 & 0 & 0 \\
v_3 & 0 & 0 & 0 & \rho & 0 & 0 & 0 & 0 & 0 & 0 & 0 & 0 & 0 & 0 & 0 & 0 \\
0 & 0 & 0 & 0 & 0 & 1 & 0 & 0 & 0 & 0 & 0 & 0 & 0 & 0 & 0 & 0 & 0 \\
0 & 0 & 0 & 0 & 0 & 0 & 1 & 0 & 0 & 0 & 0 & 0 & 0 & 0 & 0 & 0 & 0 \\
0 & 0 & 0 & 0 & 0 & 0 & 0 & 1 & 0 & 0 & 0 & 0 & 0 & 0 & 0 & 0 & 0 \\
0 & 0 & 0 & 0 & 0 & 0 & 0 & 0 & 1 & 0 & 0 & 0 & 0 & 0 & 0 & 0 & 0 \\
0 & 0 & 0 & 0 & 0 & 0 & 0 & 0 & 0 & 1 & 0 & 0 & 0 & 0 & 0 & 0 & 0 \\
0 & 0 & 0 & 0 & 0 & 0 & 0 & 0 & 0 & 0 & 1 & 0 & 0 & 0 & 0 & 0 & 0 \\
0 & 0 & 0 & 0 & 0 & 0 & 0 & 0 & 0 & 0 & 0 & 1 & 0 & 0 & 0 & 0 & 0 \\
0 & 0 & 0 & 0 & 0 & 0 & 0 & 0 & 0 & 0 & 0 & 0 & 1 & 0 & 0 & 0 & 0 \\
0 & 0 & 0 & 0 & 0 & 0 & 0 & 0 & 0 & 0 & 0 & 0 & 0 & 1 & 0 & 0 & 0 \\
J_1 & 0 & 0 & 0 & 0 & 0 & 0 & 0 & 0 & 0 & 0 & 0 & 0 & 0 & \rho & 0 & 0 \\
J_2 & 0 & 0 & 0 & 0 & 0 & 0 & 0 & 0 & 0 & 0 & 0 & 0 & 0 & 0 & \rho & 0 \\
J_3 & 0 & 0 & 0 & 0 & 0 & 0 & 0 & 0 & 0 & 0 & 0 & 0 & 0 & 0 & 0 & \rho
\end{pmatrix}
$$

$$\frac{\partial \boldsymbol{P}}{\partial \boldsymbol{Q}} = \begin{pmatrix}
1 & 0 & 0 & 0 & 0 & 0 & 0 & 0 & 0 & 0 & 0 & 0 & 0 & 0 & 0 & 0 & 0 \\
\Upsilon & \Gamma & -\Gamma v_1 & -\Gamma v_2 & -\Gamma v_3 & -\Gamma\rho\tilde{\psi}_{11} & -\Gamma\rho\tilde{\psi}_{12} & -\Gamma\rho\tilde{\psi}_{13} & -\Gamma\rho\tilde{\psi}_{21} & -\Gamma\rho\tilde{\psi}_{22} & -\Gamma\rho\tilde{\psi}_{23} & -\Gamma\rho\tilde{\psi}_{31} & -\Gamma\rho\tilde{\psi}_{32} & -\Gamma\rho\tilde{\psi}_{33} & -\Gamma H_1 & -\Gamma H_2 & -\Gamma H_3 \\
-\frac{v_1}{\rho} & 0 & \frac{1}{\rho} & 0 & 0 & 0 & 0 & 0 & 0 & 0 & 0 & 0 & 0 & 0 & 0 & 0 & 0 \\
-\frac{v_2}{\rho} & 0 & 0 & \frac{1}{\rho} & 0 & 0 & 0 & 0 & 0 & 0 & 0 & 0 & 0 & 0 & 0 & 0 & 0 \\
-\frac{v_3}{\rho} & 0 & 0 & 0 & \frac{1}{\rho} & 0 & 0 & 0 & 0 & 0 & 0 & 0 & 0 & 0 & 0 & 0 & 0 \\
0 & 0 & 0 & 0 & 0 & 1 & 0 & 0 & 0 & 0 & 0 & 0 & 0 & 0 & 0 & 0 & 0 \\
0 & 0 & 0 & 0 & 0 & 0 & 1 & 0 & 0 & 0 & 0 & 0 & 0 & 0 & 0 & 0 & 0 \\
0 & 0 & 0 & 0 & 0 & 0 & 0 & 1 & 0 & 0 & 0 & 0 & 0 & 0 & 0 & 0 & 0 \\
0 & 0 & 0 & 0 & 0 & 0 & 0 & 0 & 1 & 0 & 0 & 0 & 0 & 0 & 0 & 0 & 0 \\
0 & 0 & 0 & 0 & 0 & 0 & 0 & 0 & 0 & 1 & 0 & 0 & 0 & 0 & 0 & 0 & 0 \\
0 & 0 & 0 & 0 & 0 & 0 & 0 & 0 & 0 & 0 & 1 & 0 & 0 & 0 & 0 & 0 & 0 \\
0 & 0 & 0 & 0 & 0 & 0 & 0 & 0 & 0 & 0 & 0 & 1 & 0 & 0 & 0 & 0 & 0 \\
0 & 0 & 0 & 0 & 0 & 0 & 0 & 0 & 0 & 0 & 0 & 0 & 1 & 0 & 0 & 0 & 0 \\
0 & 0 & 0 & 0 & 0 & 0 & 0 & 0 & 0 & 0 & 0 & 0 & 0 & 1 & 0 & 0 & 0 \\
-\frac{J_1}{\rho} & 0 & 0 & 0 & 0 & 0 & 0 & 0 & 0 & 0 & 0 & 0 & 0 & 0 & \frac{1}{\rho} & 0 & 0 \\
-\frac{J_2}{\rho} & 0 & 0 & 0 & 0 & 0 & 0 & 0 & 0 & 0 & 0 & 0 & 0 & 0 & 0 & \frac{1}{\rho} & 0 \\
-\frac{J_3}{\rho} & 0 & 0 & 0 & 0 & 0 & 0 & 0 & 0 & 0 & 0 & 0 & 0 & 0 & 0 & 0 & \frac{1}{\rho}
\end{pmatrix}$$

$$
\frac{\partial \boldsymbol{F}_1}{\partial \boldsymbol{P}} = \begin{pmatrix}
v_1 & 0 & \rho & 0 & 0 & 0 & 0 & 0 & 0 & 0 & 0 & 0 & 0 & 0 & 0 & 0 & 0 \\
\Delta_1 & \Pi_1 & (\Psi_{11} + \rho E + p) & \Psi_{12} & \Psi_{13} & \Omega^1_{11} & \Omega^1_{12} & \Omega^1_{13} & \Omega^1_{21} & \Omega^1_{22} & \Omega^1_{23} & \Omega^1_{31} & \Omega^1_{32} & \Omega^1_{33} & (\rho v_1 H_1 + \alpha^2 T) & \rho v_1 H_2 & \rho v_1 H_3 \\
\Phi_{11} & 1 & 2\rho v_1 & 0 & 0 & -\frac{\sigma_{11}}{A_{11}} & -\frac{\sigma_{11}}{A_{12}} & -\frac{\sigma_{11}}{A_{13}} & -\frac{\sigma_{11}}{A_{21}} & -\frac{\sigma_{11}}{A_{22}} & -\frac{\sigma_{11}}{A_{23}} & -\frac{\sigma_{11}}{A_{31}} & -\frac{\sigma_{11}}{A_{32}} & -\frac{\sigma_{11}}{A_{33}} & 0 & 0 & 0 \\
\Phi_{12} & 0 & \rho v_2 & \rho v_1 & 0 & -\frac{\sigma_{12}}{A_{11}} & -\frac{\sigma_{12}}{A_{12}} & -\frac{\sigma_{12}}{A_{13}} & -\frac{\sigma_{12}}{A_{21}} & -\frac{\sigma_{12}}{A_{22}} & -\frac{\sigma_{12}}{A_{23}} & -\frac{\sigma_{12}}{A_{31}} & -\frac{\sigma_{12}}{A_{32}} & -\frac{\sigma_{12}}{A_{33}} & 0 & 0 & 0 \\
\Phi_{13} & 0 & \rho v_3 & 0 & \rho v_1 & -\frac{\sigma_{13}}{A_{11}} & -\frac{\sigma_{13}}{A_{12}} & -\frac{\sigma_{13}}{A_{13}} & -\frac{\sigma_{13}}{A_{21}} & -\frac{\sigma_{13}}{A_{22}} & -\frac{\sigma_{13}}{A_{23}} & -\frac{\sigma_{13}}{A_{31}} & -\frac{\sigma_{13}}{A_{32}} & -\frac{\sigma_{13}}{A_{33}} & 0 & 0 & 0 \\
0 & 0 & A_{11} & A_{12} & A_{13} & v_1 & v_2 & v_3 & 0 & 0 & 0 & 0 & 0 & 0 & 0 & 0 & 0 \\
0 & 0 & 0 & 0 & 0 & 0 & 0 & 0 & 0 & 0 & 0 & 0 & 0 & 0 & 0 & 0 & 0 \\
0 & 0 & 0 & 0 & 0 & 0 & 0 & 0 & 0 & 0 & 0 & 0 & 0 & 0 & 0 & 0 & 0 \\
0 & 0 & A_{21} & A_{22} & A_{23} & 0 & 0 & 0 & v_1 & v_2 & v_3 & 0 & 0 & 0 & 0 & 0 & 0 \\
0 & 0 & 0 & 0 & 0 & 0 & 0 & 0 & 0 & 0 & 0 & 0 & 0 & 0 & 0 & 0 & 0 \\
0 & 0 & 0 & 0 & 0 & 0 & 0 & 0 & 0 & 0 & 0 & 0 & 0 & 0 & 0 & 0 & 0 \\
0 & 0 & A_{31} & A_{32} & A_{33} & 0 & 0 & 0 & 0 & 0 & 0 & v_1 & v_2 & v_3 & 0 & 0 & 0 \\
0 & 0 & 0 & 0 & 0 & 0 & 0 & 0 & 0 & 0 & 0 & 0 & 0 & 0 & 0 & 0 & 0 \\
0 & 0 & 0 & 0 & 0 & 0 & 0 & 0 & 0 & 0 & 0 & 0 & 0 & 0 & 0 & 0 & 0 \\
v_1 J_1 + \frac{\partial T}{\partial \rho} & \frac{\partial T}{\partial p} & \rho J_1 & 0 & 0 & 0 & 0 & 0 & 0 & 0 & 0 & 0 & 0 & 0 & \rho v_1 & 0 & 0 \\
v_1 J_2 & 0 & \rho J_2 & 0 & 0 & 0 & 0 & 0 & 0 & 0 & 0 & 0 & 0 & 0 & 0 & \rho v_1 & 0 \\
v_1 J_3 & 0 & \rho J_3 & 0 & 0 & 0 & 0 & 0 & 0 & 0 & 0 & 0 & 0 & 0 & 0 & 0 & \rho v_1
\end{pmatrix}
$$

$$
\frac{\partial \boldsymbol{F_2}}{\partial \boldsymbol{P}} =
\begin{pmatrix}
v_2 & 0 & 0 & \rho & 0 & 0 & 0 & 0 & 0 & 0 & 0 & 0 & 0 & 0 & 0 & 0 & 0 \\
\Delta_2 & \Pi_2 & \Psi_{21} & (\Psi_{22}+\rho E+p) & \Psi_{23} & \Omega^2_{11} & \Omega^2_{12} & \Omega^2_{13} & \Omega^2_{21} & \Omega^2_{22} & \Omega^2_{23} & \Omega^2_{31} & \Omega^2_{32} & \Omega^2_{33} & \rho v_2 H_1 & (\rho v_2 H_2+\alpha^2 T) & \rho v_2 H_3 \\
\Phi_{21} & 0 & \rho v_2 & \rho v_1 & 0 & -\frac{\sigma_{21}}{A_{11}} & -\frac{\sigma_{21}}{A_{12}} & -\frac{\sigma_{21}}{A_{13}} & -\frac{\sigma_{21}}{A_{21}} & -\frac{\sigma_{21}}{A_{22}} & -\frac{\sigma_{21}}{A_{23}} & -\frac{\sigma_{21}}{A_{31}} & -\frac{\sigma_{21}}{A_{32}} & -\frac{\sigma_{21}}{A_{33}} & 0 & 0 & 0 \\
\Phi_{22} & 1 & 0 & 2\rho v_2 & 0 & -\frac{\sigma_{22}}{A_{11}} & -\frac{\sigma_{22}}{A_{12}} & -\frac{\sigma_{22}}{A_{13}} & -\frac{\sigma_{22}}{A_{21}} & -\frac{\sigma_{22}}{A_{22}} & -\frac{\sigma_{22}}{A_{23}} & -\frac{\sigma_{22}}{A_{31}} & -\frac{\sigma_{22}}{A_{32}} & -\frac{\sigma_{22}}{A_{33}} & 0 & 0 & 0 \\
\Phi_{23} & 0 & 0 & \rho v_3 & \rho v_2 & -\frac{\sigma_{23}}{A_{11}} & -\frac{\sigma_{23}}{A_{12}} & -\frac{\sigma_{23}}{A_{13}} & -\frac{\sigma_{23}}{A_{21}} & -\frac{\sigma_{23}}{A_{22}} & -\frac{\sigma_{23}}{A_{23}} & -\frac{\sigma_{23}}{A_{31}} & -\frac{\sigma_{23}}{A_{32}} & -\frac{\sigma_{23}}{A_{33}} & 0 & 0 & 0 \\
0 & 0 & 0 & 0 & 0 & 0 & 0 & 0 & 0 & 0 & 0 & 0 & 0 & 0 & 0 & 0 & 0 \\
0 & 0 & A_{11} & A_{12} & A_{13} & v_1 & v_2 & v_3 & 0 & 0 & 0 & 0 & 0 & 0 & 0 & 0 & 0 \\
0 & 0 & 0 & 0 & 0 & 0 & 0 & 0 & 0 & 0 & 0 & 0 & 0 & 0 & 0 & 0 & 0 \\
0 & 0 & 0 & 0 & 0 & 0 & 0 & 0 & 0 & 0 & 0 & 0 & 0 & 0 & 0 & 0 & 0 \\
0 & 0 & A_{21} & A_{22} & A_{23} & 0 & 0 & 0 & v_1 & v_2 & v_3 & 0 & 0 & 0 & 0 & 0 & 0 \\
0 & 0 & 0 & 0 & 0 & 0 & 0 & 0 & 0 & 0 & 0 & 0 & 0 & 0 & 0 & 0 & 0 \\
0 & 0 & 0 & 0 & 0 & 0 & 0 & 0 & 0 & 0 & 0 & 0 & 0 & 0 & 0 & 0 & 0 \\
0 & 0 & A_{31} & A_{32} & A_{33} & 0 & 0 & 0 & 0 & 0 & 0 & v_1 & v_2 & v_3 & 0 & 0 & 0 \\
0 & 0 & 0 & 0 & 0 & 0 & 0 & 0 & 0 & 0 & 0 & 0 & 0 & 0 & 0 & 0 & 0 \\
v_2 J_1 & 0 & 0 & \rho J_1 & 0 & 0 & 0 & 0 & 0 & 0 & 0 & 0 & 0 & 0 & \rho v_2 & 0 & 0 \\
v_2 J_2 + \frac{\partial T}{\partial \rho} & \frac{\partial T}{\partial p} & 0 & \rho J_2 & 0 & 0 & 0 & 0 & 0 & 0 & 0 & 0 & 0 & 0 & 0 & \rho v_2 & 0 \\
v_2 J_3 & 0 & 0 & \rho J_3 & 0 & 0 & 0 & 0 & 0 & 0 & 0 & 0 & 0 & 0 & 0 & 0 & \rho v_2
\end{pmatrix}
$$

$$\frac{\partial \boldsymbol{F_3}}{\partial \boldsymbol{P}} = \begin{pmatrix}
v_3 & 0 & 0 & 0 & \rho & 0 & 0 & 0 & 0 & 0 & 0 & 0 & 0 & 0 & 0 & 0 & 0 \\
\Delta_3 & \Pi_3 & \Psi_{11} & \Psi_{12} & (\Psi_{13}+\rho E+p) & \Omega^3_{11} & \Omega^3_{12} & \Omega^3_{13} & \Omega^3_{21} & \Omega^3_{22} & \Omega^3_{23} & \Omega^3_{31} & \Omega^3_{32} & \Omega^3_{33} & \rho v_3 H_1 & \rho v_3 H_2 & (\rho v_3 H_3+\alpha^2 T) \\
\Phi_{31} & 0 & \rho v_3 & 0 & \rho v_1 & -\frac{\sigma_{31}}{A_{11}} & -\frac{\sigma_{31}}{A_{12}} & -\frac{\sigma_{31}}{A_{13}} & -\frac{\sigma_{31}}{A_{21}} & -\frac{\sigma_{31}}{A_{22}} & -\frac{\sigma_{31}}{A_{23}} & -\frac{\sigma_{31}}{A_{31}} & -\frac{\sigma_{31}}{A_{32}} & -\frac{\sigma_{31}}{A_{33}} & 0 & 0 & 0 \\
\Phi_{32} & 0 & 0 & \rho v_3 & \rho v_2 & -\frac{\sigma_{32}}{A_{11}} & -\frac{\sigma_{32}}{A_{12}} & -\frac{\sigma_{32}}{A_{13}} & -\frac{\sigma_{32}}{A_{21}} & -\frac{\sigma_{32}}{A_{22}} & -\frac{\sigma_{32}}{A_{23}} & -\frac{\sigma_{32}}{A_{31}} & -\frac{\sigma_{32}}{A_{32}} & -\frac{\sigma_{32}}{A_{33}} & 0 & 0 & 0 \\
\Phi_{33} & 1 & 0 & 0 & 2\rho v_3 & -\frac{\sigma_{33}}{A_{11}} & -\frac{\sigma_{33}}{A_{12}} & -\frac{\sigma_{33}}{A_{13}} & -\frac{\sigma_{33}}{A_{21}} & -\frac{\sigma_{33}}{A_{22}} & -\frac{\sigma_{33}}{A_{23}} & -\frac{\sigma_{33}}{A_{31}} & -\frac{\sigma_{33}}{A_{32}} & -\frac{\sigma_{33}}{A_{33}} & 0 & 0 & 0 \\
0 & 0 & 0 & 0 & 0 & 0 & 0 & 0 & 0 & 0 & 0 & 0 & 0 & 0 & 0 & 0 & 0 \\
0 & 0 & 0 & 0 & 0 & 0 & 0 & 0 & 0 & 0 & 0 & 0 & 0 & 0 & 0 & 0 & 0 \\
0 & 0 & A_{11} & A_{12} & A_{13} & v_1 & v_2 & v_3 & 0 & 0 & 0 & 0 & 0 & 0 & 0 & 0 & 0 \\
0 & 0 & 0 & 0 & 0 & 0 & 0 & 0 & 0 & 0 & 0 & 0 & 0 & 0 & 0 & 0 & 0 \\
0 & 0 & 0 & 0 & 0 & 0 & 0 & 0 & 0 & 0 & 0 & 0 & 0 & 0 & 0 & 0 & 0 \\
0 & 0 & A_{21} & A_{22} & A_{23} & 0 & 0 & 0 & v_1 & v_2 & v_3 & 0 & 0 & 0 & 0 & 0 & 0 \\
0 & 0 & 0 & 0 & 0 & 0 & 0 & 0 & 0 & 0 & 0 & 0 & 0 & 0 & 0 & 0 & 0 \\
0 & 0 & 0 & 0 & 0 & 0 & 0 & 0 & 0 & 0 & 0 & 0 & 0 & 0 & 0 & 0 & 0 \\
0 & 0 & A_{31} & A_{32} & A_{33} & 0 & 0 & 0 & 0 & 0 & 0 & v_1 & v_2 & v_3 & 0 & 0 & 0 \\
v_3 J_1 & 0 & 0 & 0 & \rho J_1 & 0 & 0 & 0 & 0 & 0 & 0 & 0 & 0 & 0 & \rho v_3 & 0 & 0 \\
v_3 J_2 & 0 & 0 & 0 & \rho J_2 & 0 & 0 & 0 & 0 & 0 & 0 & 0 & 0 & 0 & 0 & \rho v_3 & 0 \\
v_3 J_3 + \frac{\partial T}{\partial \rho} & \frac{\partial T}{\partial p} & 0 & 0 & \rho J_3 & 0 & 0 & 0 & 0 & 0 & 0 & 0 & 0 & 0 & 0 & 0 & \rho v_3
\end{pmatrix}$$

Jacobian of Distortion ODEs

The Jacobian of the source function is used to speed up numerical integration of the ODE. It is derived thus:

$$\frac{\partial \operatorname{dev}(G)_{ij}}{\partial A_{mn}} = \delta_{in} A_{mj} + \delta_{jn} A_{mi} - \frac{2}{3} \delta_{ij} A_{mn} \tag{A.2}$$

Thus:

$$\begin{aligned}
\frac{\partial \left(A \operatorname{dev}(G)\right)_{ij}}{\partial A_{mn}} &= \frac{\partial A_{it}}{\partial A_{mn}} \operatorname{dev}(G)_{tj} + A_{it} \frac{\partial \operatorname{dev}(G)_{tj}}{\partial A_{mn}} \\
&= \delta_{im} \delta_{tn} \left(A_{kt} A_{kj} - \frac{1}{3} A_{kl} A_{kl} \delta_{tj} \right) + A_{it} \left(\delta_{tn} A_{mj} + \delta_{jn} A_{mt} - \frac{2}{3} \delta_{tj} A_{mn} \right) \\
&= \delta_{im} A_{kn} A_{kj} - \frac{1}{3} \delta_{im} \delta_{jn} A_{kl} A_{kl} + A_{in} A_{mj} + \delta_{jn} A_{ik} A_{mk} - \frac{2}{3} A_{ij} A_{mn}
\end{aligned} \tag{A.3}$$

Thus:

$$\begin{aligned}
J_A &\equiv \frac{-3}{\tau_1} \frac{\partial \left(\det(A)^{\frac{5}{3}} A \operatorname{dev}(G) \right)_{ij}}{\partial A_{mn}} \\
&= \frac{-3}{\tau_1} \det(A)^{\frac{5}{3}} \left(\frac{5}{3} \left(A \operatorname{dev}(G)\right)_{ij} A^{-T}_{mn} + A_{in} A_{mj} + \delta_{jn} G'_{im} + \delta_{im} G_{jn} - \frac{1}{3} \delta_{im} \delta_{jn} A_{kl} A_{kl} - \frac{2}{3} A_{ij} A_{mn} \right) \\
&= \frac{1}{\tau_1} \det(A)^{\frac{5}{3}} \left(-5 \left(A \operatorname{dev}(G)\right) \otimes A^{-T} + 2A \otimes A - 3 \left(A \otimes A\right)^{1,3} + \|A\|_F^2 \left(I \otimes I\right)^{2,3} - 3 \left(G' \otimes I + I \otimes \right.\right.
\end{aligned} \tag{A.4}$$

where $G' = AA^T$ and $X^{a,b}$ refers to tensor X with indices a, b transposed.

Jacobian of Thermal Impulse ODEs

As demonstrated in 2.2.2, we have:

$$\frac{dJ_i}{dt} = \frac{J_i}{2} \left(-a + b \left(J_1^2 + J_2^2 + J_3^2 \right) \right) \tag{A.5}$$

where

$$a = \frac{2\rho_0}{\tau_2 T_0 \rho c_v} \left(E - E_{2A}\left(A\right) - E_3\left(\boldsymbol{v}\right)\right) \tag{A.6a}$$

$$b = \frac{\rho_0 \alpha^2}{\tau_2 T_0 \rho c_v} \tag{A.6b}$$

Thus, the Jacobian of the thermal impulse ODEs is:

$$\begin{pmatrix} \frac{b}{2}\left(3J_1^2 + J_2^2 + J_3^2\right) - \frac{a}{2} & bJ_1J_2 & bJ_1J_3 \\ bJ_1J_2 & \frac{b}{2}\left(J_1^2 + 3J_2^2 + J_3^2\right) - \frac{a}{2} & bJ_2J_3 \\ bJ_1J_3 & bJ_2J_3 & \frac{b}{2}\left(J_1^2 + J_2^2 + 3J_3^2\right) - \frac{a}{2} \end{pmatrix} \tag{A.7}$$

Appendix B

Eigenstructure

B.1 Primitive System

Taking the ordering $\boldsymbol{P}$ of primitive variables in (B.13), note that (3), (1b), (1c), (1d) can be stated as:

$$\frac{D\rho}{Dt} + \rho \frac{\partial v_k}{\partial x_k} = 0 \tag{B.1a}$$

$$\frac{Dv_i}{Dt} + \frac{1}{\rho}\frac{\partial \Sigma_{ik}}{\partial x_k} = 0 \tag{B.1b}$$

$$\frac{DA_{ij}}{Dt} + A_{ik}\frac{\partial v_k}{\partial x_j} = -\frac{\psi_{ij}}{\theta_1} \tag{B.1c}$$

$$\frac{DJ_i}{Dt} + \frac{1}{\rho}\frac{\partial T\delta_{ik}}{\partial x_k} = -\frac{H_i}{\theta_2} \tag{B.1d}$$

$$\frac{DE}{Dt} + \frac{1}{\rho}\frac{\partial\left(\Sigma_{ik}v_i + TH_k\right)}{\partial x_k} = 0 \tag{B.1e}$$

where the total stress tensor $\Sigma = pI + \rho A^T\psi$. Note that:

$$\begin{aligned}\frac{DE}{Dt} &= \frac{\partial E}{\partial p}\frac{Dp}{Dt} + \frac{\partial E}{\partial \rho}\frac{D\rho}{Dt} + v_i\frac{Dv_i}{Dt} + \frac{\partial E}{\partial A_{ij}}\frac{DA_{ij}}{Dt} + H_i\frac{DJ_i}{Dt} \\ &= \frac{\partial E}{\partial p}\frac{Dp}{Dt} - \rho\frac{\partial E}{\partial \rho}\frac{\partial v_k}{\partial x_k} - \frac{1}{\rho}v_i\frac{\partial \Sigma_{ik}}{\partial x_k} - \frac{\partial E}{\partial A_{ij}}\left(A_{ik}\frac{\partial v_k}{\partial x_j} + \frac{\psi_{ij}}{\theta_1}\right) - H_i\left(\frac{1}{\rho}\frac{\partial T\delta_{ik}}{\partial x_k} + \frac{H_i}{\theta_2}\right)\end{aligned} \tag{B.2}$$

Thus, the energy equation becomes:

$$\frac{\partial E}{\partial p}\frac{Dp}{Dt} - \rho\frac{\partial E}{\partial \rho}\frac{\partial v_k}{\partial x_k} - \frac{1}{\rho}v_i\frac{\partial \Sigma_{ik}}{\partial x_k} - \frac{\partial E}{\partial A_{ij}}A_{ik}\frac{\partial v_k}{\partial x_j} - \frac{H_k}{\rho}\frac{\partial T}{\partial x_k} + \frac{1}{\rho}\frac{\partial\left(\Sigma_{ik}v_i + TH_k\right)}{\partial x_k} = \frac{\partial E}{\partial A_{ij}}\frac{\psi_{ij}}{\theta_1} + \frac{H_iH_i}{\theta_2} \tag{B.3}$$

Simplifying:

$$\frac{Dp}{Dt} + \frac{1}{\rho E_p}\left(\Sigma_{ik} - \rho A_{ji}\frac{\partial E}{\partial A_{jk}} - \rho^2\frac{\partial E}{\partial \rho}\delta_{ik}\right)\frac{\partial v_i}{\partial x_k} + \frac{T}{\rho E_p}\frac{\partial H_k}{\partial x_k} = \frac{\partial E}{\partial A_{ij}}\frac{\psi_{ij}}{\theta_1 E_p} + \frac{H_iH_i}{\theta_2 E_p} \tag{B.4}$$

We have[1][2][3]:

$$\frac{p - \rho^2 E_\rho}{\rho E_p} = \rho c_0^2 \tag{B.9a}$$

$$\frac{\alpha^2 T}{\rho E_p} = \frac{\rho c_h^2}{T_p} \tag{B.9b}$$

$$\left.\frac{\partial E}{\partial A}\right|_{\rho,p} = \left(1 - 2\rho^2 E_p \frac{\partial \log(c_s)}{\partial \rho}\right)\psi \tag{B.9c}$$

$$-\rho A^T \left.\frac{\partial E}{\partial A}\right|_{\rho,p} = \sigma + \rho^2 E_p \left(\frac{\sigma}{\rho} - \frac{\partial \sigma}{\partial \rho}\right) \tag{B.9d}$$

1

$$\begin{aligned}\frac{p - \rho^2 E_\rho}{\rho E_p} &= \frac{\rho^2 \left.E_\rho\right|_s - \rho^2 \left.E_\rho\right|_p}{\rho \left.E_p\right|_\rho} = \rho \frac{\left.E_\rho\right|_s - \left(\left.E_\rho\right|_s + \left.E_s\right|_\rho \left.s_\rho\right|_p\right)}{\left.E_s\right|_\rho \left.s_p\right|_\rho} \\ &= \rho \frac{-\left.s_\rho\right|_p}{\left.s_p\right|_\rho} = \rho \left.\frac{\partial p}{\partial \rho}\right|_s\end{aligned} \tag{B.5}$$

2

$$\frac{\alpha^2 T}{\rho E_p} = \frac{\alpha^2 T}{\rho c_v T_p} = \frac{\rho c_h^2}{T_p} \tag{B.6}$$

3

$$\left.\frac{\partial E}{\partial A}\right|_{\rho,p} = \left(c_s^2 - \frac{\rho}{\Gamma}\frac{\partial c_s^2}{\partial \rho}\right)\frac{\psi}{c_s^2} = \left(1 - 2\frac{\rho^2}{\rho\Gamma}\frac{\partial \log(c_s)}{\partial \rho}\right)\psi \tag{B.7}$$

$$\begin{aligned}\frac{\partial \sigma}{\partial \rho} &= \frac{\partial}{\partial \rho}\left(-\rho c_s^2 A^T \frac{\psi}{c_s^2}\right) = -c_s^2 A^T \frac{\psi}{c_s^2} - \rho \frac{\partial c_s^2}{\partial \rho} A^T \frac{\psi}{c_s^2} \\ &= \frac{\sigma}{\rho} + 2\frac{\partial \log(c_s)}{\partial \rho}\sigma\end{aligned} \tag{B.8}$$

The full system then becomes:

$$\frac{D\rho}{Dt}+\rho\frac{\partial v_k}{\partial x_k}=0 \tag{B.10a}$$

$$\frac{Dp}{Dt}+\rho c_0^2\frac{\partial v_i}{\partial x_i}+\left(\sigma_{ik}-\rho\frac{\partial\sigma_{ik}}{\partial\rho}\right)\frac{\partial v_i}{\partial x_k}+\frac{\rho c_h^2}{T_p}\frac{\partial J_k}{\partial x_k}=\left(1-2\rho^2E_p\frac{\partial\log\left(c_s\right)}{\partial\rho}\right)\frac{\left\|\psi\right\|_F^2}{\theta_1E_p}+\frac{\left\|H\right\|^2}{\theta_2E_p} \tag{B.10b}$$

$$\frac{DA_{ij}}{Dt}+A_{ik}\frac{\partial v_k}{\partial x_j}=-\frac{\psi_{ij}}{\theta_1} \tag{B.10c}$$

$$\frac{Dv_i}{Dt}-\frac{1}{\rho}\frac{\partial\sigma_{ik}}{\partial\rho}\frac{\partial\rho}{\partial x_k}+\frac{1}{\rho}\frac{\partial p}{\partial x_i}-\frac{1}{\rho}\frac{\partial\sigma_{ik}}{\partial A_{mn}}\frac{\partial A_{mn}}{\partial x_k}=0 \tag{B.10d}$$

$$\frac{DJ_i}{Dt}+\frac{T_\rho}{\rho}\frac{\partial\rho}{\partial x_i}+\frac{T_p}{\rho}\frac{\partial p}{\partial x_i}=-\frac{H_i}{\theta_2} \tag{B.10e}$$

Thus, the GPR system can be written in the following form:

$$\frac{\partial\boldsymbol{P}}{\partial t}+\boldsymbol{M}\cdot\nabla\boldsymbol{P}=\boldsymbol{S_p} \tag{B.11}$$

B.2 Eigenvalues

Considering the primitive system matrix (B.12), it is clear that the eigenvalues of the GPR system in the first spatial axis consist of v_1 repeated 8 times, along with the roots of:

$$\begin{vmatrix}\left(v_1-\lambda\right)I & \Xi_2\\ \Xi_1 & \left(v_1-\lambda\right)I\end{vmatrix}=0 \tag{B.15}$$

where

$$\Xi_1=\begin{pmatrix}-\frac{1}{\rho}\frac{\partial\sigma_{11}}{\partial\rho} & \frac{1}{\rho} & -\frac{1}{\rho}\frac{\partial\sigma_{11}}{\partial A_{11}} & -\frac{1}{\rho}\frac{\partial\sigma_{11}}{\partial A_{21}} & -\frac{1}{\rho}\frac{\partial\sigma_{11}}{\partial A_{31}}\\ -\frac{1}{\rho}\frac{\partial\sigma_{21}}{\partial\rho} & 0 & -\frac{1}{\rho}\frac{\partial\sigma_{21}}{\partial A_{11}} & -\frac{1}{\rho}\frac{\partial\sigma_{21}}{\partial A_{21}} & -\frac{1}{\rho}\frac{\partial\sigma_{21}}{\partial A_{31}}\\ -\frac{1}{\rho}\frac{\partial\sigma_{31}}{\partial\rho} & 0 & -\frac{1}{\rho}\frac{\partial\sigma_{31}}{\partial A_{11}} & -\frac{1}{\rho}\frac{\partial\sigma_{31}}{\partial A_{21}} & -\frac{1}{\rho}\frac{\partial\sigma_{31}}{\partial A_{31}}\\ \frac{T_\rho}{\rho} & \frac{T_p}{\rho} & 0 & 0 & 0\end{pmatrix} \tag{B.16}$$

$$
M_1 = \begin{pmatrix}
v_1 & 0 & 0 & 0 & 0 & 0 & 0 & 0 & 0 & 0 & 0 & \rho & 0 & 0 & 0 \\
0 & v_1 & 0 & 0 & 0 & 0 & 0 & 0 & 0 & 0 & 0 & \left(\rho c_0^2 + \sigma_{11} - \rho \frac{\partial \sigma_{11}}{\partial \rho}\right) & \left(\sigma_{21} - \rho \frac{\partial \sigma_{21}}{\partial \rho}\right) & \left(\sigma_{31} - \rho \frac{\partial \sigma_{31}}{\partial \rho}\right) & \frac{\rho c_h^2}{T_p} \\
0 & 0 & v_1 & 0 & 0 & 0 & 0 & 0 & 0 & 0 & 0 & A_{11} & A_{12} & A_{13} & 0 \\
0 & 0 & 0 & v_1 & 0 & 0 & 0 & 0 & 0 & 0 & 0 & A_{21} & A_{22} & A_{23} & 0 \\
0 & 0 & 0 & 0 & v_1 & 0 & 0 & 0 & 0 & 0 & 0 & A_{31} & A_{32} & A_{33} & 0 \\
0 & 0 & 0 & 0 & 0 & v_1 & 0 & 0 & 0 & 0 & 0 & 0 & 0 & 0 & 0 \\
0 & 0 & 0 & 0 & 0 & 0 & v_1 & 0 & 0 & 0 & 0 & 0 & 0 & 0 & 0 \\
0 & 0 & 0 & 0 & 0 & 0 & 0 & v_1 & 0 & 0 & 0 & 0 & 0 & 0 & 0 \\
0 & 0 & 0 & 0 & 0 & 0 & 0 & 0 & v_1 & 0 & 0 & 0 & 0 & 0 & 0 \\
0 & 0 & 0 & 0 & 0 & 0 & 0 & 0 & 0 & v_1 & 0 & 0 & 0 & 0 & 0 \\
0 & 0 & 0 & 0 & 0 & 0 & 0 & 0 & 0 & 0 & v_1 & 0 & 0 & 0 & 0 \\
-\frac{1}{\rho}\frac{\partial \sigma_{11}}{\partial \rho} & \frac{1}{\rho} & -\frac{1}{\rho}\frac{\partial \sigma_{11}}{\partial A_{11}} & -\frac{1}{\rho}\frac{\partial \sigma_{11}}{\partial A_{21}} & -\frac{1}{\rho}\frac{\partial \sigma_{11}}{\partial A_{31}} & -\frac{1}{\rho}\frac{\partial \sigma_{11}}{\partial A_{12}} & -\frac{1}{\rho}\frac{\partial \sigma_{11}}{\partial A_{22}} & -\frac{1}{\rho}\frac{\partial \sigma_{11}}{\partial A_{32}} & -\frac{1}{\rho}\frac{\partial \sigma_{11}}{\partial A_{13}} & -\frac{1}{\rho}\frac{\partial \sigma_{11}}{\partial A_{23}} & -\frac{1}{\rho}\frac{\partial \sigma_{11}}{\partial A_{33}} & v_1 & 0 & 0 & 0 \\
-\frac{1}{\rho}\frac{\partial \sigma_{21}}{\partial \rho} & 0 & -\frac{1}{\rho}\frac{\partial \sigma_{21}}{\partial A_{11}} & -\frac{1}{\rho}\frac{\partial \sigma_{21}}{\partial A_{21}} & -\frac{1}{\rho}\frac{\partial \sigma_{21}}{\partial A_{31}} & -\frac{1}{\rho}\frac{\partial \sigma_{21}}{\partial A_{12}} & -\frac{1}{\rho}\frac{\partial \sigma_{21}}{\partial A_{22}} & -\frac{1}{\rho}\frac{\partial \sigma_{21}}{\partial A_{32}} & -\frac{1}{\rho}\frac{\partial \sigma_{21}}{\partial A_{13}} & -\frac{1}{\rho}\frac{\partial \sigma_{21}}{\partial A_{23}} & -\frac{1}{\rho}\frac{\partial \sigma_{21}}{\partial A_{33}} & 0 & v_1 & 0 & 0 \\
-\frac{1}{\rho}\frac{\partial \sigma_{31}}{\partial \rho} & 0 & -\frac{1}{\rho}\frac{\partial \sigma_{31}}{\partial A_{11}} & -\frac{1}{\rho}\frac{\partial \sigma_{31}}{\partial A_{21}} & -\frac{1}{\rho}\frac{\partial \sigma_{31}}{\partial A_{31}} & -\frac{1}{\rho}\frac{\partial \sigma_{31}}{\partial A_{12}} & -\frac{1}{\rho}\frac{\partial \sigma_{31}}{\partial A_{22}} & -\frac{1}{\rho}\frac{\partial \sigma_{31}}{\partial A_{32}} & -\frac{1}{\rho}\frac{\partial \sigma_{31}}{\partial A_{13}} & -\frac{1}{\rho}\frac{\partial \sigma_{31}}{\partial A_{23}} & -\frac{1}{\rho}\frac{\partial \sigma_{31}}{\partial A_{33}} & 0 & 0 & v_1 & 0 \\
\frac{T_\rho}{\rho} & \frac{T_p}{\rho} & 0 & 0 & 0 & 0 & 0 & 0 & 0 & 0 & 0 & 0 & 0 & 0 & v_1 \\
0 & 0 & 0 & 0 & 0 & 0 & 0 & 0 & 0 & 0 & 0 & 0 & 0 & 0 & 0 \\
0 & 0 & 0 & 0 & 0 & 0 & 0 & 0 & 0 & 0 & 0 & 0 & 0 & 0 & 0
\end{pmatrix}
\tag{B.12}
$$

$$\Xi_2 = \begin{pmatrix} \rho & 0 & 0 & 0 \\ \left(\rho c_0^2 + \sigma_{11} - \rho \frac{\partial \sigma_{11}}{\partial \rho}\right) & \left(\sigma_{21} - \rho \frac{\partial \sigma_{21}}{\partial \rho}\right) & \left(\sigma_{31} - \rho \frac{\partial \sigma_{31}}{\partial \rho}\right) & \frac{\rho c_h^2}{T_p} \\ A_{11} & A_{12} & A_{13} & 0 \\ A_{21} & A_{22} & A_{23} & 0 \\ A_{31} & A_{32} & A_{33} & 0 \end{pmatrix} \tag{B.17}$$

By the properties of block matrices[4], the remaining eigenvalues are v_1 and the roots of $\left|(v_1 - \lambda)^2 I - \Xi_1 \Xi_2\right| = 0$. Thus, $\lambda_i = v_1 \pm \sqrt{\tilde{\lambda}_i}$ where the $\tilde{\lambda}_i$ are the eigenvalues of the following matrix:

$$\Xi = \Xi_1 \Xi_2 = \begin{pmatrix} \Omega_{11}^1 + \left(c_0^2 + \frac{\sigma_{11}}{\rho} - \frac{\partial \sigma_{11}}{\partial \rho}\right) & \Omega_{12}^1 + \left(\frac{\sigma_{21}}{\rho} - \frac{\partial \sigma_{21}}{\partial \rho}\right) & \Omega_{13}^1 + \left(\frac{\sigma_{31}}{\rho} - \frac{\partial \sigma_{31}}{\partial \rho}\right) & \frac{c_h^2}{T_p} \\ \Omega_{21}^1 & \Omega_{22}^1 & \Omega_{23}^1 & 0 \\ \Omega_{31}^1 & \Omega_{32}^1 & \Omega_{33}^1 & 0 \\ T_\rho + T_p \left(c_0^2 + \frac{\sigma_{11}}{\rho} - \frac{\partial \sigma_{11}}{\partial \rho}\right) & T_p \left(\frac{\sigma_{21}}{\rho} - \frac{\partial \sigma_{21}}{\partial \rho}\right) & T_p \left(\frac{\sigma_{31}}{\rho} - \frac{\partial \sigma_{31}}{\partial \rho}\right) & c_h^2 \end{pmatrix} \tag{B.18}$$

where Ω is given shortly. Similar results hold for the other two spatial directions. In general it is not possible to express the eigenvalues of Ξ in terms of the eigenvalues of its submatrices. Note, however, that if $\alpha = 0$ then one of the eigenvalues is 0 and the remaining eigenvalues can be found analytically, using the form given in the appendix of [14].

It is straightforward to verify the following:

$$\frac{\partial \sigma_{ij}}{\partial A_{mn}} = -c_s^2 \rho \begin{pmatrix} \delta_{in} \left(A \operatorname{dev}(G)\right)_{mj} + \delta_{jn} \left(A \operatorname{dev}(G)\right)_{mi} \\ + A_{mi} G_{jn} + A_{mj} G_{in} - \frac{2}{3} G_{ij} A_{mn} \end{pmatrix} \tag{B.19}$$

The quantity Ω is named here the *acoustic tensor*, due to its similarity to the acoustic tensor described in [4]:

[4] If A is invertible, $\det \begin{pmatrix} A & B \\ C & D \end{pmatrix} = \det(A) \det\left(D - CA^{-1}B\right)$

$$\begin{aligned}
\Omega_{ij}^{d} &= -\frac{1}{\rho}\frac{\partial \sigma_{id}}{\partial A_{kd}} A_{kj} - \frac{\sigma_{id}}{\rho}\delta_{dj} \\
&= c_s^2 \begin{pmatrix} \delta_{id}\left(G\,\mathrm{dev}\left(G\right)\right)_{dj} + \left(G\,\mathrm{dev}\left(G\right)\right)_{id}\delta_{dj} \\ + \left(G\,\mathrm{dev}\left(G\right)\right)_{ij} + G_{ij}G_{dd} + \frac{1}{3}G_{dj}G_{id} \end{pmatrix} \\
&= c_s^2 \left(E^d G\,\mathrm{dev}\left(G\right) + G\,\mathrm{dev}\left(G\right)E^d + G\,\mathrm{dev}\left(G\right) + G_{dd}G + \frac{1}{3}G_d G_d^T\right)
\end{aligned} \tag{B.20}$$

where $E_{ij}^{d} = \delta_{id}\delta_{jd}$.

B.3 Eigenvectors

With Heat Conduction

By hyperbolicity of the system, Ξ can be expressed as:

$$\Xi = Q^{-1}D^2Q \tag{B.21}$$

where D is a diagonal matrix with positive diagonal entries. The eigenvectors corresponding to $\lambda_i = v_1 \pm \sqrt{\tilde{\lambda}_i}$ take the form $\begin{pmatrix} \hat{u} & 0_6 & \tilde{u} & 0_2 \end{pmatrix}^T$ where $\boldsymbol{\hat{u}} \in \mathbb{R}^5, \boldsymbol{\tilde{u}} \in \mathbb{R}^4$ satisfy:

$$\begin{pmatrix} v_1 I & \Xi_2 \\ \Xi_1 & v_1 I \end{pmatrix} \begin{pmatrix} \boldsymbol{\hat{u}} \\ \boldsymbol{\tilde{u}} \end{pmatrix} = \left(v_1 \pm \sqrt{\tilde{\lambda}_i}\right) \begin{pmatrix} \boldsymbol{\hat{u}} \\ \boldsymbol{\tilde{u}} \end{pmatrix} \tag{B.22}$$

Thus, $\Xi_2\boldsymbol{\tilde{u}} = \pm\sqrt{\tilde{\lambda}_i}\boldsymbol{\hat{u}}$ and $\Xi_1\boldsymbol{\hat{u}} = \pm\sqrt{\tilde{\lambda}_i}\boldsymbol{\tilde{u}}$. Combining these results, $\Xi\boldsymbol{\tilde{u}} = \tilde{\lambda}_i\boldsymbol{\tilde{u}}$. Thus, $\boldsymbol{\tilde{u}}$ is a right eigenvector of Ξ and, taking the form $Q^{-1}\boldsymbol{e_i}$ for some $i = 1 \dots 4$.

The four eigenvectors corresponding to eigenvalues of the form $v_1 + \sqrt{\tilde{\lambda}_i}$ are columns 1-4 of matrix R in (B.23). Those corresponding to eigenvalues of the form $v_1 - \sqrt{\tilde{\lambda}_i}$ are columns 5-8. By inspection, it can be verified that the remaining 9 eigenvectors (corresponding to eigenvalue v_1) are the remaining columns.

A similar analysis yields the left eigenvectors as the rows of (B.25).

$$R = \left\{ \begin{pmatrix} \frac{1}{2}\Xi_2 \left(D^2 Q\right)^{-1} & \frac{1}{2}\Xi_2 \left(D^2 Q\right)^{-1} \\ 0_{6,4} & 0_{6,4} \\ \frac{1}{2}\left(DQ\right)^{-1} & -\frac{1}{2}\left(DQ\right)^{-1} \\ 0_{2,4} & 0_{2,4} \end{pmatrix}, \begin{pmatrix} -cT_p \\ cT_\rho \\ c\Pi_d^{-1}\boldsymbol{w} \\ 0_{12,1} \end{pmatrix}, \begin{pmatrix} 0_{2,3} & 0_{2,3} \\ -\Pi_1^{-1}\Pi_2 & -\Pi_1^{-1}\Pi_3 \\ I_3 & 0_{3,3} \\ 0_{3,3} & I_3 \\ 0_{6,3} & 0_{6,3} \end{pmatrix}, \begin{pmatrix} 0_{15,2} \\ I_2 \end{pmatrix} \right\} \tag{B.23}$$

where

$$\boldsymbol{w} = T_p \frac{\partial \boldsymbol{\sigma_d}}{\partial \rho} + T_\rho \boldsymbol{e_d} \tag{B.24a}$$

$$c = \frac{1}{\boldsymbol{e_d^T}\left(\Pi_d A\right)^{-1}\boldsymbol{w} + \frac{T_p}{\rho}} \tag{B.24b}$$

$$L = \left\{ \begin{array}{c} \begin{pmatrix} Q\Xi_1 & -\frac{1}{\rho}Q_{:,1:3}\Pi_2 & -\frac{1}{\rho}Q_{:,1:3}\Pi_3 & DQ & 0_{4,2} \\ Q\Xi_1 & -\frac{1}{\rho}Q_{:,1:3}\Pi_2 & -\frac{1}{\rho}Q_{:,1:3}\Pi_3 & -DQ & 0_{4,2} \end{pmatrix} \\ \begin{pmatrix} -\frac{1}{\rho} & 0 & \boldsymbol{e_d^T}A^{-1} & \boldsymbol{e_d^T}A^{-1}\Pi_1^{-1}\Pi_2 & \boldsymbol{e_d^T}A^{-1}\Pi_1^{-1}\Pi_3 & 0_{1,6} \end{pmatrix} \\ \begin{pmatrix} 0_{3,5} & I_3 & 0_{3,3} & 0_{3,6} \\ 0_{3,5} & 0_{3,3} & I_3 & 0_{3,6} \end{pmatrix} \\ \begin{pmatrix} 0_{2,15} & I_2 \end{pmatrix} \end{array} \right\} \tag{B.25}$$

Without Heat Conduction

If the system does not include the heat conduction terms, the eigenstructure of the system matrix changes. Ξ_1, Ξ_2, Ξ now take the following values:

$$\Xi_1 = \begin{pmatrix} -\frac{1}{\rho}\frac{\partial \sigma_{11}}{\partial \rho} & \frac{1}{\rho} & -\frac{1}{\rho}\frac{\partial \sigma_{11}}{\partial A_{11}} & -\frac{1}{\rho}\frac{\partial \sigma_{11}}{\partial A_{21}} & -\frac{1}{\rho}\frac{\partial \sigma_{11}}{\partial A_{31}} \\ -\frac{1}{\rho}\frac{\partial \sigma_{21}}{\partial \rho} & 0 & -\frac{1}{\rho}\frac{\partial \sigma_{21}}{\partial A_{11}} & -\frac{1}{\rho}\frac{\partial \sigma_{21}}{\partial A_{21}} & -\frac{1}{\rho}\frac{\partial \sigma_{21}}{\partial A_{31}} \\ -\frac{1}{\rho}\frac{\partial \sigma_{31}}{\partial \rho} & 0 & -\frac{1}{\rho}\frac{\partial \sigma_{31}}{\partial A_{11}} & -\frac{1}{\rho}\frac{\partial \sigma_{31}}{\partial A_{21}} & -\frac{1}{\rho}\frac{\partial \sigma_{31}}{\partial A_{31}} \end{pmatrix} \tag{B.26}$$

$$\Xi_2 = \begin{pmatrix} \rho & 0 & 0 \\ \left(\rho c_0^2 + \sigma_{11} - \rho\frac{\partial \sigma_{11}}{\partial \rho}\right) & \left(\sigma_{21} - \rho\frac{\partial \sigma_{21}}{\partial \rho}\right) & \left(\sigma_{31} - \rho\frac{\partial \sigma_{31}}{\partial \rho}\right) \\ A_{11} & A_{12} & A_{13} \\ A_{21} & A_{22} & A_{23} \\ A_{31} & A_{32} & A_{33} \end{pmatrix} \tag{B.27}$$

$$\Xi = \Xi_1\Xi_2 = \begin{pmatrix} \Omega^1_{11} + \left(c_0^2 + \frac{\sigma_{11}}{\rho} - \frac{\partial\sigma_{11}}{\partial\rho}\right) & \Omega^1_{12} + \left(\frac{\sigma_{21}}{\rho} - \frac{\partial\sigma_{21}}{\partial\rho}\right) & \Omega^1_{13} + \left(\frac{\sigma_{31}}{\rho} - \frac{\partial\sigma_{31}}{\partial\rho}\right) \\ \Omega^1_{21} & \Omega^1_{22} & \Omega^1_{23} \\ \Omega^1_{31} & \Omega^1_{32} & \Omega^1_{33} \end{pmatrix} \tag{B.28}$$

Using the eigendecomposition $\Xi = Q^{-1}D^2Q$ as before, we have:

$$R = \left\{ \begin{pmatrix} \frac{1}{2}\Xi_2\left(D^2Q\right)^{-1} & \frac{1}{2}\Xi_2\left(D^2Q\right)^{-1} \\ 0_{6,3} & 0_{6,3} \\ \frac{1}{2}\left(DQ\right)^{-1} & -\frac{1}{2}\left(DQ\right)^{-1} \end{pmatrix}, \begin{pmatrix} 1 & 0 \\ 0 & 1 \\ -\Pi_1^{-1}\frac{\partial\boldsymbol{\sigma_1}}{\partial\rho} & \Pi_1^{-1}\boldsymbol{e_1} \\ \mathbf{0_9} & \mathbf{0_9} \end{pmatrix}, \begin{pmatrix} 0_{2,3} & 0_{2,3} \\ -\Pi_1^{-1}\Pi_2 & -\Pi_1^{-1}\Pi_3 \\ I_3 & 0_{3,3} \\ 0_{3,3} & I_3 \\ 0_{3,3} & 0_{3,3} \end{pmatrix} \right\} \tag{B.29}$$

By considering their products with the first 8 columns of R, two of the left eigenvectors corresponding the the 7th and 8th right eigenvectors must come in the form of the rows of the following matrix:

$$\begin{pmatrix} W & X & Y & Z \end{pmatrix} \tag{B.30}$$

where $W \in \mathbb{R}^{2,5}$ and $X, Y, Z \in \mathbb{R}^{2,3}$, and:

$$W\Xi_2\left(D^2Q\right)^{-1} + Z\left(DQ\right)^{-1} = 0 \tag{B.31a}$$

$$W\Xi_2\left(D^2Q\right)^{-1} - Z\left(DQ\right)^{-1} = 0 \tag{B.31b}$$

$$W\begin{pmatrix} 0_{2,3} \\ -\Pi_1^{-1}\Pi_2 \end{pmatrix} + X = 0 \tag{B.31c}$$

$$W\begin{pmatrix} 0_{2,3} \\ -\Pi_1^{-1}\Pi_3 \end{pmatrix} + Y = 0 \tag{B.31d}$$

Thus:

$$Z = 0 \tag{B.32a}$$

$$X = W_{:,3:5}\Pi_1^{-1}\Pi_2 \tag{B.32b}$$

$$Y = W_{:,3:5}\Pi_1^{-1}\Pi_3 \tag{B.32c}$$

and

$$W \begin{pmatrix} \rho & 0 & 0 & 1 & 0 \\ \left(\rho c_0^2 + \sigma_{11} - \rho \frac{\partial \sigma_{11}}{\partial \rho}\right) & \left(\sigma_{21} - \rho \frac{\partial \sigma_{21}}{\partial \rho}\right) & \left(\sigma_{31} - \rho \frac{\partial \sigma_{31}}{\partial \rho}\right) & 0 & 1 \\ A_{11} & A_{12} & A_{13} & \vdots & \vdots \\ A_{21} & A_{22} & A_{23} & -\Pi_1^{-1} \frac{\partial \boldsymbol{\sigma_1}}{\partial \rho} & \Pi_1^{-1} \boldsymbol{e_1} \\ A_{31} & A_{32} & A_{33} & \vdots & \vdots \end{pmatrix} = WM = \begin{pmatrix} 0 & 0 & 0 & 1 & 0 \\ 0 & 0 & 0 & 0 & 1 \end{pmatrix} \tag{B.33}$$

By the properties of block matrices:

$$M^{-1} = \begin{pmatrix} -A^{-1}C \left(I - BA^{-1}C\right)^{-1} & A^{-1} \left(I + C \left(I - BA^{-1}C\right)^{-1} BA^{-1}\right) \\ \left(I - BA^{-1}C\right)^{-1} & -\left(I - BA^{-1}C\right)^{-1} BA^{-1} \end{pmatrix} \tag{B.34}$$

where

$$B = \begin{pmatrix} \rho & 0 & 0 \\ \left(\rho c_0^2 + \sigma_{11} - \rho \frac{\partial \sigma_{11}}{\partial \rho}\right) & \left(\sigma_{21} - \rho \frac{\partial \sigma_{21}}{\partial \rho}\right) & \left(\sigma_{31} - \rho \frac{\partial \sigma_{31}}{\partial \rho}\right) \end{pmatrix} \tag{B.35a}$$

$$C = \begin{pmatrix} \cdots & -\Pi_1^{-1} \frac{\partial \boldsymbol{\sigma_1}}{\partial \rho} & \cdots \\ \cdots & \Pi_1^{-1} \boldsymbol{e_1} & \cdots \end{pmatrix}^T \tag{B.35b}$$

Thus:

$$W = \left(\left(I - BA^{-1}C\right)^{-1} \; -\left(I - BA^{-1}C\right)^{-1} BA^{-1} \right) \tag{B.36}$$

$$W = \left(I - BA^{-1}C\right)^{-1} \left(I_2 \; -BA^{-1} \right) \tag{B.37a}$$

$$X = -\left(I - BA^{-1}C\right)^{-1} BA^{-1} \Pi_1^{-1} \Pi_2 \tag{B.37b}$$

$$Y = -\left(I - BA^{-1}C\right)^{-1} BA^{-1} \Pi_1^{-1} \Pi_3 \tag{B.37c}$$

$$L = \left\{ \begin{matrix} \begin{pmatrix} Q\Xi_1 & -\frac{1}{\rho}Q\Pi_2 & -\frac{1}{\rho}Q\Pi_3 & DQ \\ Q\Xi_1 & -\frac{1}{\rho}Q\Pi_2 & -\frac{1}{\rho}Q\Pi_3 & -DQ \end{pmatrix} \\ (I_2 - BA^{-1}C)^{-1} \begin{pmatrix} I_2 & -BA^{-1} & -BA^{-1}\Pi_1^{-1}\Pi_2 & -BA^{-1}\Pi_1^{-1}\Pi_3 & 0_{2,3} \end{pmatrix} \\ \begin{pmatrix} 0_{3,5} & I_3 & 0_{3,3} & 0_{3,3} \\ 0_{3,5} & 0_{3,3} & I_3 & 0_{3,3} \end{pmatrix} \end{matrix} \right\} \tag{B.38}$$

$$\boldsymbol{P} = \begin{pmatrix} \rho \\ p \\ A_{11} \\ A_{21} \\ A_{31} \\ A_{12} \\ A_{22} \\ A_{32} \\ A_{13} \\ A_{23} \\ A_{33} \\ v_1 \\ v_2 \\ v_3 \\ J_1 \\ J_2 \\ J_3 \end{pmatrix} \tag{B.13}$$

$$
\boldsymbol{S_p} = \frac{1}{\theta_1}\begin{pmatrix} 0 \\ \left(\frac{1}{E_p} - 2\rho^2 \frac{\partial \log(c_s)}{\partial \rho}\right) \|\psi\|_F^2 \\ -\psi_{11} \\ -\psi_{21} \\ -\psi_{31} \\ -\psi_{12} \\ -\psi_{22} \\ -\psi_{32} \\ -\psi_{13} \\ -\psi_{23} \\ -\psi_{33} \\ 0 \\ 0 \\ 0 \\ 0 \\ 0 \\ 0 \end{pmatrix} + \frac{1}{\theta_2}\begin{pmatrix} 0 \\ \frac{1}{E_p}\|\boldsymbol{H}\|^2 \\ 0 \\ 0 \\ 0 \\ 0 \\ 0 \\ 0 \\ 0 \\ 0 \\ 0 \\ 0 \\ 0 \\ 0 \\ -H_1 \\ -H_2 \\ -H_3 \end{pmatrix} \tag{B.14}
$$

Appendix C

Model Parameters

The parameters for different materials under different equations of state are given in the tables below. All variables are given in SI units.

C.1 Material Properties

Material	ρ_0	p_0	T_0	c_v	c_s	μ	α	κ	P_r
Air	1.18	10100		721	1	1.85×10^{-5}	1		0.714
Helium	0.163	10100		3127	1	1.99×10^{-5}	1		0.688
Water	1000	10000		950	10^{-4}	10^{-3}	10^{-4}		7
PBX	1840	10000		-	10^{-4}	10^{-5}	-		-
C4	1590								
Copper	8930	0		390		-			
Aluminium						-			
Steel	7860		298			-			

Table C.1: Reference parameters for various materials

C.2 Equation of State Parameters

	Ideal/Stiffened Gas		Shock Mie-Gruneisen			Godunov-Romenski			
	γ	p_∞	Γ_0	c_0	s	c_0	α	β	$\dot{\gamma}$
Air	1.4	-							
Helium	1.66	-							
Water	4.4	6×10^8							
PBX	2.85	-							
C4	-	-	1.99	3909	1.48				
Copper									
Aluminium									
Steel									

Table C.2: Parameters for the Ideal-/Stiffened-Gas, Shock Mie-Gruneisen, and Godunov-Romenski equations of state

Material	τ_1	σ_Y	n
Copper	0.1	9×10^8	10
Aluminium	1	4×10^8	20

Table C.3: Plasticity parameters for various materials

C.3 Combustion Parameters